MECHANISTIC STUDY ON THE CONVERSION OF FATTY ACID TO LONG CHAIN OLEFINS OVER TITANATE-BASED CATALYSTS

PRATYA PROMCHANA

A THESIS SUBMITTED IN PARTIAL FULFILLMENTOF THE REQUIREMENT FOR THE DEGREE OFMASTER OF SCIENCE IN PETROCHEMICALS AND HYDROCARBON CHEMISTRY

DEPARTMENT OF CHEMISTRY

FACULTY OF SCIENCE

KING MONGKUT'S INSTITUTE OF TECHNOLOGY LADKRABANG

2016

KMITL-2016-SC-M-015-015

Thesis Title	Mechanistic study on the conversion of fatty acid to Long chain olefins over titanate-based catalysts
Student	Mr. Pratya Promchana
Student ID.	56605051
Degree	Master of Science (Petrochemicals and Hydrocarbon Chemistry)
Department	Chemistry
Year	2016
Thesis Advisor	Assoc. Prof. Dr. Tawan Sooknoi
Thesis Coadvisor	Dr. Tosapol Maluangnont

Abstract

The mechanistic study on the conversion of fatty acid to long chain olefins over titanate-based catalysts has been investigated using heptanoic acid as model compound. Catalysts studied include $A_2Ti_6O_{13}$ (A = Li, Na and K; tunneled structure), $Na_2Ti_3O_7$ and $K_2Ti_4O_9$. It was found by temperature programmed reduction (TPR) that the most facile reduction occurs with $K_2Ti_6O_{13}$. While basicity and basic strength of the catalysts are much less than that of the commercial MgO that is commonly used as a catalyst in decarboxylation of carboxylic acid. The catalytic characterization for decarboxylation of carboxylic acid were primarily tested using acetic acid as probe molecule. It was found that acetone and CO_2 obtained over all catalysts suggesting that ketonization is primarily promoted. The activity (400 °C, in N_2) is in the order of: $K_2Ti_6O_{13}$ > $Li_2Ti_6O_{13}$ > $Na_2Ti_6O_{13}$ > $K_2Ti_4O_9$ > $Na_2Ti_3O_7$ and Anatase TiO_2. The activity of $K_2Ti_6O_{13}$ can be enhanced by *in situ* reduction at 400 °C which generates more oxygen vacancy sites. However, a decrease in the activity was observed upon reduction at high temperature (500 °C), due to the electron transfer from Ti^{3+} at surface to the bulk.

The deoxygenation of heptanoic acid (400 °C, N_2) over reducible $K_2Ti_6O_{13}$, gives mainly 7-tridecanone and small amount of cracking products such as 2-octanone, 6-dodecanone and 5-undecane with 24% conversion. Incorporating Pt on $K_2Ti_6O_{13}$ gives long chain olefins (7-tridecene) via hydrogenation of 7-tridecanone and subsequently dehydration. In addition, direct decarboxylation and hydrogenolysis of heptanoic acid were promoted, resulting in all isomer of hexene and heptane. The mechanistic pathway over the Pt loaded $K_2Ti_6O_{13}$ is claimed by the ketonization of heptanoic acid

to 7-tridecanone and CO_2 over oxygen vacancy sites. However, direct decarbonylation of heptanoic acid to hexene and hydrogenolysis to heptane are also obtained with lesser extent. Hence, the ketone is further converted either by carbon-carbon bond cracking at at α-position to 2-octanone and *n*-pentene or hydrogenation-dehydration to 7-tridecene.

ACKNOWLEDGEMENT

The authors take this opportunity to acknowledge advisors Assoc.Prof.Dr. Tawan Sooknoi and Co-Advisor Dr. Tosapol Maluangnont, for the continually suggestion, graceful knowledge and useful discussion throughout this research. In addition, we would like to sincere appreciate chairperson and committee member, Dr. Amnat Permsubskul, Assoc. Prof. Dr. Siriporn Jongpatiwut and Asst. Dr. Montree Thongkam, respectively, for the opinions and the guidance with a graceful.

We would like to distribute a kindness thank to Catalytic Chemistry Research Unit members for their contribution of the ideas and facilities and most importantly their support.

We would like to extend our thanks to Mr. Boonyawat Wuttitham and Mr. Pornanan Arsa for their help and advices in working the data analysis, support and encouragement.

Furthermore, we would like to express our appreciation thanks to Department of Chemistry, Faculty of Science, King Mongkut's Institute of Technology Ladkrabang for advanced laboratory instruments, equipment, chemical and accommodation.

Last but not least, the authors would like to gracefully thank the parents and families, who give an encouragement. This thesis would not be possible without them.

The thesis is dedicated for the world citizen, who want to be a technical and theoretical expert.

Pratya Promchana

CONTENTS

Page

ABSTRACT I

ACKNOWLEDGEMENT III

CONTENTS IV

LIST OF TABLES VII

LIST OF FIGURES VIII

CHAPTER 1 Introduction 1

1.1 Introduction 1

1.2 Objectives 2

1.3 Scopes of study 3

1.4 Expected results 3

CHAPTER 2 Theory and Literature Reviews 4

2.1 Fatty acids 4

2.1.1 Acetic acid 6

2.1.2 Heptanoic acid 6

2.2 Chemical reaction of fatty acids 7

2.2.1 Reaction associated with double bonds of fatty acid 7

2.2.2 Reaction of carboxyl group of fatty acids 7

2.3 Long chain olefins 10

2.4 Titania (TiO_2) 11

2.5 Titanate-based materials 13

2.5.1 Alkali-titanate $A_2O{\cdot}nTiO_2$ 13

2.5.2 Reducibility vs Basicity in Alkali Titanates 14

2.6 Literature reviews 15

CHAPTER 3 Experimental 18

3.1 Reagents 18

3.2 Apparatuses 18

3.3 Preparation and characterization of catalysts 19

3.3.1 Synthesis of titanate-based catalysts 19

3.3.2 Preparation of 1% $Co/K_2Ti_6O_{13}$ 20

3.3.3 Powder X-ray diffraction 20

CONTENTS (CONTINUED)

Page

3.3.4 Chemical analysis 20
3.3.5 Surface area measurement and pore size distribution 21
3.3.6 Thermal stability 21
3.3.7 Morphology 21
3.3.8 Temperature-programmed reduction 21
3.3.9 Temperature-programmed desorption of CO_2 22
3.3.10 X-ray photoelectron spectroscopy 22
3.4 Catalytic activity testing 23
CHAPTER 4 Results and Discussions 25
4.1 Characterization of catalysts 25
4.1.1 Powder x-ray diffraction pattern, PXRD 25
4.1.2 Elemental analysis 29
4.1.3 Surface area and textural properties 30
4.1.4 Thermal stability 32
4.1.5 Temperature programmed reduction profile 33
4.1.6 Basic properties 38
4.2 Catalytic characterization 40
4.2.1 Deoxygenation of acetic acid 40
4.2.2 Aldol-condensation of acetone 47
4.3 Production of long chain olefins from heptanoic acid 48
4.3.1 Effect of reaction temperature 48
4.3.2 Effect of contact time 50
4.2.3 Effect of incorporated metals 56
4.2.4 Production of long chain olefins from lauric acid 62
CHAPTER 5 Conclusion and Suggestion 65
5.1 Conclusions 65
5.2 Suggestions 66
References 67
APPENDIX A 77
APPENDIX B 80
APPENDIX C 82

CONTENTS (CONTINUED)

Page

APPENDIX D.....84
APPENDIX E.....91
AUTHOR BIOGRAPHY.....97

LIST OF TABLES

Table		Page
2.1	Saturated fatty acid and their physical properties	4
2.2	The use of long chain olefins in industrial application	11
3.1	A list of reagents	18
4.1	Unit cell parameter of the metal titanates prepared in this work	28
4.2	Elemental composition of titanate catalysts	29
4.3	Surface area and pore volume of the catalysts	30
4.4	Hydrogen consumption of the catalysts studied	34
4.5	Basic site of catalysts studied	39
4.6	the aldol-condensation activity of the catalysts	47
4.7	Application of products derivative from parent fatty acid	63

LIST OF FIGURES

Figure Page

2.1 Molecular structure of acetic acid 6

2.2 Molecular structure of heptanoic acid 6

2.3 Direct hydrogenation of unsaturated fatty acid and the side reaction. 7

2.4 Acid-catalyzed esterification 8

2.5 Base-catalyzed esterification 8

2.6 Decarboxylative ketonization of acetic acid to acetone 9

2.7 Hydrocarbon production from fatty acid via
(a) decarboxylation, and (b) decarbonylation 10

2.8 The crystal structure of (a) anatase and (b) rutile phase TiO_2. 13

2.9 Skeletal structure of (a) $Na_2Ti_3O_7$ and (b) $Na_2Ti_6O_{13}$. 14

3.1 Schematic diagram of the catalytic testing rig 24

4.1 X-ray diffraction pattern of a) $K_2Ti_6O_{13}$, b) 1% wt $Co/K_2Ti_6O_{13}$,
c) 1% wt $Pt/K_2Ti_6O_{13}$, d) $Na_2Ti_6O_{13}$ and e) $Li_2Ti_6O_{13}$ 25

4.2 X-ray diffraction pattern of a) Commercial $Na_2Ti_3O_7$, b) $Na_2Ti_3O_7$,
c) reheated-$Na_2Ti_3O_7$, d) $K_2Ti_4O_9$ and e) reheated-$K_2Ti_4O_9$ 27

4.3 SEM images of a) $Na_2Ti_6O_{13}$, b) $K_2Ti_6O_{13}$, c) $Li_2Ti_6O_{13}$, d) $Na_2Ti_3O_7$ e) commercial-
$Na_2Ti_3O_7$, f) $K_2Ti_4O_9$, g) 1% wt $Co/K_2Ti_6O_{13}$ and h) 1% wt $Pt/K_2Ti_6O_{13}$. 31

4.4 Thermal stability of all titanate-catalysts. 32

4.5 Temperature programmed reduction profiles of the catalysts studied. 33

4.6 X-ray diffraction pattern of all catalysts studied 36

4.7 TPR profiles of metal-free and impregnated $K_2Ti_6O_{13}$ 37

4.8 CO_2-Temperature programmed desorption profiles
of all catalysts studied. 38

4.9 The deoxygenation activity of various catalyst
with and without reduction at 400 °C for 2 h 40

4.10 The conversion of acetic acid over non-reduced catalysts
and 400°C-reduced catalysts versus specific surface area of each catalyst 42

4.11 The conversion of acetic acid over reduced catalysts vs
the oxygen vacancy sites density at selected reduction temperature. 43

LIST OF FIGURES (CONTINUED)

Figure Page

4.12 Effect of the reduction temperature of $K_2Ti_6O_{13}$ on the conversion of acetic acid and the yield of acetone. 44
4.13 Ti 2p -XPS spectra of $K_2Ti_6O_{13}$ at various reduction temperatures. 45
4.14 O 2s XPS spectra of $K_2Ti_6O_{13}$ at various reduction temperatures in H_2 atmosphere. 46
4.15 The conversion of heptanoic acid and yield of major product (a) and yield of by-products (b) at different reaction temperatures. 49
4.16 The conversion of heptanoic acid and yield of major product (a) and yield of by-products (b) at different contact times 51
4.17 The conversion of heptanoic acid and yield of major product (a) and yield of by-products (b) at different contact times 52
4.18 The conversion of heptanoic acid at contact time 150 gh/mol in N_2 and H_2. 53
4.19 Catalytic pathway of the conversion of heptanoic acid in both N_2 and H_2 atmostphere over $K_2Ti_6O_{13}$. 55
4.20 The conversion of heptanoic acid and yield of various products over different metal-loaded $K_2Ti_6O_{13}$-based catalysts 57
4.21 The conversion of heptanoic acid and yield of various products at different contact times 58
4.22 The extended mechanistic pathway of $Pt/K_2Ti_6O_{13}$ 60
4.23 The conversion of heptanoic acid and yield of various products over $K_2Ti_6O_{13}$-based catalysts loaded with different amount of Pt. 61
4.24 The conversion of lauric acid and yield of major product (a) and yield of by-products (b). 62

CHAPTER 1
Introduction

1.1 Introduction

The demand for long chain olefins has been tremendously growing as they are building blocks in a wide variety of industrial processes, such as the synthesis of copolymers, detergent alcohols, surfactants, or laboratorial chemicals [1].

The main manufacturing routes of long chain olefins in an industrial scale include (i) the oligomerization of ethylene, and (ii) Fischer-Tropsch synthesis. In addition, they could be produced commercially in a small-scale batch via the dehydration of long chain alcohols [2]. The depletion of petroleum-oil and hydrocarbon storage, in addition to the pollution evolving from the use of petrochemical feedstock, has driven the search for alternative, clean, eco-friendly and more sustainable sources for the manufacturing of long chain olefins. Therefore, renewable feedstock such as biomass, natural wax and extracted oil, are significant candidates [3].

Fatty acids can be derived from triglycerides in vegetable oils such as palm, soybean and coconut oil. A monomolecular reaction capable of producing long chain olefins from the acids involves the removal of oxygen atoms, known collectively as deoxygenation. Supported noble metal such as Pd and Pt/ activated carbon has been extensively studied. In this studied the deoxygenation can be accomplished via either the directly removal of CO (i.e., decarbonylation) or of CO_2 (i.e., decarboxylation). However, high partial pressure of hydrogen was co-fed, acting as oxygen accepter and decreasing olefins yield by rapid hydrogenation. Alternatively, a bimolecular reaction known as ketonization, partial deoxygenation, where two molecules of and carboxylic acids are coupled into a ketone and release H_2O and CO_2, would also produce long chain olefins by cracking of the ketone with less H_2 consumption.

Metal oxide-based catalysts have been widely studied in deoxygenation [4]. Among them, catalysts based on titanium dioxide (TiO_2, or titania) which are relatively inexpensive and less toxic, show moderate activity [5]. The common phase of TiO_2 is rutile and anatase, where the TiO_6 building blocks are linked together differently, resulting in relatively dense crystal structures. The moderate activity is a result of low surface area and low reducibility of the surface. Therefore, it is interesting to study several types of materials with Ti and O atoms, showing a more complex assembly of

TiO_6 into a less dense structure. Titanate-based materials with different crystal structures would affect the reducibility of the materials and the associated catalytic deoxygenation activity. In addition, the ability to synthesize some of the titanates into nanostructured ones would increase the surface area of the solid, thereby increasing the catalytic activity.

As mentioned previously, the deoxygenation of carboxylic acids with H_2-least approach can be proceeded through either (i) the direct decarboxylation /decarbonylation over a basic site or, (ii) the ketonization over an oxygen vacancy site [6]. In both cases, cracking of the primary products (whether they be alkane, alkene, or ketone) into smaller ones could occur. Hydrogen transfer can also take place, resulting in the conversion of unsaturated compounds into saturated ones. For the production of long chain olefins from carboxylic acids is required, the hydrogen transfer reaction must therefore be limited. This thesis will investigate the use of titanate-based materials as a non-acidic deoxygenation catalyst that minimize hydrogen transfer problem. Moreover, the associated mechanism for the production of long chain olefins will also be focused. The effect of several parameters including the structure (tunneled *vs* layered structure), the type of compensating cations and the presence of other active metal, surface area, morphology, and the reduction temperature, on catalytic activities will also be highlighted.

1.2 Objectives

1.2.1 To obtain long chain olefins from the deoxygenation of fatty acid over titanate-based catalysts.

1.2.2 To understand the mechanism on the conversion of fatty acid to long chain olefins over titanate-based catalyst.

1.2.3 To understand the use of titanate-based materials as a deoxygenation catalyst, focusing on the following parameters: the influences of the structure (tunneled *vs* layered structure), the type of compensating cation and the presence of other active metal, surface area, morphology, and the reduction temperature on deoxygenation of fatty acid.

1.3 Scopes of study

1.3.1 Synthesis of several types of titanates, such as alkali hexatitanates $A_2Ti_6O_{13}$ (A = Li, Na and K), sodium trititanate $Na_2Ti_3O_7$ and potassium tetratitanate $K_2Ti_4O_9$, as the catalysts for the production of long chain olefins from fatty acids. Some of these materials will be doped with cobalt metal and platinum.

1.3.2 Acetic acid and heptanoic acid will be employed as model compounds to investigate the ability of titanate-based catalysts in the deoxygenation and the production of long chain olefins, respectively. In addition, the acid-catalyzed aldol-condensation will also be evaluated using acetone as a reactant, such that the contribution of the basic site to the deoxygenation activity can be quantified.

1.3.3 The catalysts will be characterized by the following techniques:

1.3.3.1 Powder X-ray diffraction (PXRD)

1.3.3.2 Scanning electron microscopy (SEM)

1.3.3.3 Surface area measurement and pore size distribution analysis

1.3.3.4 Temperature programmed reduction by hydrogen gas (H_2 TPR)

1.3.3.5 CO_2 Temperature programmed desorption (CO_2 TPD)

1.3.3.6 Thermogravimetric analysis (TGA)

1.3.3.7 X-ray photoelectron spectroscopy (XPS)

1.3.4 Catalytic activity testing will be carried out in a fixed-bed down flow reactor at 300-400 °C, at the contact time of 5-250 g·h mol^{-1}, for a time on stream (TOS) of 0-360 min. The reduction temperature will also be studied from 400-500 °C. Moreover, the type of the carrier gas includes N_2 and H_2, both at atmospheric pressure.

1. 3. 5 The liquid products from the reactions will be qualitatively and quantitatively analyzed by a gas chromatograph (GC) equipped with a mass spectrometer (GC/MS) or a flame ionization detector (GC/FID), respectively.

1.4 Expected results

The mechanistic understanding obtained from this study can be used as a guide for the rational design of other types of titanate-based deoxygenation catalysts for the production of long chain olefins from long chain fatty acids.

CHAPTER 2

Theory and Literature Reviews

2.1 Fatty acids

Fatty acids are long chain organic molecules with four or more carbon atoms and a carboxylic (-COOH) group. Fatty acids are the main component of vegetable oil and derivative fat. They are categorized either as saturated (without double bond) or as unsaturated ones (with one or more double bonds in the hydrocarbon chain). Natural fatty acids can be obtained from dietary plants such as palm kernel, sunflower seed, rape seed, linseed, sesame, and soy beans. They can also be obtained from animal products such as dairy fat, butter, milk and animal fats. Moreover, fatty acids could be extracted from organic wastes from wood and crop. The difference in the number of carbon atoms gives rise to distinguishable physical properties of different fatty acids as shown in Table 2.1.

Table 2.1 Saturated fatty acid and their physical properties [7]

Chain length	Systematic Name	Trivial name	Acid		Methyl ester	
			m.p./ °C	b.p./ °C	m.p./ °C	b.p./ °C
1	Methanoic	Formic	8.4	101	-	32
2	Ethanoic	Acetic	16.6	118	-	57
3	Propanoic	Propionic	-20.8	141	-	80
4	Butanoic	Butyric	-5.3	164	-	103
5	Pentanoic	Valeric	-34.5	186	-80.7	127
6	Hexanoic	Caproic	-3.2	206	-69.6	151
7	Heptanoic	Enanthic	-7.5	223	-55.7	174
8	Octanoic	Caprylic	16.5	240	-36.7	195
9	Nonanoic	Pelargonic	12.5	256	-34.3	214
10	Decanoic	Capric	31.6	271	-12.8	228
11	Hendecanoic	-	29.3	284	-11.3	250
12	Dodecanoic	Lauric	44.8	130	5.1	262
13	Tridecanoic	-	41.8	140	5.8	-

Table 2.1(continued) Saturated fatty acid and their physical properties

Chain length	Systematic Name	Trivial name	Acid		Methyl ester	
			m.p./ °C	b.p./ °C	m.p./ °C	b.p./ °C
14	Tetradecanoic	Myristic	54.4	149	19.1	114
15	Pentadecanoic	-	52.5	158	19.1	127
16	Hexadecanoic	Palmitic	62.9	167	30.7	136
17	Heptadecanoic	Margenic	61.3	175	29.7	148
18	Octadecanoic	Stearic	70.1	184	37.8	156
19	Nonadecanoic	-	69.4	-	38.5	191
20	Eicosanoic	Arachidic	76.1	204	46.4	188
21	Heneicosanoic	-	75.2	-	-	207
22	Docosanoic	Behenic	80.0	-	51.8	206
23	Trocosanoic	-	79.6	-	59.3	-
24	Tetracosanoic	Lignoceric	84.2	-	57.4	222
25	Pentacosanoic	-	83.5	-	59.5	-
26	Hexacosanoic	Cerotic	87.8	-	63.5	237
27	Heptacosanoic	-	87.6	-	64.6	-
28	Octacosanoic	Montanic	90.9	-	67.5	-
29	Nonacosanoic	-	90.4	-	68.8	-
30	Triacontanoic	Melissic	93.6	-	71.5	-

Considering a wide variety of uses of fatty acids, the separation and isolation of fatty acids are extremely important. Since the distillation depends on differences in the boiling point, the chain length is more important than degree of unsaturation. It is possible to fractionate a mixture of fatty acids with different numbers of carbon atoms. In addition, steam distillation can provide the fatty acids as short as C6, but usually in the range C7-C12 [8]. The characteristics and applications of two types of carboxylic acids used as a model compound in this study, acetic acid and heptanoic acid, will be described below.

2.1.1 Acetic acid

Acetic acid (Figure 2.1), known as ethanoic acid, is the chemical that is responsible for the characteristic odor of vinegar. Acetates (salts of acetic acid) are common constituents of animal and plant tissues, and are formed during the metabolism of food substances [9]. Typical concentrations of acetic acid occurring naturally in foods are 700 to 1,200 mg/kg in wines, up to 860 mg/kg in aged cheeses, and 2.8 mg/kg in fresh orange juice [10]. Acetic acid was first isolated by the distillation of vinegar, and was industrially used in textile industries such as cellulose acetate (for the production of films and textiles). Acetic acid is also used in the preparation of pharmaceuticals such as aspirin [11].

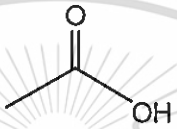

Figure 2.1 Molecular structure of acetic acid

2.1.2 Heptanoic acid

Heptanoic acid (Figure 2.2), also called enanthic acid, is the acid with seven carbon atoms. It is the oily liquid with unpleasant, rancid odor. It contributes to the odor of some rancid oils. Heptanoic acid is slightly soluble in water, but very soluble in ethanol and ether, and has been naturally found in oily seed [12]. Alternatively, heptanoic acid can be derived from the methyl ester of ricinoleic acid (which is a constituent of caster bean oil) from a process comprising of hydrolyzation and oxidation [13]. The bio-transformation of ricinoleic acid has also been studied by a multi-step enzymatic activation [14]. Heptanoic has been employed as a model chemical in the ketonization study over oxides of Mn, Ce and Zr depositing on supports such as alumina, silica or titania [15]. It has been used as a building block for the synthesis of an industrial lubricant, flavor, fragrance for cosmetics, and cigarette additive. Additionally, the salts of heptanoic acid (i.e., heptanoates) are a corrosion inhibitor, and are a representative precursor for drugs such as esterify steroid [16].

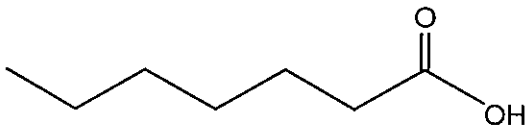

Figure 2.2 Molecular structure of heptanoic acid

2.2 Chemical reaction of fatty acids

2.2.1 Reaction associated with double bonds of fatty acid

2.2.1.1 Hydrogenation

Hydrogenation of fatty acid is the addition of molecular hydrogen to eliminate a double bond, thereby saturating the acids (Figure 2.3). As full hydrogenation produced exclusively saturated fatty acids which are too waxy to be used in food production, the partial hydrogenation is preferable. The hydrogenation process has a side reaction, such as the double bond isomerization at about 180 to 270 °C. The widely-used catalyst is nickel supported on inert material [17]. The hydrogenation of fatty acids finds some use in the production of magarine. In other applications, however, it is more useful to limit the hydrogenation, thereby retaining the unsaturation of the fatty acids. For example, olefins have high heating value than alkanes when used as fuels. Also, olefins are essential chemicals in the synthesis of polymers [18].

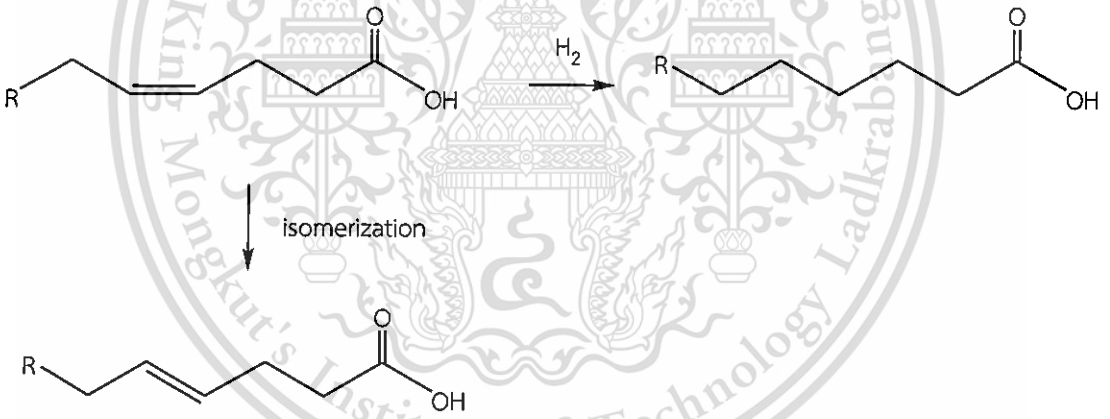

Figure 2.3 Direct hydrogenation of unsaturated fatty acid and the side reaction.

2.2.2 Reaction of carboxyl group of fatty acids

2.2.2.1 Esterification

Esterification refers to the conversion of acids (RCOOH) into esters (RCOOR) as shown in Figure 2.4 and 2.5. The esters can be used as alternative fuels, i.e., the biodiesel from the transesterfication of triglycerides with alcohols [19]. Fatty acid methyl esters (also known as FAMEs) are generally referred to as the first generation of the biodiesel [20]. Some physical characteristics of the methyl esters of fatty acids are shown in Table 2.1.

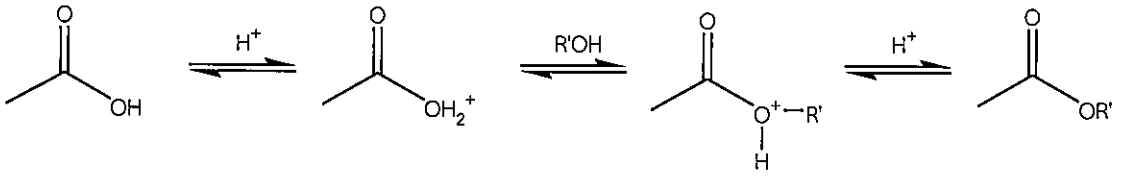

Figure 2.4 Acid-catalyzed esterification [Adapted from 21]

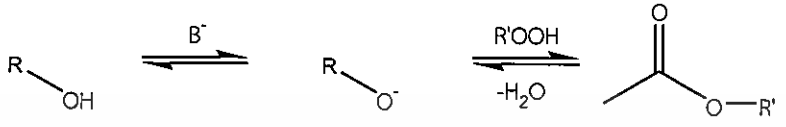

Figure 2.5 Base-catalyzed esterification [Adapted from 22]. The letter B stands for the basic site.

The reaction is catalyzed either by acid catalysts such as H-ZSM5 and amberlyst, or basic catalysts such as aqueous NaOH or MgO [23]. However, the use of homogeneous basic catalysts generates a large amount of liquid waste. On the other hand, the use of some heterogeneous basic catalysts gives rise to the saponification of the acids, thereby producing soap. Saponification is due to the presence of a high amount of free fatty acid (FFA) in large excess. Therefore, alternative catalysts with high reactivity but limited production of the undesirable soap are sought [24].

2.2.2.2 Ketonization

Ketonization is a bimolecular reaction where organic acids couple together forming a ketone as shown in Figure 2.6. The reaction enthalpy for the conversion of acetic acid to acetone of 4.4 kcal/ (mol of acetic acid) has been reported. Such transformation is catalyzed by several oxides such as $BaCO_3$, MgO, ThO_2, UO_2, CdO, ZnO, NiO, Bi_2O_3, and SnO_2 catalysts. Several ketonization mechanisms have been proposed [25]:

(i) An acid anhydride intermediate loses CO_2 to produce ketone. This mechanism is used to explain the production of cyclic ketones from dicarboxylic acids.

(ii) A beta-keto acid intermediate formed from two monodentate carboxylates via α-hydrogen abstraction.

(iii) A concerted mechanism involving two monodentate carboxylates. It has been claimed that this mechanism is restricted to ketonization of aromatic acids only.

(iv) An intermediate formed from two adsorbed molecules of carboxylic acid. Isotopic labeling studies showed that molecular acetic acid adsorbed on the surface is not directly involved in ketonization.

(v) A ketene intermediate that reacts with a carboxylate to produce ketone.

(vi) A bimolecular coupling of two carboxylates bound to the same cation.

Figure 2.6 Decarboxylative ketonization of acetic acid to acetone

2.2.2.3 Deoxygenation

Deoxygenation is a chemical reaction that removes oxygen atoms from starting molecules. Deoxygenation can be divided into decarboxylation (figure 2.7a) and decarbonylation (figure 2.7b). Decarboxylation yields CO_2, water and alkanes, whereas decarbonylation yields CO, water and alkenes. Therefore, the decarbonylation of fatty acid is capable of producing long chain olefins, given that hydrogen transfer/hydrogenation of the formed long chain olefins is limited. Both deoxygenation and decabonylation are thermodynamically favorable above 300 °C [26]. The decarboxylation of carboxylic acids to the corresponding hydrocarbons in the gas phase over heterogeneous metal catalysts has been known for many years [27]. It has been simply used in the production of liquid fuel from free fatty acid. The mechanism of deoxygenation of small organic acids over metal catalysts has been described based on the strength of the metal-oxygen bond [28]. Moreover, partially-reducible metal oxides such as SnO_2 and TiO_2 which produce oxygen vacancy sites have been reported as active catalysts in this reaction, usually in combination with noble metals [29].

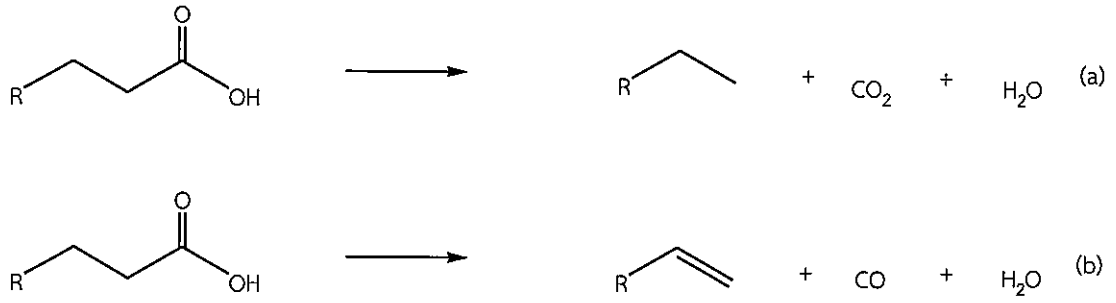

Figure 2.7 Hydrocarbon production from fatty acid via (a) decarboxylation, and (b) decarbonylation.

2.3 Long chain olefins

Olefins are hydrocarbons having one or more unsaturation. The smallest example is ethylene, which can be produced from the thermal cracking of naptha or natural gas [30]. Ethylene can be further oligomerized into long chain α-olefins, or reacts with another olefin to form longer chain olefins via metathesis by organometallic catalyst [31]. The term "linear α-olefins" are olefins that has a double bond at the terminal position, in contrast to internal olefins where the double bond is not at the terminal position [32]. Long chain olefins have been employed in various chemical industries, especially in a polymer field. Some examples on the use of long chain olefins are shown in Table 2.2.

Table 2.2 The use of long chain olefins in industrial application [33].

Long chain olefins in range of C_4-C_8	▪ Precursor in the production of linear aldehyde ▪ Manufacturing of linear alcohol for plasticizer ▪ Production of short chain carboxylic acid ▪ Synthesis of poly α-olefins used as synthetic lubricant ▪ Use as surfactant in a blend with the others long chain olefins
Long chain olefins in range of C_{10}-C_{14}	▪ Production of linear alkyl benzene surfactant ▪ Use as the drilling fluid base stock to replace diesel or kerosene
Long chain olefins in range of C_{16}-C_{18}	▪ Hydrophobes in oil-soluble surfactant ▪ Lubricating fluids ▪ Synthetic drilling fluids ▪ Production of maleic acid for paper sizing chemicals
Long chain olefins in range of C_{20}-C_{30}	▪ Chemical feedstock for heavy linear alkyl benzene ▪ Chemical feedstock for low molecular weight polymer

As long chain olefins are normally derived from petroleum, oil or natural gas, all of them are depleting, the production of long chain olefins by alternative, environmentally-friendly approach is being investigated [34, 35, 36, 37, 38 and 39]. Fatty acids which are abundantly found in various types of renewable feedstock are being considered as a promising candidate for the production of long chain olefins. This thesis will explore the use of TiO_2 (titania) and titanate-based materials as the catalyst for the transformation of fatty acids into long chain olefins. Some backgrounds of these materials are described below.

2.4 Titania (TiO_2)

TiO_2 is one of the most studied metal oxides for the deoxygenation of carboxylic acids [40]. An oxygen vacancy site is generally described as the active sites. Such a vacancy on the surface can be generated via UV-irradiation, annealing, calcination, particle bombardment, or the reaction of the solid with reducing gas such as hydrogen

[41]. The presence of an oxygen vacancy site might also induce the reduction of the metal atoms into a lower oxidation number, i.e., a Ti^{3+} defect in TiO_2.

The catalytic activity of TiO_2 is dependent on the nature and the composition of the surface defect sites [42]. Consider the formation of an oxygen vacancy and Ti^{3+} defects by the treatment of TiO_2 with H_2 gas as an example [43]. Initially, hydrogen gas was adsorbed on the surface of TiO_2 at high temperature. An electron from hydrogen atom was then transferred to the lattice oxygen of TiO_2. Secondly, the lattice oxygen reacts with hydrogen gas, forming water molecules. Water molecules desorbs form the surface, resulting in an oxygen vacancy site. Finally, the electron remaining there at the oxygen vacancy site could transfer to an adjacent Ti^{4+}, thereby forming the Ti^{3+} defect. Besides TiO_2, other metal oxides well known to contain an oxygen vacancy site include CeO_2 [44], which has also been studied in the deoxygenation and ketonization of various fatty acids [45].

The commonly found polymorphs of TiO_2 are those having anatase, rutile, and to a lesser extent brookite structure. The crystal structure of anatase and rutile is shown in Figure 2.8a and 2.8b respectively. Anatase is the most unstable TiO_2 crystal [46]. It crystallizes in the tetragonal system with TiO_6 octahedra linked via the edges, producing relatively dense structure. The rutile phase of TiO_2 is the high stability polymorph at all ranges of temperature. This phase crystallizes in a body-centered tetragonal unit cell [47]. The structure is built from infinite columns of edge sharing TiO_6 octahedra, where each edge-shared oxygen is corner-shared with an adjacent infinite chain.

The mixture of these two phases, known commercially as P25, has been widely studied and employed as catalysts. P25 is produced by the Aerosil process, involving flame hydrolysis where the titanium source was introduced into a burner with dry air and hydrogen gas [48]. The well-dispersed particles in combination with the presence of two phases with similar size [49] results in the synergistic effect boosting the catalytic activity in several reactions. The superior catalytic activity has also been attributed to a relatively high surface area [50] P25 TiO_2 has found numerous applications in photodegradation of pollutants [51], or as the starting material for the synthesis of other titanium-containing materials [52].

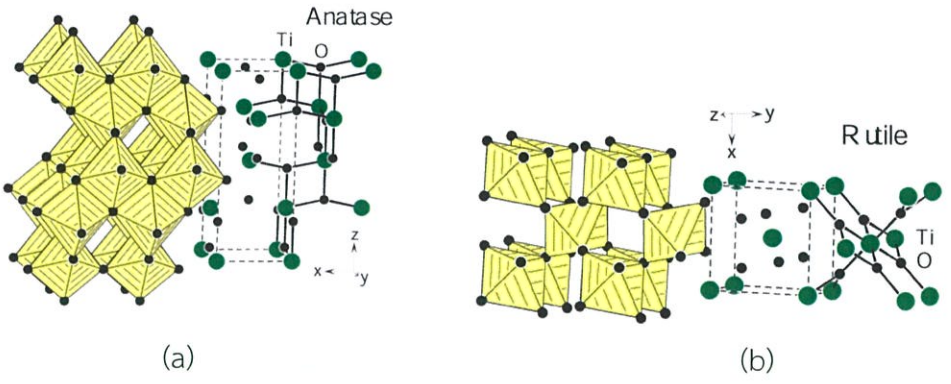

Figure 2.8 The crystal structure of (a) anatase and (b) rutile phase TiO_2 [53].

The activity of TiO_2 in the ketonization of acetic acid has been reported [54]. It is a relatively inexpensive and non-toxic solid. However, the presence of only Ti and O atoms limits the range of available crystal structure and the associated surface chemistry. It is interesting to investigate the formation of an oxygen vacancy on a solid consisting of titanium and oxygen possessing a more complex crystal structure, as will be described in Section 2.6.

2.5 Titanate-based materials

2.5.1 Alkali-titanate $A_2O{\cdot}nTiO_2$

Alkali-titanate of the general formula $A_2O{\cdot}nTiO_2$ can be considered as an oxide constructed from two components, the alkali metal part and the titanate part. The latter has a negative charge. Therefore, the suffix "-ate" to the name in contrast to titanium dioxide TiO_2 where the skeleton is neutral. In alkali-titanate, the rigid TiO_6 octahedra are linked together in different ways, depending on the number n. This thesis considers the case where n = 3 giving sodium trititanate $Na_2Ti_3O_7$, n = 4 giving potassium tetratitanate $K_2Ti_4O_9$, and n = 6 giving alkali hexatitanate $A_2Ti_6O_{13}$ (A = Li, Na and K). The n = 3 and 4 have a layered structure, whereas the n = 6 has the tunneled structure [55].

The structure of the $Na_2Ti_3O_7$ is shown in Figure 2. 9a. This material crystalizes in a monoclinic unit cell consisting of three edge-share TiO_6 units held together forming a layer (also called a ribbon). Each layer is linked with another layer via the edge, resulting in a "step 3 layer" structure. $K_2Ti_4O_9$ has similar structure, but having *four* TiO_6 linked together forming a layer, and one layer is linked with another layered via the corner. In this layered structure, the alkali metal cations reside at the

interlayer space, preserving charge neutrality [56]. This skeleton arrangement is also a basis for other titanate-based nanostructures such as nanowire [57], nanotube [58], nanoribbon [59], or for different morphologies including whiskers [60], spheres [61] and rods [62].

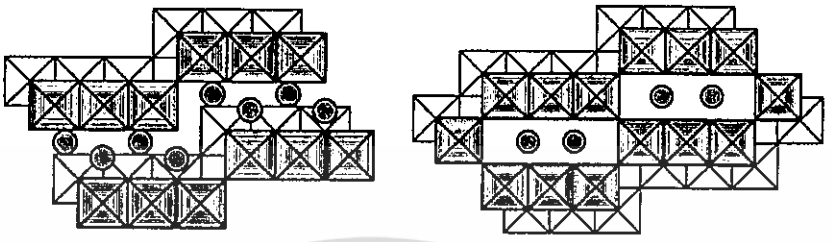

(a) (b)

Figure 2.9 Skeletal structure of (a) $Na_2Ti_3O_7$ and (b) $Na_2Ti_6O_{13}$. The dots represent alkali metal cations, and the squares the TiO_6 octahedral unit [6].

The structure of $A_2Ti_6O_{13}$ can be described based on the "step 3" layered structure, as shown in Figure 2.9b. One can consider that the 3-octahedra long ribbon in the trititanate migrates close to each other and condense at the edge [63]. As a result, the interlayer space is lost, and the structure now possesses the "tunnel" instead of the layer. The alkali metal cations A (A = Li, Na, and K) reside in the tunnel, although their exact locations and their geometry are dependent on the type of the cations. Both layered ($Na_2Ti_3O_7$, $K_2Ti_4O_9$) and tunneled titanates ($M_2Ti_6O_{13}$) are known to undergo ion exchange, therefore finding uses in Li-on battery [64], or in the treatment of radioactive cations [65]. They are also studied in the hydrogen production via the photocatalytic splitting of water [66].

2.5.2 Reducibility vs Basicity in Alkali Titanates

The active site for the ketonization of acids over TiO_2 is proposed to be an oxygen vacancy, as discussed previously in Section 2.2. Alkali titanates possess a crystal structure which is less dense than that of TiO_2. The spaces are inside the tunnel (for $A_2Ti_6O_{13}$). The more open structure might exhibit different reactivity toward the formation of an oxygen vacancy site, which has remained unexplored so far.

In addition to the oxygen vacancy site, there are also basic sites on the surface of TiO_2 and on titanates. Basicity in titania is well documented [67]. Generally, basic sites on the surface are described to the O^{2-} surface species having different

coordination numbers, depending on the location whether it be on the faces, edges, or terraces of the crystals. The O^{2-} moiety can be either originally existed, or is formed by the surface hydroxylation (via atmospheric moisture) and surface dehydroxylation (via calcination). The basic sites are known to be active for various kinds of reactions including deoxygenation [68] and aldol condensation [69]. Aldol condensation exothermically generates a C-C bond from two starting molecules. It is essential in the removal of polynuclear bio-mass derived. In this thesis, it is necessary to quantitate the contribution of basic sites toward the deoxygenation activity, the latter is generally catalyzed by an oxygen vacancy site. The extent to which a basic site involves in the deoxygenation could be appreciated by studying the basic- catalyzed aldol condensation of acetone, in comparison to the oxygen-vacancy-catalyzed ketonization of acetone. Besides, the differences in the catalytic activity of an oxygen vacancy site and a basic site in catalysts with related yet different crystal structures may be anticipated. For example, alkali titanates $A_2O{\cdot}nTiO_2$ with different n might be able to donate/accept electrons to a different extent. This issue will also be addressed in this work.

2.6 Literature reviews

Glinski *et al.* [70] have conducted experiments screening 32 metal oxides depositing on surface inorganic support, regarding their catalytic activity in catalytic ketonization of propanoic acid. The metal oxides were divided into three groups according to the reactivity. The most effective ones are the oxides of Mn, Zr, Ce, Th and U. It has been suggested that their reducibility promotes the catalytic ketonization.

Eduardo *et al.* [71] has studied the use of Ni-Al layered double hydroxide as a catalyst for the conversion of fatty acids and triglycerides to fuel-like hydrocarbons. It was found that the catalytic activity depended on hydrogen partial pressure, and the specific surface area of the catalysts. The formation of strong basic site during the regeneration step favored the deoxygenation.

Chaline *et al.* [72] studied the deoxygenation of soybean oil over palladium metal supported on clays. The testing was performed in batch mode using Pd metal supported on pillared Brazillian Montmorillonite as a catalyst, at 30 bar of hydrogen. A 74.5% conversion of soybean oil was obtained at the reaction time of 6 h. The selectivity to n-alkane and iso-alkane was about 69 and 29% respectively.

Jae *et al.* [73] investigated the use of ceria-based catalysts for the deoxygenation of oleic acid. It was found that $Ce_{0.6}Zr_{0.4}O_2$ exhibited the highest oleic acid conversion and high selectivity to C9-C17 hydrocarbons at the reaction temperature of 300 °C. The high activity/selectivity of $Ce_{0.6}Zr_{0.4}O_2$ catalyst was correlated to its reducibility, oxygen storage capacity, and crystallite size.

The production of long chain, linear olefins from the decarboxylation of palmitic acid has been recently reported by Dararat *et al.* [74] over ceria-based catalysts. The effect of surface oxygen vacancy site on the catalytic activity and the product selectivity have been demonstrated. C31 ketone can be generated from the keteonization of palmitic acid (C16 acid). Additionally, these catalysts can reduce palmitic acid over the vacancy sites to C16 aldehyde. The latter subsequently underwent hydrogenation to saturated hydrocarbons.

The use of lepidocrocite titanate $K_{0.8}Zn_{0.4}Ti_{1.6}O_4$ as a catalyst for the deoxygenation of palmitic acid has been recently reported by Limsakul *et al.* [75]. It was proposed that palmitic acid can be deoxygenated into C13-C17 hydrocarbons over the basic sites, very likely via the ketonization of the acids into C31 ketone. However, neither the basicity nor reducibility of the catalyst has been reported.

The reducibility of TiO_2 and the generation of an oxygen vacancy site or Ti^{3+} defect is well documented. Tu *et al.* [76] has reported the reaction kinetics and mechanisms in the ketonization of aliphatic carboxylic acids over Ru/TiO_2 catalyst. While Ru itself is inactive for the ketonization of carboxylic acids, it reinforces the reduction of titanium(IV) oxide to Ti^{3+} species which provides the active site. A bimolecular reaction between carboxylic acids (adsorbed in a bidentate-bridging mode) which proceeds through the beta-ketoacid intermediate is proposed.

There are a few works on the reducibility and the formation of an oxygen vacancy sites in layered/tunneled titantes besides those on the more frequently found anatase or rutile TiO_2. Jinmeng *et al.* [77] reported that $Pt/K_2Ti_6O_{13}$ nanowire can be easily reduced, owing to the strong metal support interaction (SMSI) which increase the coverage by H_2 spillover. However, the reducibility of $K_2Ti_6O_{13}$ without Pt has not been mentioned.

Szilvia *et al.* [6] has investigated the thermal stability of $Na_2Ti_3O_7$ and $Na_2Ti_6O_{13}$. The tunneled titanate $Na_2Ti_6O_{13}$ has a higher thermal stability, compared to the layered titanate $Na_2Ti_3O_7$. It was found that $Na_2Ti_3O_7$ transformed into $Na_2Ti_6O_{13}$ at above 600 °C.

Jing *et al.* [78] has studied the low temperature synthesis of $K_2Ti_6O_{13}$. The use of KNO_3 (instead of the more commonly used K_2CO_3) and the active P25 TiO_2 (instead of anatase TiO_2) is effective in lowering the synthesis temperature. Moreover, the room temperature photoluminescence was observed and gave a supporting evidence on the presence of an oxygen vacancy sites (or other crystal defects) in this material.

CHAPTER 3

Experimental

3.1 Reagents

Details on the reagents used in this thesis are summarized in Table 3.1.

Table 3.1 A list of reagents

Chemical	Grade of purity	Manufacturer
Acetone	≥ 99.80 %	CARLO ERBA
Acetic acid	99.70 %	J.T. Baker
Heptanoic acid	99.50 %	ALDRICH
p-Xylene	≥ 99.00 %	CARLO ERBA
P25 titanium dioxide	≥ 99.50 %	Aerosil
Anatase titanium dioxide	≥ 99.80 %	CARLO ERBA
Potassium nitrate	≥ 99.50 %	CARLO ERBA
Sodium carbonate anhydrous	≥ 99.70 %	CARLO ERBA
Lithium nitrate	≥ 98.00 %	Labochemie
Cobalt(II) nitrate hexahydrate	≥ 99.80 %	Rankem
Sodium metatitanate $Na_2Ti_3O_7$	99.00 %	ALDRICH
Carbon dioxide gas	99.99 %	PRAXAIR
Air zero gas	99.99 %	PRAXAIR
Nitrogen gas	99.99 %	PRAXAIR
Hydrogen gas	99.99 %	PRAXAIR
Hydrogen in Argon gas	10 %	PRAXAIR
Helium gas	99.99 %	PRAXAIR

3.2 Apparatuses

1. Alumina crucible
2. Agate mortar
3. Glass bead
4. Glass wool
5. Glass tube
6. Glass syringe, SGE Analytical Science
7. GC needle, SGE Analytical Science

8. Graduate pipette and red bulb
9. Hot air oven, UM500, Memmert
10. Mass flow controller, GFC-1105, Dwyer
11. Mass flow controller, GFC17, AALBORG
12. Box furnace, Controller P 320, Nabertherm
13. Laboratory glassware
14. Protector laboratory hood, Science Technology
15. Quartz wool
16. Quartz tube
17. Syringe pump, KDS-100, KD-scientific
18. Tube furnace, VCTF4, Vecstar
19. Powder X-ray diffractometer, a DMAX2200 Ultima+, Rigaku
20. Surface area and pore size analyzer, Autosorb-1, Quantachrome
21. Thermogravimetric analyzer, Pyris, Perkin Elmer
22. Scanning electron microscope, EVO®MA10, ZEISS
23. X-ray photoelectron spectrophotometer, AXIS ULTRA, KRATOS ANALYTICAL
24. Wavelength dispersive X-ray fluorescence spectrophotometer, Bruker, Tiger
25. Raman spectrophotometer, DXR Smart Raman, Thermoscientific
26. Thermal conductivity detector, TCD2-c, Valco Instrument
27. Gas chromatography, Varian 3800
28. Gas chromatography, Hewlett Packard 6890

3.3 Preparation and characterization of catalysts

3.3.1 Synthesis of titanate-based catalysts

Prior to the synthesis, alkali metal carbonates/nitrates were dried at least overnight at 120 °C prior to use. Other chemicals were used as received.

The $Na_2Ti_6O_{13}$, $K_2Ti_6O_{13}$ and $K_2Ti_4O_9$ catalysts were synthesized via a conventional solid-state synthesis. For $Na_2Ti_6O_{13}$ [79], a stoichiometric amount of Na_2CO_3 was mixed with anatase TiO_2. The mixture was ground manually in a mortar for 20 min, followed by a calcination in a muffle furnace at 800 °C for 20 h. The synthesis of $K_2Ti_4O_9$ [80] can be done similarly, but replacing Na_2CO_3 by K_2CO_3. For

$K_2Ti_6O_{13}$ [81], a stoichiometric mixture of KNO_3 and P25-TiO_2 was used, followed by a calcination at 700 °C for 10 h. $Li_2Ti_6O_{13}$ was synthesized by the ion-exchange of $Na_2Ti_6O_{13}$ with $LiNO_3$ molten salt. $Na_2Ti_6O_{13}$ and $LiNO_3$ (100% excess) was mixed and consecutively grinded in an agate mortar for 20 min and pelletized, followed by a calcination at 350 °C for 7 days at heating rate 10 °C/min and washing with Deionized water [82]. All samples were naturally cooled down to room temperature after the heating was completed. The sodium trititanate $Na_2Ti_3O_7$ is a commercial product of Aldrich. All samples were kept in a desiccator.

3.3.2 Preparation of 1% Co/$K_2Ti_6O_{13}$

An amount of 0.0163 g of $Co(NO_3)_2 \cdot 6H_2O$ was dissolved in 20 mL deionized water to make a solution with a concentration of 0.8 mol·L^{-1}. $K_2Ti_6O_{13}$ (5 g) which acts as the support was impregnated by this solution of Co^{2+} (20 mL) via a sprayed-impregnation method. The amount of Co corresponds to a 1% by weight loading of cobalt on $K_2Ti_6O_{13}$. After that, the wet solid was isothermally heated at 60 °C overnight. The dried solid was subsequently calcined at 450 °C for 10 h with the heating rate of 5 °C/min in a tube furnace at atmospheric pressure.

3.3.3 Powder X-ray diffraction

The data on phase identification, including the determination of unit cell parameters and the crystallite size can be obtained by Powder X-ray diffraction (PXRD). The PXRD patterns were recorded on a DMAX2200 Ultima+ (Rigaku) diffractometer using CuKα radiation. The 2¤ covered was 5-100° with a scan step of 5° min^{-1}.

3.3.4 Chemical analysis

The chemical composition of a catalyst was analyzed by a wavelength-dispersive X- ray fluorescence spectrophotometer (WD- XRF) , Bruker, Tiger. Approximately 0.5 g of a catalyst was mixed with 4.5 g of boric acid. The mixture was then manually grinded, and was compressed into a pellet. The data was recorded by CuKα x-ray source and quantitative calculated by Theoretical formulas, "fundamental parameter calculations".

3.3.5 Surface area measurement and pore size distribution

Specific surface area of a catalyst was measured on an Autosorb- 1 (Quantachrome). Each sample (weighed approximately 0.1 g) was degassed at 300 °C for 12 hours prior to analysis. After that, nitrogen gas was adsorbed on the surface of the sample at -60 °C. The adsorbate pressure was fixed at 1 torr, the equilibration time at each point at 3 min, the scaled tolerances were set at zero. The surface area was analyzed employing BET equation [89]. The BJH pore size distribution was next calculated [90].

3.3.6 Thermal stability

The thermal stability of a catalyst was measured by a thermogravimetric analyzer (Pyris). The sample was manually grinded in a mortar to homogeneous fine particles. Then, approximately 10 mg was put into a platinum pan. The measurement was conducted in 20 mL/min of nitrogen atmosphere, from 30 to 900 °C with heating rate of 5 °C/min. The mass of the sample as the function of temperature was recorded by the instrument.

3.3.7 Morphology

The catalyst powder was dispersed in acetone by ultrasonication. A small amount of the suspended powder in the liquid was dropped on a glass slide. Afterward, the stub with carbon tape was pressed on those dispersed particles which have been previously deposited on a glass slide. The powder on the stub was coated with Au by ion-sputtering before being imaged by an electron microscope (SEM, ZEISS) at the magnification of 20,000 and 60,000×.

3.3.8 Temperature-programmed reduction

The amount/strength of oxygen vacancy sites can be determined by a temperature-programmed reduction by H_2 gas (H_2-TPR). The measurement was performed in a quartz tube connected with a thermal conductivity detector (VICI). Prior to an analysis, the sample (0.1 g approximately) was activated in air (flow rate of 30 mL min^{-1}) from room temperature to 500 °C at a heating rate 10 °C min^{-1}, followed by an isothermal treatment at 500 °C for 2 h. Subsequently, the system was naturally cooled down in the atmosphere of nitrogen gas (flow rate of 30 mL min^{-1}) to room

temperature. Then, the temperature reduction profile was recorded using 10% H_2 in Ar at the heating rate 5 °C min^{-1}, from 50 to 900 °C. The TCD signal was calibrated employing a known mass of CuO as a standard, considering that CuO is reduced stoichiometrically and completely to Cu and H_2O. The reduction profile of CuO and the calculation of the hydrogen consumption can be found in Appendix A. The amount of oxygen vacancy sites is expressed as mmol of H_2 consumed per mass of a catalyst (mmol H_2/g).

3.3.9 Temperature-programmed desorption of CO_2

The basic functionality of a catalyst can be quantified with temperature-programmed desorption of CO_2 (CO_2 TPD). Approximately 0.2 g of the sample was activated inside a reactor by a procedure similar to that described in Section 3.3.9. The CO_2 adsorption was conducted at room temperature for a total of 60 min. After that, excess CO_2 was flushed away from the surface by helium gas (flow rate 30 mL/h) for an hour. The desorption profile was recorded from the temperature of 30 to 600 °C, with a heating rate 5 °C min^{-1}. The TCD signal was calibrated employing a known mass of MgO as a standard. The CO_2 desorption profile from MgO and the calculation of basicity can be found in Appendix A. The basicity is expressed as mmol of CO_2 desorbed per mass of a catalyst (mmol CO_2/g).

3.3.10 X-ray photoelectron spectroscopy

The sample was pelletized and pressed onto a stub with a carbon tape. The measurement was done by an X-ray photoelectron spectrophotometer, AXIS ULTRA, KRATOS ANALYTICAL with monochromatic Al X-ray. The sample was placed in a chamber, and the internal pressure was decreased down to 1×10^{-8} torr. After that, the temperature inside the chamber was naturally increased to 500°C which is the reduction temperature obtained from TPR measurement (Section 3.3.9). H_2 gas (1 bar) was fed into the chamber for 2 h, followed by the collection of the spectrum for qualitative analysis. Next, the sample was naturally cooled down inside the chamber to below 100°C, and the quantitative spectrum was collected. The correction of the background due to a carbon substrate was also performed.

3.4 Catalytic activity testing

At the first step, the ketonization was carried out in a fixed-bed flow reactor operated at atmospheric pressure. A solution of model chemical, 90% vol/vol acetic acid in *p*-xylene, was fed to the reactor by a 10-mL syringe connected to a syringe-pump (KD Scientific). The contact time (W/F) was set constant at 15 g·h mol^{-1}. Prior to the testing, the samples were activated from room temperature to 500 °C (heating rate 10 °C min^{-1}) followed by an isothermal period at 500 °C for 2 h under air (flow rate of 40 mL min^{-1}). After that, the reduction by H_2 (flow rate of 30 mL min^{-1}) was performed at a selected temperature (400, 450, 500 and 600 °C) for a total of 2 h. Acetic acid was then fed to the reactor and the reaction began. The liquid products were collected by a water-ice trap (at 10-15 °C approximately) every 60 min for a total time on stream (TOS) of 360 min. The liquid products were quantitatively analyzed by a gas chromatograph (Varians 3800) equipped with a DB-wax column (30m×0.53 mm) and a flame ionization detector (FID). *p*-Xylene was employed as an internal standard.

For aldol condensation, the catalytic testing was performed similarly. The commercial MgO was used as a reference catalyst. As the products from this reaction have lower boiling point than those from ketonization, the liquid nitrogen trap was employed.

The deoxygenation of heptanoic acid (10%vol/vol in *p*-xylene) was performed by the procedure similar to the ketonization of acetic acid. The exception is that the W/F was varied in the range 100-250 g·h mol^{-1}. The liquid products were analyzed on an HP gas chromatograph (HP) equipped with a DB-1 column (30m×0.32 mm).

The catalytic system for those three systems was schematically shown in Figure 3.0.

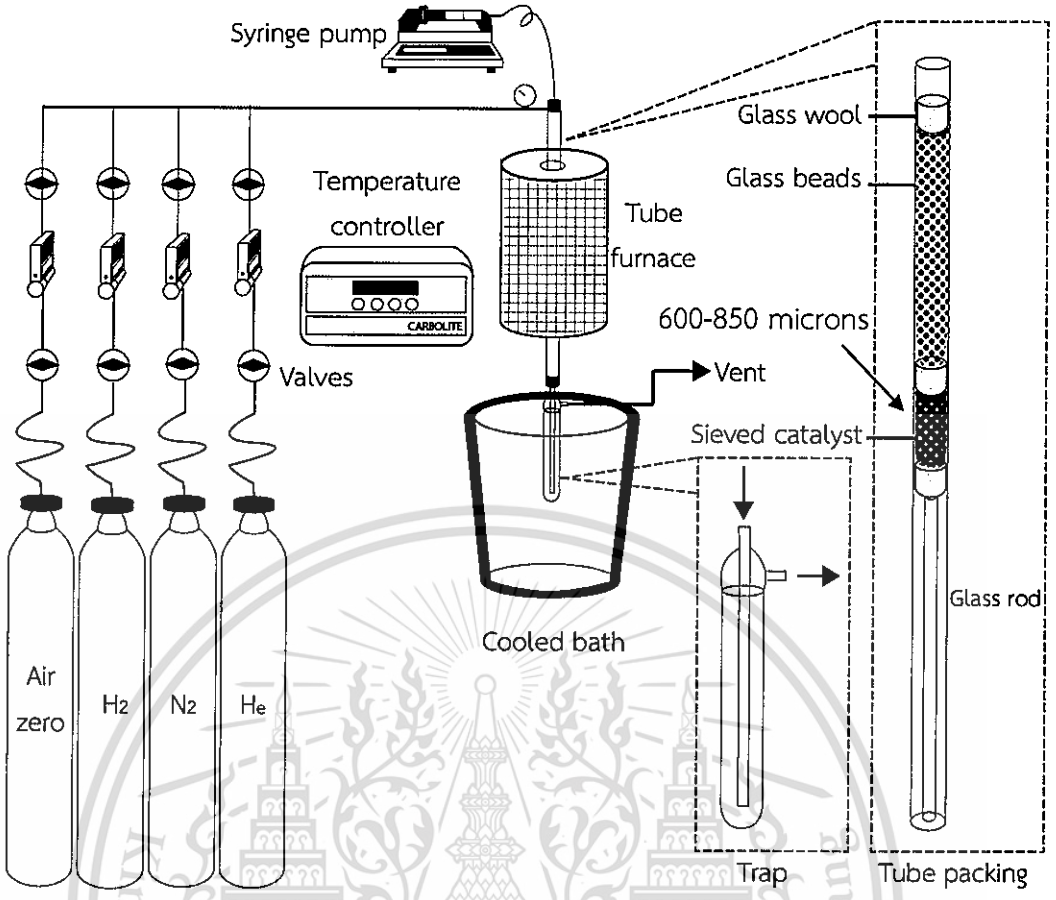

Figure 3.1 Schematic diagram of the catalytic testing rig

CHAPTER 4

Results and Discussions

4.1 Characterization of catalysts

4.1.1 Powder X-ray diffraction pattern, PXRD

All synthesized materials are white opaque powders. The PXRD patterns were recorded and the phase of each product confirmed by the comparison with JCPDS databases and/or the literatures. XRD spectra of alkali all hexatitanates are shown in Figure 4.1.

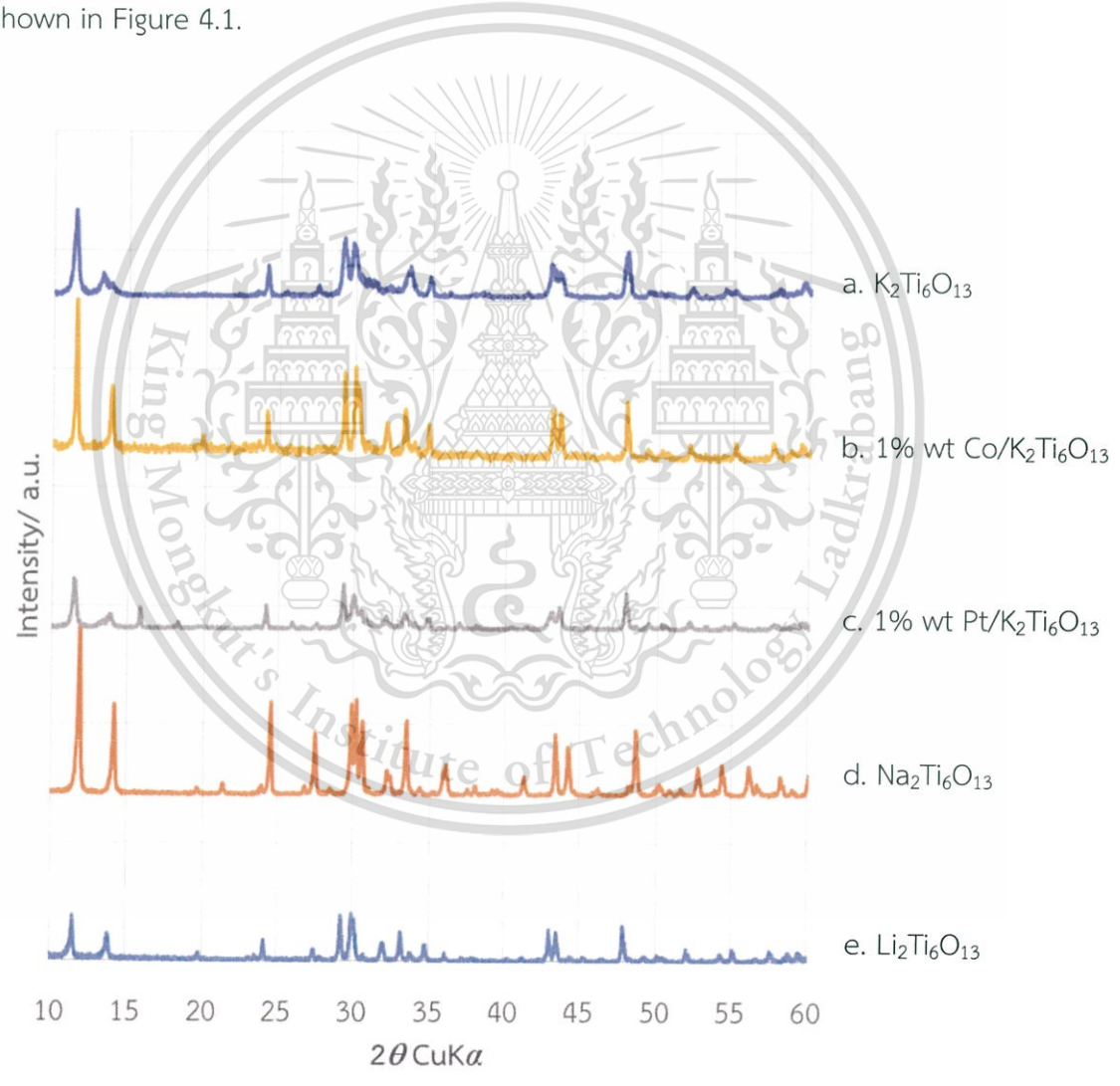

Figure 4.1 X-ray diffraction pattern of a) $K_2Ti_6O_{13}$, b) 1% wt $Co/K_2Ti_6O_{13}$, c) 1% wt $Pt/K_2Ti_6O_{13}$, d) $Na_2Ti_6O_{13}$ and e) $Li_2Ti_6O_{13}$

Taking potassium hexatitanate ($K_2Ti_6O_{13}$, Figure 4.1a) as an example, the strongest peak is at 2θ = 11.899, or d = 0.7431 nm, in agreement with the literature [6]. This peak is the reflection from the (*200*) plane, equivalent to the shortest distance between the tunnels (Figure 2.3). There is no crystalline impurity phase found. Sodium hexatitanate ($Na_2Ti_6O_{13}$) can be similarly synthesized, Figure 4.1d. The higher peak intensity of the sodium-form indicates its higher crystallinity compared to the K-form, likely due to the use of higher temperature in the synthesis (i.e., 800 °C for $Na_2Ti_6O_{13}$ *vs* 700 °C for $K_2Ti_6O_{13}$). The strongest peak for $Na_2Ti_6O_{13}$ is at 2θ = 11.460, or d = 0.7715 nm, in agreement with the literature [83]. Because the large size K^+ will require more space at the tunnel than the small size Na^+, the (*200*) spacing increases in this order.

Similarly, $Li_2Ti_6O_{13}$ can be synthesized from the ion exchange of $Na_2Ti_6O_{13}$ with molten $LiNO_3$. The (*200*) plane of $Li_2Ti_6O_{13}$ was slightly shifted to lower angle (2θ = 11.412, or d = 0.7702 nm, Figure 4.1e), indicating the expansion of the distance between the tunnel despite the smaller ionic radius of Li^+ compared to Na^+. However, this finding is in agreement with the literature [84], and can be explained considering the different exact positions of Li^+ *vs* Na^+. The accommodation of small Li^+ results in the repulsion between three edge-shared, which subsequently results in the distortion of the framework and the relatively larger unit cell. The crystallinity of $Li_2Ti_6O_{13}$ was, however, lower than the precursor ($Na_2Ti_6O_{13}$). The crystallite site was determined by applying the Scherrer equation to the (*200*) peak. The values obtained are 27.46 nm for $K_2Ti_6O_{13}$ and 38.22 nm for $Na_2Ti_6O_{13}$. This finding is in agreement with a general expectation that smaller crystallites are obtained at lower reaction temperature and vice versa.

XRD of 1% Co and Pt/$K_2Ti_6O_{13}$ (Figure 4.1b and 4.1c) show the base diffraction of $K_2Ti_6O_{13}$ as the same metal-free support. The Co impregnated sample has the small diffraction peak of Co_3O_4 at 2θ = 36.978 and 65.488 while the Pt one does not show any diffraction of Pt species. The disappearance of this peak does not mean no platinum, but in a small particle (e.g. higher dispersion of Pt). The crystallite size of the supports of metal-loaded catalysts from the (*200*) peak are not changed significantly (49.00 and 31.02 nm for 1% wt Co and 1% wt Pt/$K_2Ti_6O_{13}$ respectively).

The PXRD patterns of $Na_2Ti_3O_7$ and $K_2Ti_4O_9$ are also shown in Figure 4.2b and 4.2e respectively.

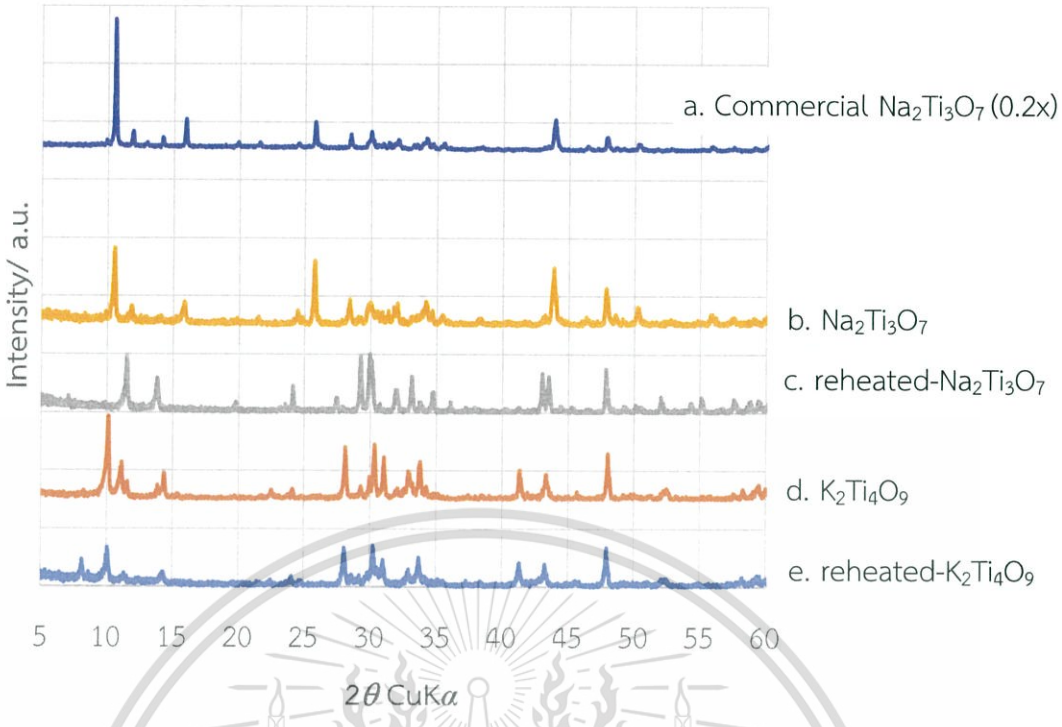

Figure 4.2 X-ray diffraction pattern of a) Commercial $Na_2Ti_3O_7$, b) $Na_2Ti_3O_7$, c) reheated-$Na_2Ti_3O_7$, d) $K_2Ti_4O_9$ and e) reheated-$K_2Ti_4O_9$; label reheated catalysts mean the catalysts were reheated at 800 °C

The majority of the peaks match well with the reference [85]. The strongest peak for $Na_2Ti_3O_7$ ($K_2Ti_4O_9$) is at 2θ = 10.05° (10.53°), representing the repeating distance of 0.8402 nm (0.7926 nm) along the *a*-direction of the monoclinic symmetry. The unit cell parameters of $Na_2Ti_3O_7$ and $K_2Ti_4O_9$ shown in Table 4.1 are also in reasonable agreement with those in the literature. The crystallite size of $Na_2Ti_3O_7$ and $K_2Ti_4O_9$ are found to be 43.11 and 41.03 nm respectively from the use of Scherrer equation of the (*200*) peak. However, in these two samples, there are impurity peaks as also marked in Figure 4.2. The impurity phase was assigned to the respective alkali hexatitanate. The attempt to obtain a single phase $K_2Ti_4O_9$ and $Na_2Ti_3O_7$ by re-calcining at 800 °C 10 h was unsuccessful. The PXRD patterns of the reheated $Na_2Ti_3O_7$ and reheated $K_2Ti_4O_9$ (Figure 4.2d and 4.2f respectively) show that the diffraction peaks of the respective alkali hexatitanate grow in intensity at the expense of the parental phase. This finding supports the low thermal stability of the layered titanates, in agreement with the previous report [6]. The peaks corresponding to the impurity phase(s) are also found in the commercially available $Na_2Ti_3O_7$ as shown in Figure 4.2a. From Scherrer equation of (*200*) peak, the crystallite size of the commercial $Na_2Ti_3O_7$ is 73.02 nm.

Table 4.1 Unit cell parameter of the metal titanates prepared in this work.

Sample	*a* (nm)	*b* (nm)	*c* (nm)	*β* (°)
$Na_2Ti_6O_{13}$	1.511(3)	0.3744(4)	0.9138(4)	99.109
$K_2Ti_6O_{13}$	1.54(2)	0.378(3)	0.920(3)	99.894
$Li_2Ti_6O_{13}$	1.562(3)	0.379(3)	0.910(3)	99.893
Commercial $Na_2Ti_3O_7$	0.858(3)	0.3805(4)	0.912(3)	101.339
$Na_2Ti_3O_7$	0.8563(4)	0.3803(4)	0.9107(4)	101.285
$K_2Ti_4O_9$	1.274(3)	0.3820(4)	0.889(3)	104.023

The lattice parameters *a*, *b*, c and *β* of the alkali hexatitanate can be obtained following the indexing in the literature. These values are shown in Table 4.1. The *b*- and *c*-parameter are very close for the three phases, suggesting that the in-plane structure (along the *bc* plane) is similar. The change in the *a*-parameter has been discussed previously in relation to the position of the (*200*) peak.

4.1.2 Elemental analysis

The chemical compositions of some catalysts were determined by XRF.

Table 4.2 Elemental composition of titanate catalysts

Samples	Theoretical composition (% wt)				Experimental composition (% wt)			
	Pt	Co	A_2O*	TiO_2	Pt	Co	A_2O*	TiO_2
$Na_2Ti_6O_{13}$	-	-	11.43	88.57	-	-	10.20	88.00
$K_2Ti_6O_{13}$	-	-	16.42	83.59	-	-	14.00	86.00
$Li_2Ti_6O_{13}$	-	-	5.28	94.13	-	-	4.85	95.15
1.0% wt Co/$K_2Ti_6O_{13}$	-	1.00	16.26	82.70	-	1.15	16.70	81.00
0.1% wt Pt/$K_2Ti_6O_{13}$	0.10	-	16.40	83.51	0.11	-	13.98	85.91
0.5% wt Pt/$K_2Ti_6O_{13}$	0.50	-	16.34	83.08	0.41	-	13.94	85.65
1.0% wt Pt/$K_2Ti_6O_{13}$	1.00	-	16.26	82.70	0.80	-	13.89	87.30

* A_2O refers to the oxide of the alkali metal, K_2O (for $K_2Ti_6O_{13}$), Na_2O (for $Na_2Ti_6O_{13}$) and Li_2O (for $Li_2Ti_6O_{13}$). The content of Li_2O is deduced from the difference in the Na_2O content before and after the molten ion exchange. The decrease in Na_2O content is assumed as the amount of Li_2O.

Results are in agreement with the theoretical composition. From molten Li-salt exchange of $Na_2Ti_6O_{13}$, the results reveal the 100% successful $Li_2Ti_6O_{13}$. The content of Co which is impregnated to $K_2Ti_6O_{13}$ is also in agreement with the expected loading.

4.1.3 Surface area and textural properties

The specific surface areas for each catalyst are presented in Table 4.3.

Table 4.3 Surface area of the catalysts

Samples	S_{BET} (m^2/g)
Anatase TiO_2	6
$Na_2Ti_6O_{13}$	9
$K_2Ti_6O_{13}$	21
$Li_2Ti_6O_{13}$	16
$Na_2Ti_3O_7$	5
Commercial $Na_2Ti_3O_7$	3
$K_2Ti_4O_9$	6
1.0% wt Co/$K_2Ti_6O_{13}$	16
0.1% wt Pt/$K_2Ti_6O_{13}$	7
0.5% wt Pt/$K_2Ti_6O_{13}$	20
1.0% wt Pt/$K_2Ti_6O_{13}$	19

The surface area is in the range 3-21 m^2/g. Such low values indicate that only the external surface area of the particles contributes to the N_2 adsorption. That is, the materials are essentially dense and non-porous. Some minor adsorption indeed occurred at the inter-particle voids resulting in the secondary porosity. So, the respective pore size distributions are not reported here as they do not reflect the true nature of the catalysts. (The N_2 adsorption-desorption isotherm for all catalysts can be found in Appendix E.)

The higher specific surface area of $K_2Ti_6O_{13}$ compared to that of $Na_2Ti_6O_{13}$ and $Li_2Ti_6O_{13}$ is as expected, considering the lower crystallinity and smaller crystallite size in the former, as deduced from XRD measurement. $Na_2Ti_3O_7$ and $K_2Ti_4O_9$ has a similar specific surface area. Commercial and prepared $Na_2Ti_3O_7$ show a very close specific surface area as well.

SEM images of all catalysts are shown in Figure 4.3.

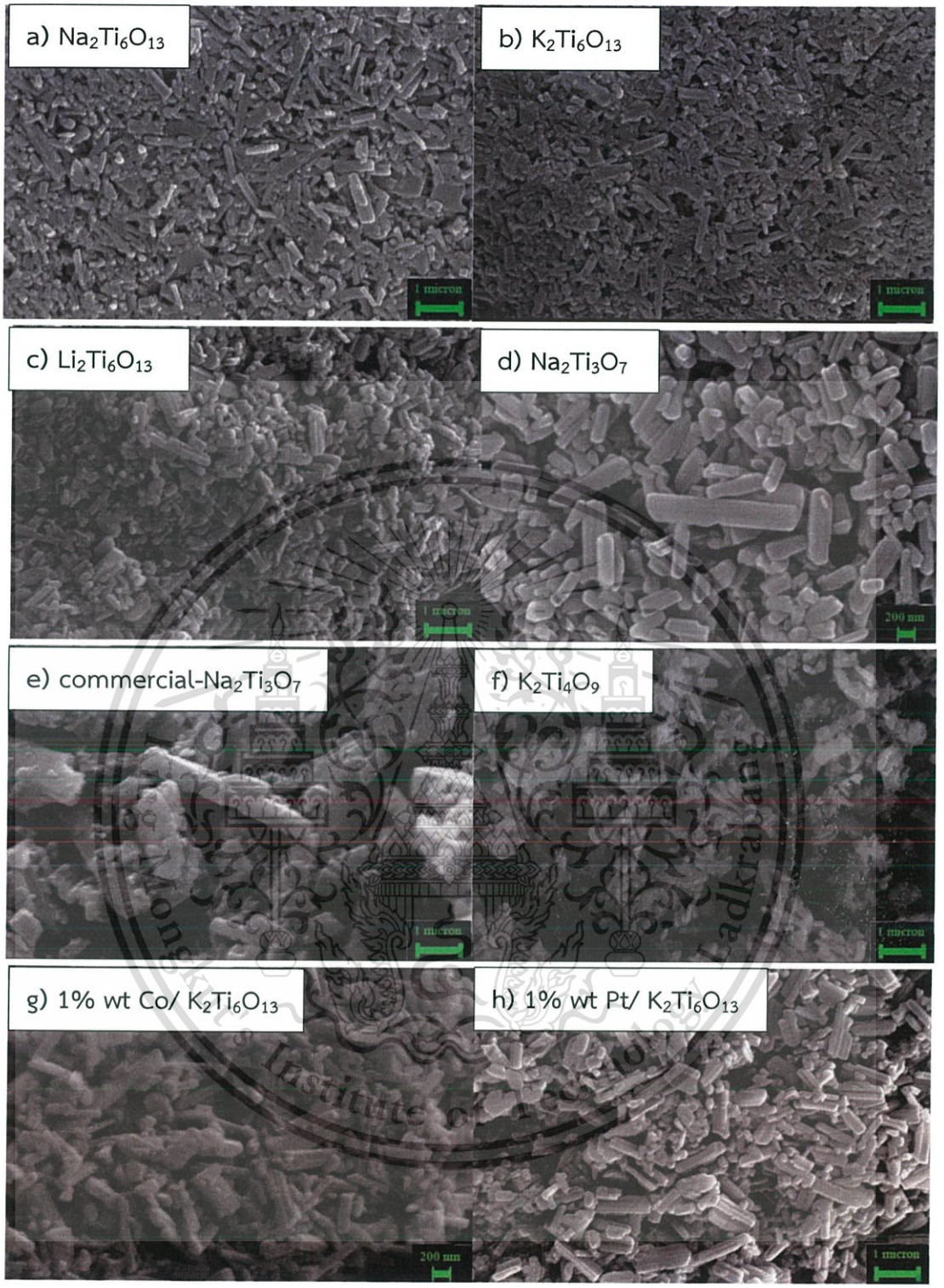

Figure 4. 3 SEM images of a) $Na_2Ti_6O_{13}$, b) $K_2Ti_6O_{13}$, c) $Li_2Ti_6O_{13}$, d) $Na_2Ti_3O_7$ e) commercial- $Na_2Ti_3O_7$, f) $K_2Ti_4O_9$, g) 1% wt Co/$K_2Ti_6O_{13}$ and h) 1% wt Pt/$K_2Ti_6O_{13}$. The scale bars represent the length 0.2 μm in (d) and (g), and 1 μm in others.

All bulk titanate samples are aggregates composed of rod-like particles. The length the rod is in the order: 0.18-01.73 μm ($Li_2Ti_6O_{13}$), 0.2-1.5 μm ($Na_2Ti_6O_{13}$) < 0.2 μm ($K_2Ti_6O_{13}$), 0.5-3.5 μm ($Na_2Ti_3O_7$) and 0.5-3.5 μm ($K_2Ti_4O_9$). However, commercial-$Na_2Ti_3O_7$ appears as the mixture of plates and rods with the size 0.73×1.73 μm and 2.85 μm. After metal loading onto $K_2Ti_6O_{13}$ (both 1% wt Co and Pt), the structures are still remained rod shape with the length closed the metal free $K_2Ti_6O_{13}$.

4.1.4 Thermal stability

The mass loss curves of all samples are shown in Figure 4.4.

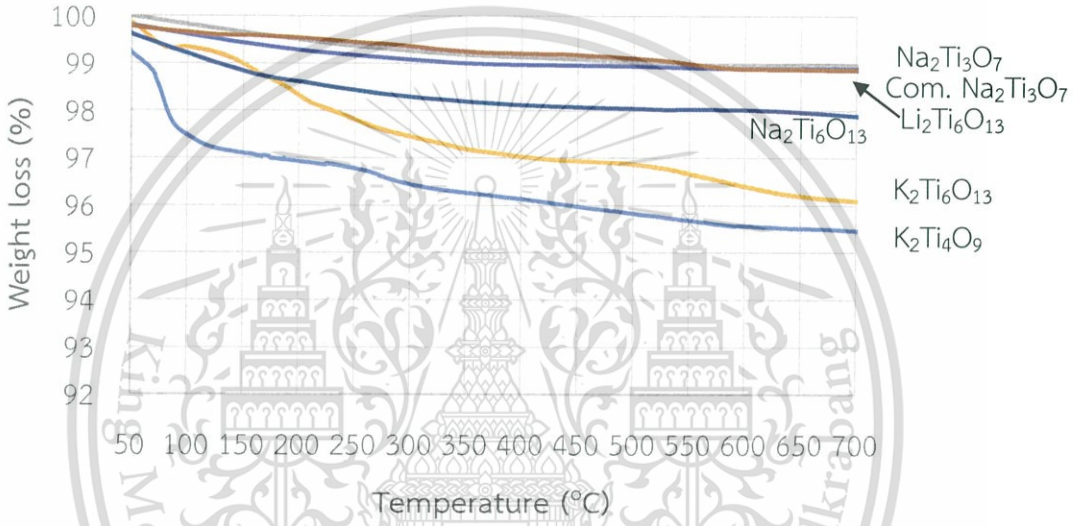

Figure 4.4 Thermal stability of all titanate-catalysts.

The alkali hexatitanates show the mass loss starting at around 30 °C ($Na_2Ti_6O_{13}$, 0.3%; $K_2Ti_6O_{13}$, 1.2% and $Li_2Ti_6O_{13}$, 0.4%), ascribed to the loss of physisorbed water on the surface of a catalyst. The amount of physisorbed water as deduced from the first mass loss is in the order $K_2Ti_6O_{13}$ > $Li_2Ti_6O_{13}$ > $Na_2Ti_6O_{13}$, following the trend in the specific surface area.

The layered titanates $Na_2Ti_3O_7$ and $K_2Ti_4O_9$ show two regions of the mass loss. $Na_2Ti_3O_7$ lost 0.6% of the mass starting at 30 °C (i.e., physisorbed water), while $K_2Ti_4O_9$ lost 1.0% of the mass. At 100 °C or higher, the losing was determined to be the inter-lamellar water molecules present in the layered $Na_2Ti_3O_7$ and $K_2Ti_4O_9$. For $Na_2Ti_3O_7$, another high temperature loss starting at 500 °C is also observed, ascribed to the transformation to $Na_2Ti_6O_{13}$ [6]. The transformation of $Na_2Ti_3O_7$ to $Na_2Ti_6O_{13}$ is also in agreement with XRD results mentioned in Figure 4.2. The relative lower thermal

stability of the layered titanate limits the activation temperature to be used during catalytic activity testing. So, all catalysts will be activated in air at 500 °C as will be mentioned later.

4.1.5 Temperature programmed reduction profile

The TPR profiles of all catalysts are shown in Figure 4.5. The y-axis represents the signal from the TCD detector normalized by the sample mass.

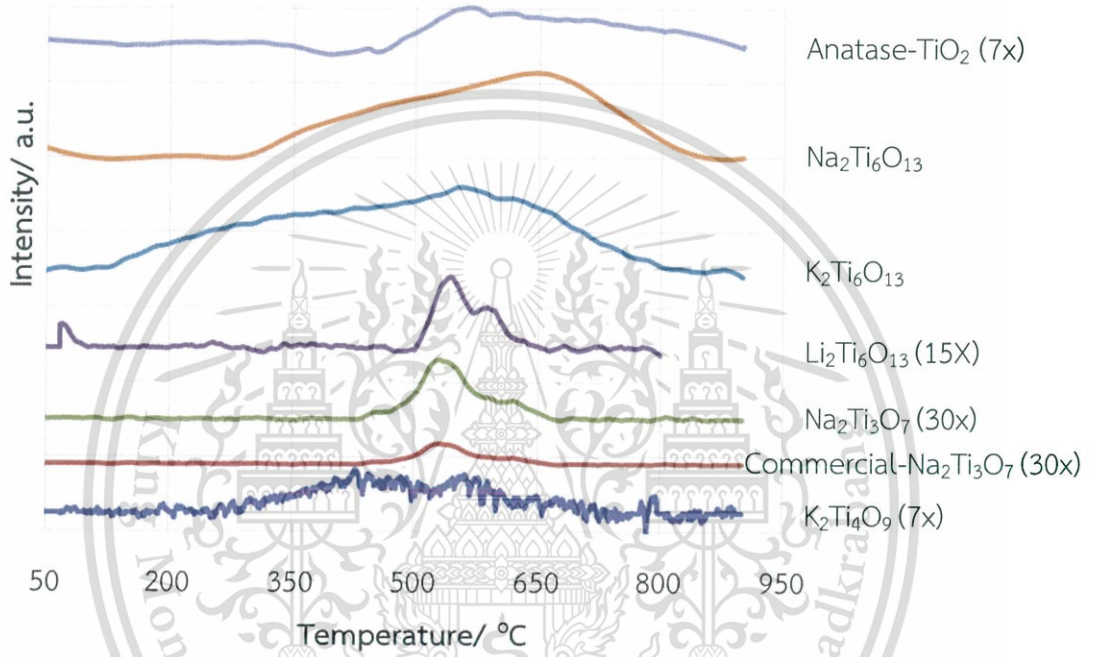

Figure 4.5 Temperature programmed reduction profiles of the catalysts studied.

All profiles show a broad peak that is ascribed to the reduction of reducible metal oxide (Ti in this case) via the removal of oxygen atoms. Such reduction generates oxygen vacancy sites and Ti^{3+} surface defects from the original Ti^{4+} cations [86]. The different reducibility of a catalyst can be seen as the difference in the reduction temperature (i.e., position on the x-axis) and the magnitude of the reduction (i.e., peak area). These results could be explained considering the different surroundings of oxygen atoms as present in different crystal structures. Anatase TiO_2 shows the peak maximum (T_p) at 550 °C, similar to previous report [87].

One can see that the start of the reduction for *all* alkali metal titanates has shifted to lower temperature in comparison to anatase. Relevant values are shown in Table 4.4.

Table 4.4 Hydrogen consumption of the catalysts studied.

Catalysts	T_{onset} (°C)	$T_{maximum}$ (°C)	T_{offset} (°C)	Hydrogen consumption	
				μmol/g	μmol/m^2
Anatase TiO_2	406	610	834	55	9.3
$K_2Ti_6O_{13}$	131	563	851	1,352	64
$Na_2Ti_6O_{13}$	284	553	841	1,200	133
$Li_2Ti_6O_{13}$	500	545	650	4.6	0.3
$Na_2Ti_3O_7$	426	531	679	2.6	0.5
Commercial $Na_2Ti_3O_7$	434	543	595	7.6	2.5
$K_2Ti_4O_9$	262	550	761	5.2	8.6

Comparing $A_2Ti_6O_{13}$ having the tunnel structure but with different alkali metal cations, the onset temperatures are in the order $K_2Ti_6O_{13}$ (131 °C) < $Na_2Ti_6O_{13}$ (284 °C) < $Li_2Ti_6O_{13}$ (545 °C). This order parallels the order of the *b* parameter of the monoclinic unit cell. It is here proposed that the larger distance between the tunnel (i.e., *b*-parameter) results in a weaker attraction between the negatively charged Ti-O framework and the positively charge alkali metal cations. This situation enables a facile removal of oxygen atoms in the alkali hexatitanates with relatively large d200. However, in spite of the fact that $Li_2Ti_6O_{13}$ has *b* parameter larger than the Na-form, the reducibility is weakened. Li^+ coordinated 4 oxygen atom whereas Na^+ coordinated 8 oxygen atom.

When comparing the reduction profile of $Na_2Ti_3O_7$ *vs* $Na_2Ti_6O_{13}$, one can see that it is more difficult to reduce the layered titanates compared the tunneled titanates. This conclusion is deduced from the higher onset temperature in the former. For example, the onset reduction temperature of $Na_2Ti_3O_7$ is at 426 °C while the onset reduction temperature of $Na_2Ti_6O_{13}$ is as low as 300 °C. The tunneled structure is relatively more rigid than the layered structure. Such rigidity would impose the strain to the Ti-O connectivity of the framework. The large strain serves as the driving force for a facile removal of oxygen atoms, such that the resulting material has a more relaxed structure. Similar conclusion can be drawn when comparing the layered $K_2Ti_4O_9$ (T_{onset} = 262 °C) with the tunneled $K_2Ti_6O_{13}$ (T_{onset} = 116 °C). In this case, however, a different number of TiO_6 making up the ribbon (4 in $K_2Ti_4O_9$, but 3 in $K_2Ti_6O_{13}$) makes a direct comparison difficult.

The individual hydrogen consumption is also shown in Table 4.4. These values are compared both on the mass basis and on the area basis. The hydrogen consumption (or reducibility) based on the mass, i.e., micromole H_2/g catalyst, is in the order: $K_2Ti_6O_{13}$ > $Na_2Ti_6O_{13}$ > $K_2Ti_4O_9$ > Commercial $Na_2Ti_3O_7$ > $Na_2Ti_3O_7$ > Anatase TiO_2. Such order is nicely parallel the specific surface area. This finding is due to the fact that the reduction of a metal oxide requires the adsorption of gaseous H_2 upon the surface.

Nevertheless, the hydrogen consumptions based on the surface area for tunneled titanates ($A_2Ti_6O_{13}$) are roughly 4 times larger than those for the layered titanates ($Na_2Ti_3O_7$ and $K_2Ti_4O_9$). The reducibility of TiO_2 anatase is very low.

This order can be arranged by the *b*-axis in the crystal or, on the other hand, lattice strain. High lattice strain generally interrupts the overlap of the orbital between Ti and O atom suiting the formation of oxygen vacancy site which is an active site for the ketonization. The strain is partially originated from the structure and size of interstitial cations. Comparing $K_2Ti_6O_{13}$ and $K_2Ti_4O_9$ (Tunneled *vs* Layered structure), the tunnel is more rigid and less flexible than the other, so the relative large K^+ ion can be parted the framework away only at their accommodation but the layer can be stretch out all of the plane. Comparing $K_2Ti_6O_{13}$ and $Na_2Ti_6O_{13}$ (different cation), undoubtedly, the larger one needed the space than the smaller one.

Even though non-reduced $Na_2Ti_6O_{13}$ has an activity lower than the Li-form, but after reduction this trend is clearly inversed. From TPR results the Li-form is hardly reduced, starting at high temperature, while the Na-form is easily reduced.

Comparing the same structure, the H_2 consumption (per surface area) is similar for $Na_2Ti_6O_{13}$ and $K_2Ti_6O_{13}$. However, $Li_2Ti_6O_{13}$ is different, it has the lowest H_2 consumption among hexatitanate. This result suggests that the type of alkali cation at the tunnel plays an insignificant role in the reduction.

XRD of all catalysts after calcination at 500 °C and reduction at 400 °C are shown in Figure 4.6.

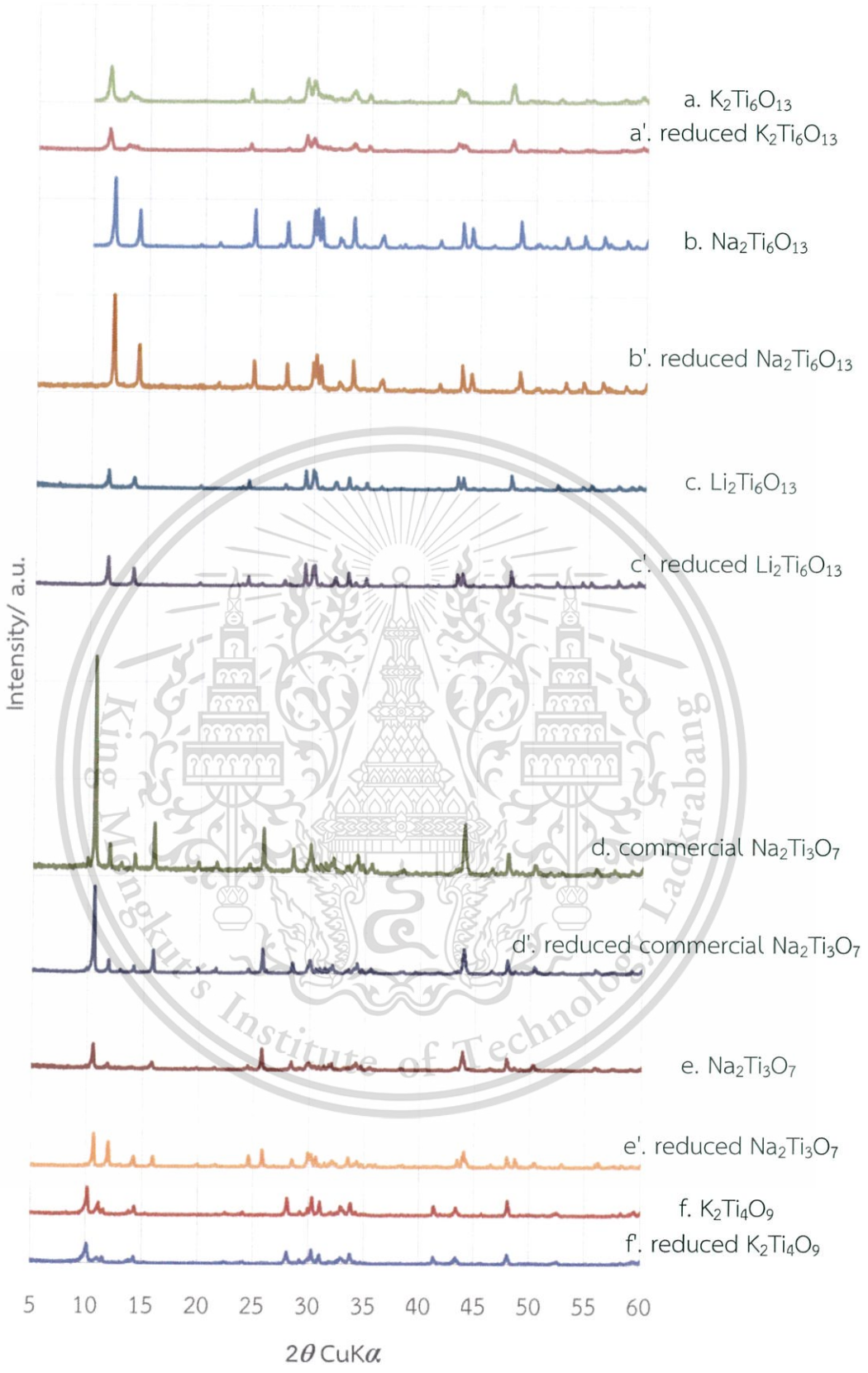

Figure 4.6 X-ray diffraction pattern of all catalysts studied; reduced catalysts means the catalysts calcined at 500 °C and reduced 400 °C

The XRD patterns indicate that the structure has no changed during the reduction including lattice parameters (*a*, *b* and *c* axis). However, these white dispersed particles turn grey after reduction assuming the identical character of Ti^{3+} coordination that consistent the TPR profiles.

Figure 4.7 shows TPR profiles of metal impregnated $K_2Ti_6O_{13}$ (both 1% wt Co and Pt) and parent supports.

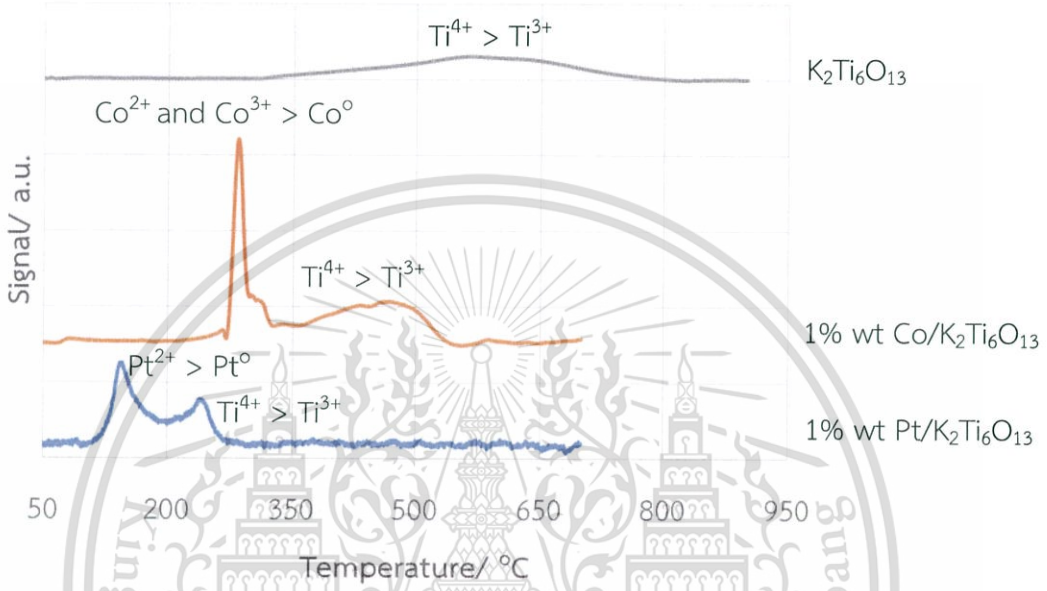

Figure 4.7 TPR profiles of metal-free and impregnated $K_2Ti_6O_{13}$

1% wt Co/ $K_2Ti_6O_{13}$ shows the reduction peaks at 280 °C corresponding to Co^{3+} to Co^{2+} and 310 °C for Co^{2+} to metallic Co. In addition, the reduction of Ti^{4+} to Ti^{3+} over the surface of $K_2Ti_6O_{13}$ seems to be easily promoted; the peak shifts to lower temperature because the interaction of H_2 with the Co species assist the reduction of the support. 1% Pt/ $K_2Ti_6O_{13}$ shows two reduction peaks at 154 °C (Pt^{2+} to metallic Pt) and 240 °C (Ti^{4+} to Ti^{3+}). Titanium species at interface between Pt and $K_2Ti_6O_{13}$ is more easily reduced, as compared to the Co/$K_2Ti_6O_{13}$ due to the higher support-metal interaction, so called Strong Metal Support Interaction (SMSI) as will be discussed in Section 4.2.3 [88].

4.1.6 Basic properties

The CO_2-TPD profiles characterizing the basic properties are depicted in Figure 4.8.

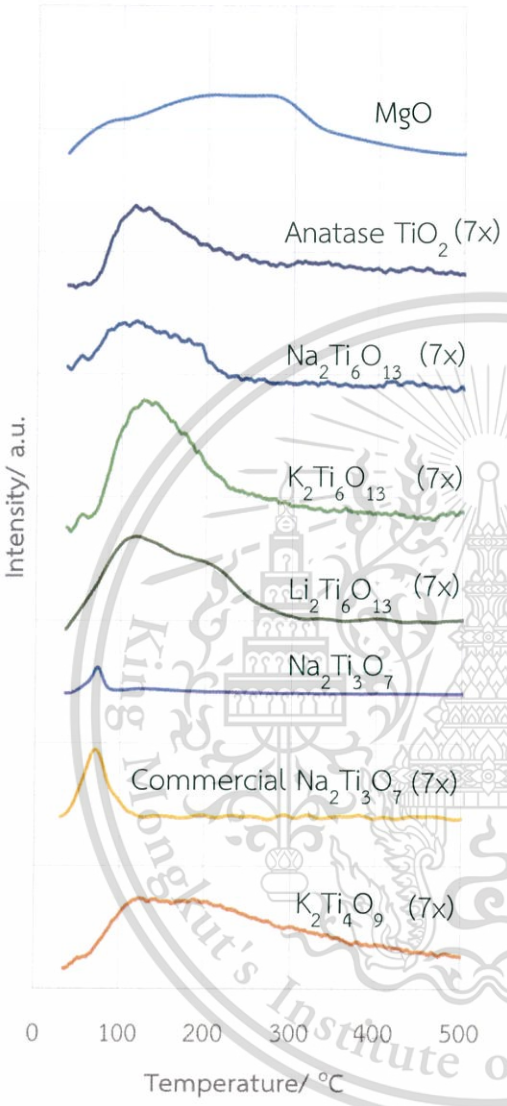

Figure 4.8 CO_2-Temperature programmed desorption profiles of all catalysts studied.

The profiles indicate both of basic strength (determined from adsorption temperature) and basicity (determined from amount of adsorbed CO_2 i.e. the area under the peak). All catalysts were compared to the strong basic MgO. Adsorption of CO_2 over MgO is relatively high, both of temperature and integration of peak area. This results show that MgO possessed high basicity and basic strength, while alkali titanate samples unfortunately has lower basic properties. All of hexatitanates shows the only one step desorption similar to anatase TiO_2. While $Na_2Ti_3O_7$ exhibits two peaks at 75 °C. The $K_2Ti_4O_9$ possessed only one adsorption at 100 °C. The low temperature CO_2 adsorption is deduced as the physisorbed CO_2 species. As with TPR, the basicity will be compared either per mass (μmol CO_2/ g) or per area (μmol CO_2/ m^2) in Table 4.5.

Table 4.5 Basic site of catalysts studied

Catalysts	T_{onset} (°C)	$T_{maximum}$ (°C)	T_{offset} (°C)	Basicity	
				μmol/g	μmol/m^2
MgO	30	276	834	2,790	-
Anatase TiO_2	54.3	120	476	68	2.3
$K_2Ti_6O_{13}$	30	128	232	96	0.9
$Na_2Ti_6O_{13}$	30	105	235	39	0.9
$Li_2Ti_6O_{13}$	30	105	309	30	2.8
Commercial $Na_2Ti_3O_7$	30	94	118	45	3.0
$Na_2Ti_3O_7$	30	77	91	241	9.7
$K_2Ti_4O_9$	30	124	580	221	7.4

As expected, MgO shows the highest basic properties (2,790 μmol/ g) . Comparing TiO_2 samples, the basicity is decreased from MgO > $K_2Ti_4O_9$ > $Na_2Ti_3O_7$ > $K_2Ti_6O_{13}$ > Anatase TiO_2 > commercial $Na_2Ti_3O_7$ > $Na_2Ti_6O_{13}$ > $Li_2Ti_6O_{13}$. Furthermore, the basicity is arranged in an order of; $Na^+ < Li^+ < K^+$ according to their *b*-axis and polarizability. The more polarizable cations would induce electron around oxygen framework affecting the high electron density except for Li-form which is cation at different accommodation.

4.2 Catalytic characterization

The activity of each catalyst was first screened via (i) the deoxygenation of a simple model carboxylic acid such as acetic acid and (ii) aldol condensation of acetone. The later (ii) can provide information for basicity of the catalysts. The contribution of basic sites toward the deoxygenation was proposed in the literature that the hydrogen abstraction is a proper step on the deoxygenation. The production of long chain olefins from heptanoic acid would be encountered at next section by the contribution of these conclusive estimations.

4.2.1 Deoxygenation of acetic acid

The conversion of acetic acid over various catalysts under atmospheric N_2 at 400 °C is shown in Figure 4.9.

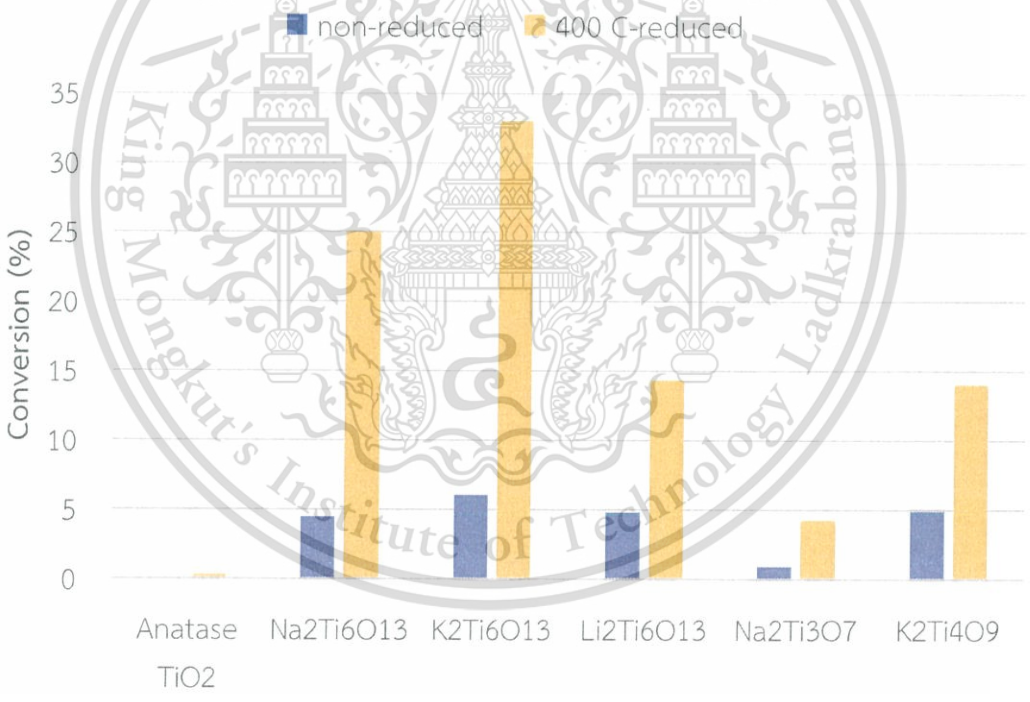

Figure 4.9 The deoxygenation activity of various catalyst with and without reduction at 400 °C for 2 h. Reaction conditions: reaction temperature 400 °C, atmospheric N_2, W/F 15 gh/mol. Results were averaged from 60-360 min on stream.

The steady state conversion of acetic acid was obtained over each catalyst after the TOS of 60 min without obvious deactivation of the catalyst. The results shown here are the average of the values from 60 to 360 min. In all cases, acetone was the only product detected. The partial deoxygenation of acetic acid in this case can be referred to as ketonization. The highest conversion was obtained over $K_2Ti_6O_{13}$ (6.1%) followed by $Li_2Ti_6O_{13}$ (5.1%), $K_2Ti_4O_9$ (4.9%), $Na_2Ti_6O_{13}$ (4.5%) and $Na_2Ti_3O_7$ (0.9%). Anatase TiO_2 could not convert acetic acid into products under this experimental condition.

Considering that the conversion of acetic acid under N_2 gas is rather low, all catalysts were in situ reduced at 400 °C for 2 h prior to the activity testing under 90 mL/h H_2 gas. Similar to the reaction under N_2 mentioned above, the reaction under H_2 here comes to the steady state after 60 min, and results are the averaged from 60 to 360 TOS. Figure 4.9 shows that the pre-reduction enhances the conversion of acetic acid for all catalysts while acetone is the only product obtained. The conversion of acetic acid from high to low is in the order: $K_2Ti_6O_{13}$ (33.0%) followed by $Na_2Ti_6O_{13}$ (25.1%), $Li_2Ti_6O_{13}$ (14.3%), $K_2Ti_4O_9$ (14.0%) and $Na_2Ti_3O_7$ (4.3%). The order of the activity is not different from that of non-reduced catalysts. From the TPR experiments show in Figure 4.5, it can be assumed that oxygen vacancy sites and/or reducible surfaces are created on the surface of these catalysts upon reduction at 400 °C. The higher conversion of acetic acid over the reduced catalysts, as compared to the non-reduced ones, confirms that oxygen vacancy sites and/or reducible surfaces are beneficial in the ketonization [89].

Figure 4.10 shows that the conversion of acetic acid on both non-reduced and reduced catalysts is proportional to the specific surface area of the catalyst as expected.

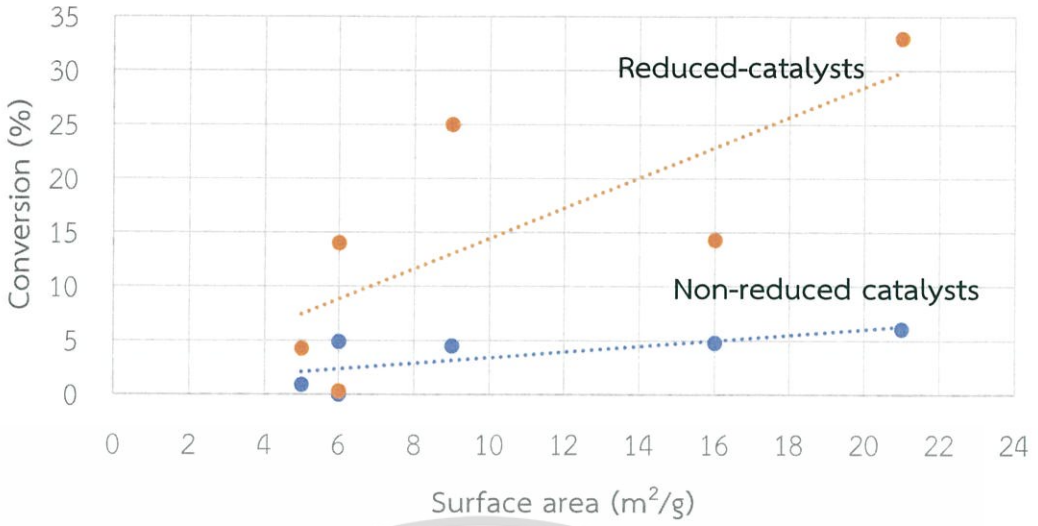

Figure 4.10 The conversion of acetic acid over non-reduced catalysts and 400°C-reduced catalysts versus specific surface area of each catalyst. Reaction conditions: reaction temperature 400 °C, reduction temperature (when available) 400 °C, atmospheric N_2, W/F 15 gh/mol. *Results were averaged from 60-360 min time on stream.*

Again, the catalysts reduced at 400 °C give higher acetic acid conversion, as compared to the non-reduced one. It can be seen that in both reduced and non-reduced catalysts, the conversion significantly depends on the specific area. As the surface area is increased, the number oxygen vacancy sites are increased. Accordingly, it is worth to consider the reducibility of the catalysts by normalization with surface area as shown in Figure 4.11. The catalyst's reducibility can be deduced from the area density of oxygen vacancy sites in micromole H_2/ g catalyst.

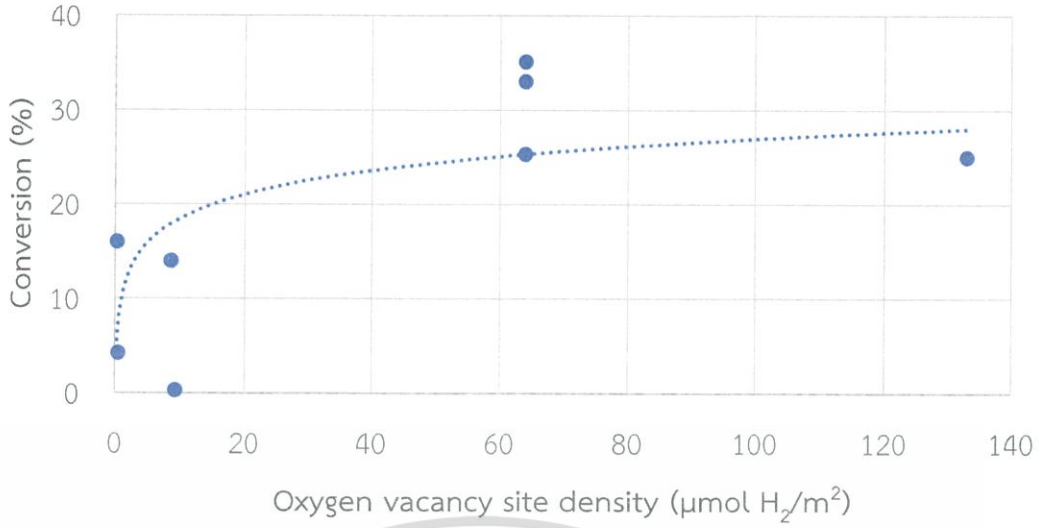

Figure 4.11 The conversion of acetic acid over reduced catalysts *vs* the oxygen vacancy sites density at selected reduction temperauture. All catalysts were reduced at 400 °C except $K_2Ti_6O_{13}$ where results with the reduction temperature of 450 and 500 °C were also shown as indicated. *Reaction conditions: reaction temperature 400 °C, atmospheric N_2, W/F 15 gh/mol, as averaged from 60-360 min time on stream.*

One can see that there is a logarithmic relationship between the conversion of acetic acid and the oxygen vacancy sites density over various titanate- based catalysts. Hence, the number of oxygen vacancy sites is importance for the ketonization of acetic acid over all alkali-titanate catalysts.

It was suggested that oxygen exposed at surface of the catalysts contacts with the adsorbed hydrogen species that is formed by the dissociative adsorption of hydrogen gas. Then, hydrogen species can transfer electron to the oxygen lattice of the catalysts and leaving as water molecule. This step produced single electron in the vacancy that is subsequently transfer to adjacent Ti^{4+} forming Ti^{3+} surface defects. The formation of this sites can be explained using Scheme 4.1.

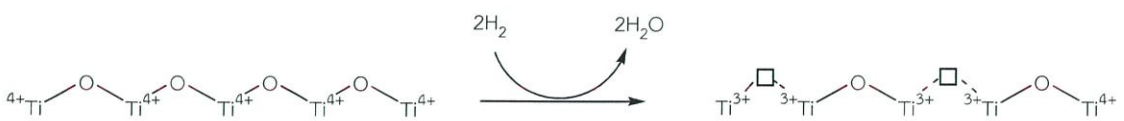

Scheme 4.1

Among the low surface area alkali titanates, $K_2Ti_6O_{13}$ was selected for further study on the effect of reduction temperature (i.e., 400, 450, and 500 °C) on the catalytic activity, employing N_2 as a carrier gas. Note that even the low surface area the K titanates yields high acetone. Therefore, reduction of the surface would play role for the observed activity.

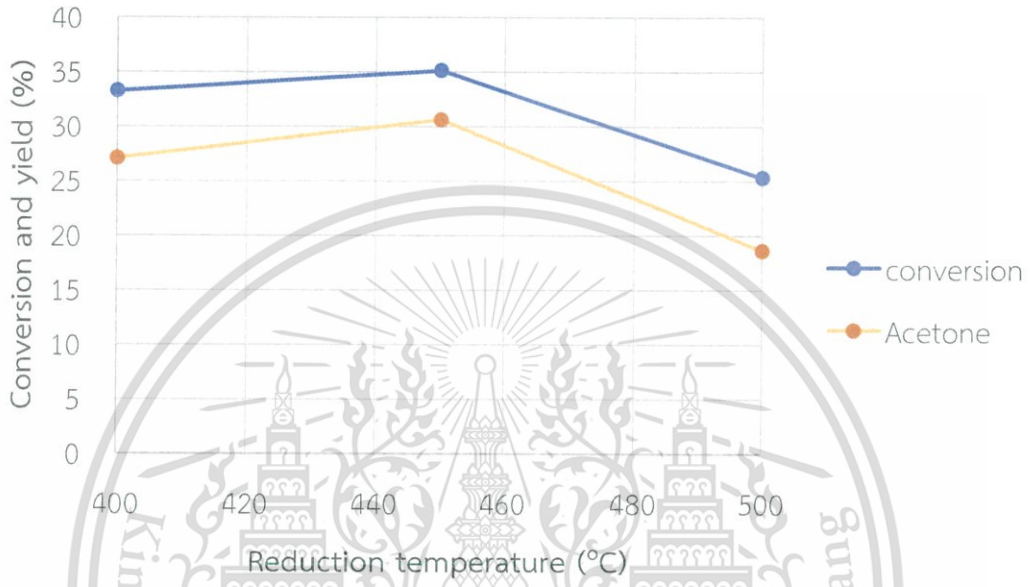

Figure 4.12 Effect of the reduction temperature of $K_2Ti_6O_{13}$ on the conversion of acetic acid and the yield of acetone. *Reaction conditions: reaction temperature 400 °C, reduction temperature 400, 450, or 500 °C as indicated, atmospheric N_2, W/F 15 gh/mol, averaged from 60-360 min time on stream.*

As shown in Figure 4.12, the conversion of acetic acid is increased from 33.4% to 35.1% upon increasing the reduction temperature from 400 to 450 °C. However, the reactivity drops to 25.3% upon reduction at 500 °C. The yield of acetone, follows the same trend, is increased with temperature but decreased upon reduction at 500 °C. However, the decrease in the conversion and the yield when the reduction temperature is high, does not relate to the change in the crystal structure or the surface area. XRD results show that $K_2Ti_6O_3$ reduced at 500 °C retained the alkali hexatitanate structure (Section 4.1) and had similar specific surface area, as compared to the value of 21 m^2/g for the as-made catalyst. It is proposed that the (i) electron transfer from surface to bulk [90] or (ii) oxygen lattice replenishment from bulk to surface [91] of

$K_2Ti_6O_{13}$ is responsible for such decline in activity. In line with this view, Figure 4.13 shows a decrease in Ti^{3+} on the external surface of $K_2Ti_6O_{13}$ catalysts when reduced at 500 °C (XPS spectra of Ti species).

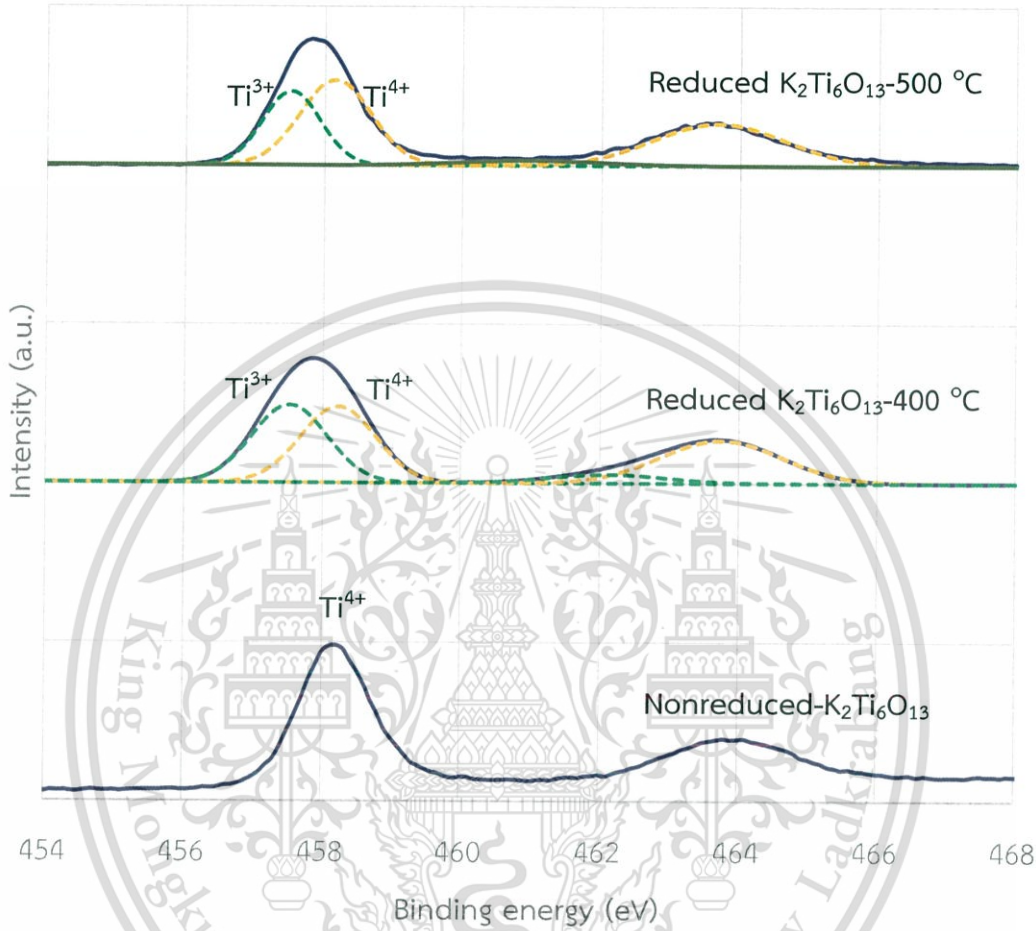

Figure 4.13 Ti 2p -XPS spectra of $K_2Ti_6O_{13}$ at various reduction temperatures; green dash line; Ti^{3+} species and yellow dash line; Ti^{4+} species.

It can be seen that non-reduced $K_2Ti_6O_{13}$ possess only Ti^{4+} species on the surface while Ti^{3+} species stand out upon reduction at 400 and 500 °C. The Ti^{3+}/Ti^{4+} ratio of the catalyst reduced at 400 °C is higher than that at 500 °C. This finding supports the lower concentration of the oxygen vacancy sites in the sample reduced at 500 C, which is also in good agreement with the observed activity. It is indicated that at high reduction temperature (500 °C), the electron trapped in the surface oxygen vacancy sites may well be ejected to the bulk, leading to the decrease in *surface* Ti^{3+}. Therefore, the surface become less active for the ketonization. Alternatively, the observed decrease in surface Ti^{3+} would be resulted from the movement of lattice oxygen. As

temperature is increased, mobility of the oxygen in the lattice would be increased. It is possible that some of oxygen can immigrate onto the surface. In this case, the single electron from the surface would move to lattice-orbital that enhance mobility of the oxygen. Accordingly, the bulk oxygen can readily replenish the surface oxygen vacancy at high temperature.

The binding energy of titanium for non-reduced $K_2Ti_6O_{13}$ is at 458.2 eV for 1/2, and 464.0 eV for 3/2. This is indicated that the higher electron density of the Ti^{4+} species in support manner (Figure 4.14 shows the oxygen 2s XPS spectra of $K_2Ti_6O_{13}$).

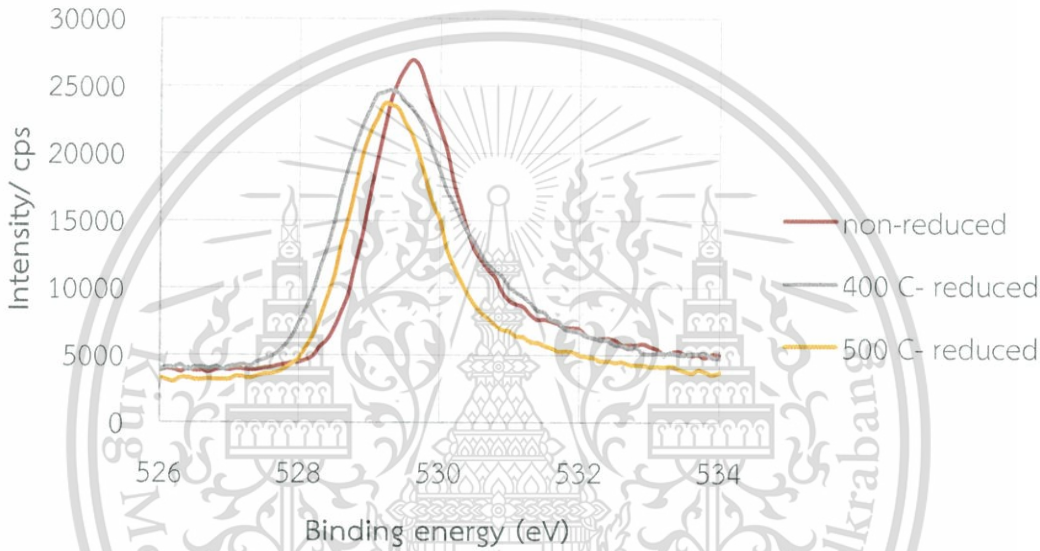

Figure 4.14 O 2s XPS spectra of $K_2Ti_6O_{13}$ at various reduction temperatures in H_2 atmosphere.

The O 2s XPS spectra of reduced catalysts show lower binding energy (529.3 eV), as compared to that of the non-reduced one (529.7 eV). This observation can be explained considering that the interaction between oxygen and titanium is relatively weak for O-Ti^{3+}, as compared to O-Ti^{4+}. Moreover, the weaker intensity of the peak found in the reduced $K_2Ti_6O_{13}$ sample, suggests a relatively less concentration of surface oxygen, in comparison to the non-reduced sample.

4.2.2 Aldol-condensation of acetone

While the results in the previous section point to importance of oxygen vacancy sites or reducible surfaces in the ketonization of acetic acid, the contribution from the basic sites should not be overlooked. Some catalysts are known to catalyze the deoxygenation via the basic sites [92]. The activity of high basicity possessed titanate-based catalysts in the basic-catalyzed aldol condensation of acetone was then evaluated at 450 °C as shown in Table 4.6.

Table 4.6 the aldol-condensation activity of the catalysts

Catalysts	Acetone conversion (%)	Yield (%)	
		α-hydroxyketone	Mesityl oxide
MgO	40.0	32.2	5.4
$K_2Ti_4O_9$	0.0	0.0	0.0
$K_2Ti_6O_{13}$	0.0	0.0	0.0

Reaction conditions: reaction temperature 400 °C, atmospheric N2, W/F 50 gh/mol, averaged from 60-360 min time on stream.

However, the zero conversion of acetic acid was obtained in potassium titanates. For comparison, the basic MgO gives ~40.0% conversion. Therefore, the basic sites detected by CO_2 TPD (Figure 4.8) are rather weak and inactive toward acetone aldol condensation. One could deduce that the contribution of basic sites in the ketonization of acetic acid is rather limited. This finding support the fact that there is not direct correlation between the conversion of acetic acid and the mmol of CO_2, as mentioned previously.

4.3 Production of long chain olefins from heptanoic acid

As $K_2Ti_6O_{13}$ is readily reduced and active for ketonization of acetic acid, the sample was studied further as a catalytically active material for the production of long chain olefins from heptanoic acid. Several parameters have been investigated including the effect of reaction temperature, contact time, and metal loading.

4.3.1 Effect of reaction temperature

Using *non- reduced* $K_2Ti_6O_{13}$, the effect of the temperature on the conversion of heptanoic acid was investigated. The reaction was conducted at 400-500 °C under atmospheric N_2 at the W/F = 250 gh/mol. As shown in Figure 4.15a, the conversion of 24.2-100.0% was obtained, with 7-tridecanone as a major product.

a)

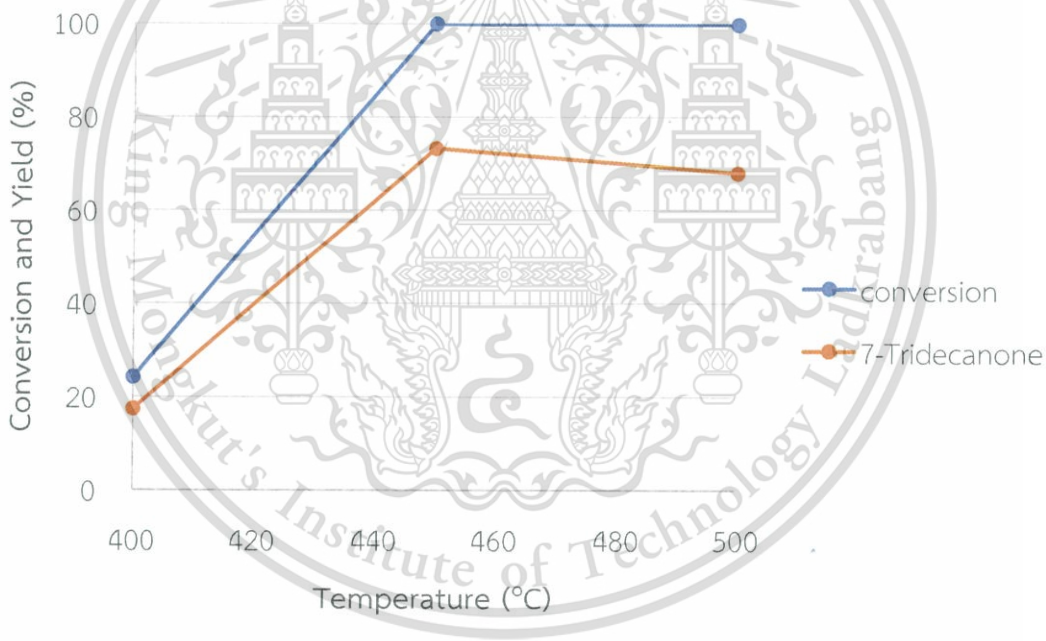

b)

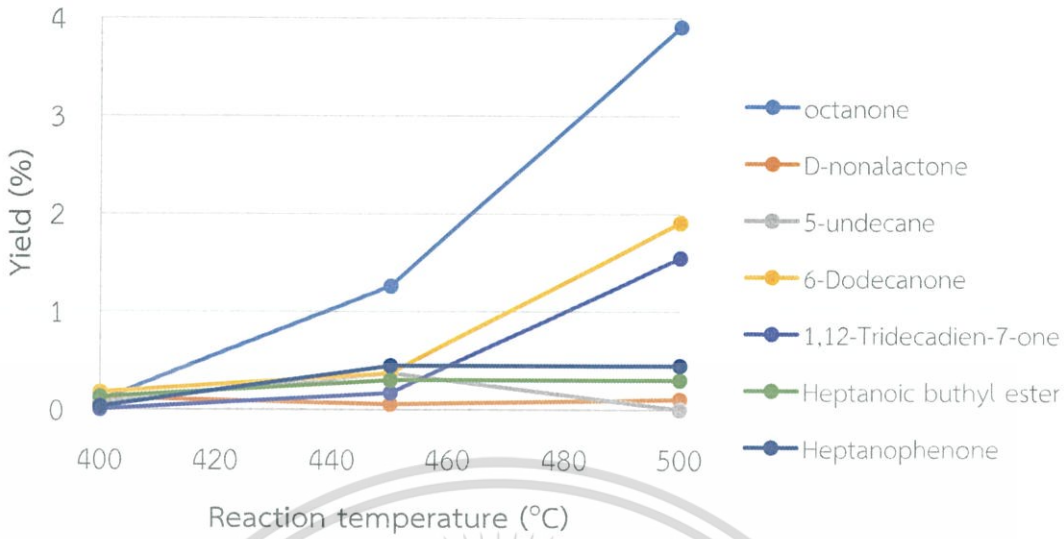

Figure 4.15 The conversion of heptanoic acid and yield of major product **(a)** and yield of by-products **(b)** at different reaction temperatures. Reaction conditions: nonreduced-$K_2T_6O_{13}$, W/F 250 gh/mol, 400-500 °C in N_2, at the time on stream of 60 min.

As the temperature is increased, the conversion of heptanoic acid is increased. 7-tridecanone (17.4%) is predominantly primary product which is increased along the reaction temperature. Furthermore, at 500 °C the cracking of 7-tridecanone is favored. In line with the catalytic characterization of acetic acid (Section 4.2), the 7-tridecanone is a symmetrical ketone obtained via the ketonization of heptanoic acid as shown in Equation 4.1.

(Equation 4.1)

Other products (less than 2%) are 2-octanone, D-nonalactone, 5-undecane, 6-dodecanone, 1,12-tridecadien-7-one, heptanoic anhydride, heptanoic butylester, heptanophenone and 1-(4-methylphenyl)-1-pentanone (Figure 4.15b). As the higher ketone is observed by ketonization, one can deduce that these products resulted from the cracking of 7-tridecanone (which is energetically endothermic). The major product among the cracked ketone is 2-octanone, which is produced from the cleavage of

7-tridecanone at the α-position (Equation 4.2). The cracking at the α-carbon can be explained by Norrish type II mechanism of the six-membered carbon intermediate via the radical process. The mechanism involves γ-hydrogen abstraction by the excited carbonyl group at high temperature [93].

(Equation 4.2)

4.3.2 Effect of contact time

To verify the reaction pathway, Figure 4. 16 shows the conversion of heptanoic acid and the yield of various products as a function of the contact time. The experiments were performed over $K_2Ti_6O_{13}$ reduced at 400 °C in H_2, and the reaction was tested at 400 °C in N_2 atmosphere.

a)

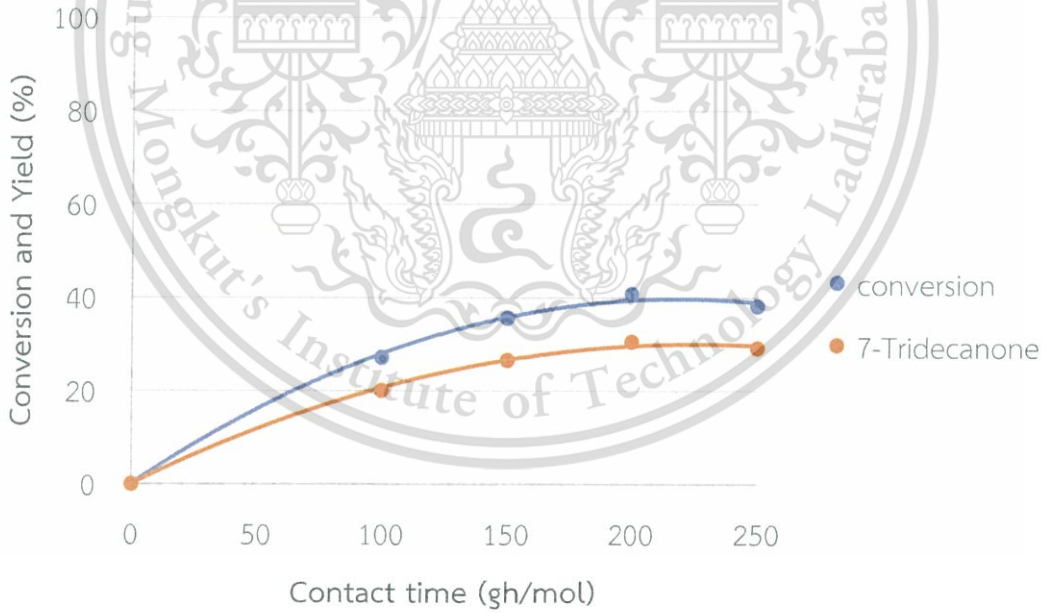

b)

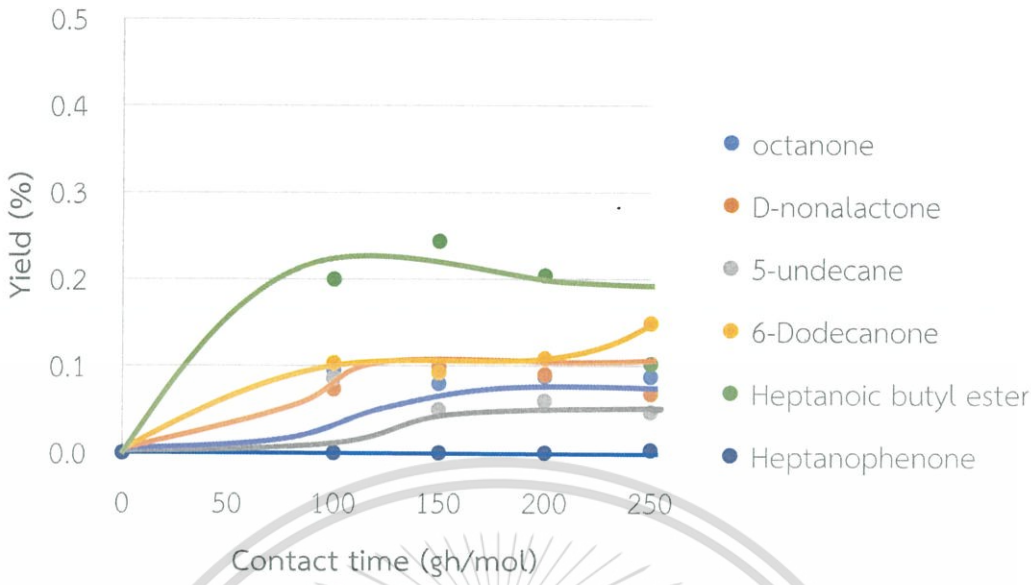

Figure 4.16 The conversion of heptanoic acid and yield of major product **(a)** and yield of by-products **(b)** at different contact times. Reaction conditions: $K_2T_6O_{13}$, reaction temperature 400 °C, reduction temperature 400 °C, under atmospheric N_2 at 60 min time on stream.

The conversion of heptanoic acid increased from 27 to 40% when the contact time is increased from 100 to 250 gh/mol. The increased conversion at longer contact time is understandable, because heptanoic acid spends a longer time in contact with the active sites on the surface of a catalyst. In all cases, the only dominant product is 7-tridecanone (Figure 4.16a). Very small amount of cracked ketone (0.45%), light hydrocarbon (0.07%), and products from basic-catalyzed reaction of heptanoic acid (0.16%, i.e., heptanoic butylester and heptanophenone) was also observed in a trace amount (Figure 4.16b). As oxygen vacancy sites play role on the conversion of heptanoic acid, H_2 atmosphere would affects the heptanoic acid conversion. Accordingly, the effect of the contact time under H_2 atmosphere is presented in Figure 4.17.

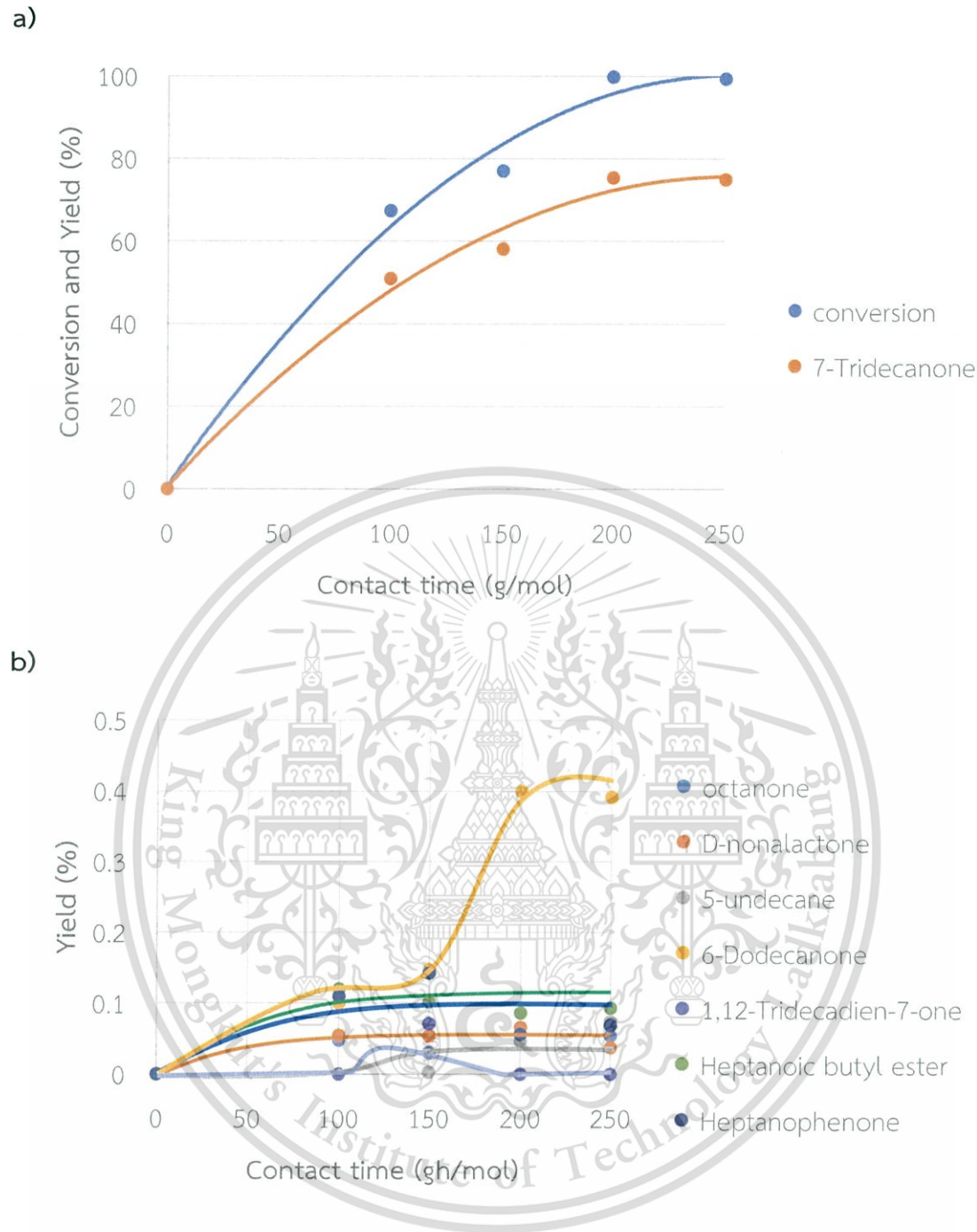

Figure 4. 17 The conversion of heptanoic acid and yield of major product **(a)** and yield of by- products **(b)** at different contact times. *Reaction conditions: $K_2T_6O_{13}$, reaction temperature 400 °C, reduction temperature 400 °C, atmospheric H_2, as averaged from 60-300 min time on stream.*

Comparing to N_2 atmosphere, the conversion of heptanoic acid under H_2 is significantly improved to 70- 100% when W/F is increased in the same range of 100- 250 gh/mol. The major product is still 7-tridecanone, hence, the atmospheric H_2 does not affect the reaction sequence (Figure 4. 17a). The higher conversion here can be

explained by the beneficial role of hydrogen gas. H_2 assists in the production of oxygen vacancy sites/ reducible surface and enhances the hydrogen transfer reaction, preventing the deposition of coke on the surface of the catalyst.

In addition to the increase in activity, using H_2 as carrier gas improve stability of $K_2Ti_6O_{13}$ as shown in Figure 4.18.

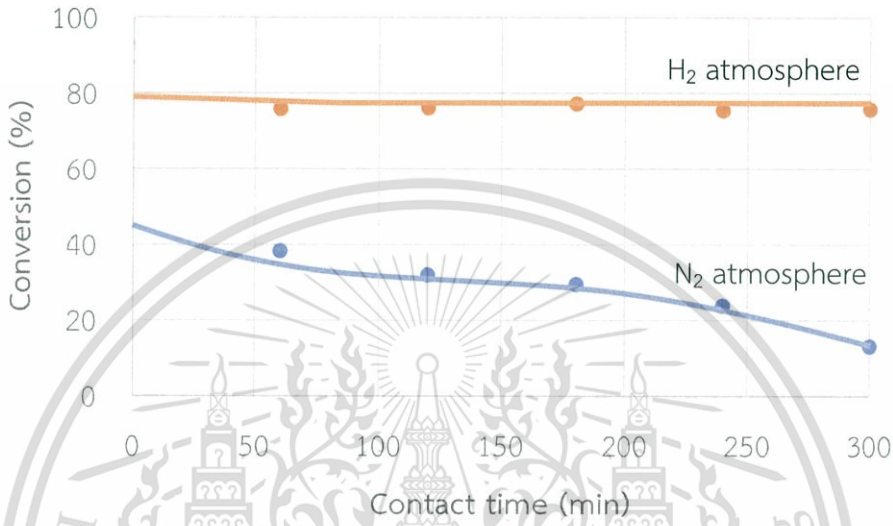

Figure 4.18 The conversion of heptanoic acid at contact time 150 gh/mol in N_2 and H_2. *Reaction conditions: $K_2T_6O_{13}$, reaction temperature 400 °C, reduction temperature 400 °C, atmospheric H_2, as averaged from 60-300 min time on stream.*

It can be seen that the conversion is slightly decreased under N_2 while a better stability is obtained for the reaction under H_2. The deactivation observed for the reaction under N_2 can be derived from (i) coking during the reaction progress and/or (ii) the competitive adsorption between the acid and the products. The carbon deposition was described by a great deal of unsaturated species such as higher molecular weight compounds formed by the olefins isomerization and cyclization (i). The H_2 can also prevent the formation of the primary unsaturated compound via the hydrogenation process. Moreover, H_2 helps the product desorption from the surface of the catalysts (ii).

From the product distribution as mentioned previously, the atomic-level of the ketonization of heptanoic acid over $K_2Ti_6O_{13}$ might be explained following the mechanism proposed by *Pham et. al.* [94] over Ru/TiO_2. The oxygen atom of heptanoic

acid attaches to the Ti^{3+} on the surface of $K_2Ti_6O_{13}$. (Ti^{3+} is indeed detected by XPS in Figure 4.13) Simultaneously, the –OH end of the acid could interact with the hydroxyl group of the Ti site. As a result, a water molecule is released and the heptanoate species is formed as shown in Scheme 4.2. This heptanoate species then undergoes enolization, in combination with the hydrogen abstraction from adjacent hydroxyl group, forming a semi-enol compound, Scheme 4.3.

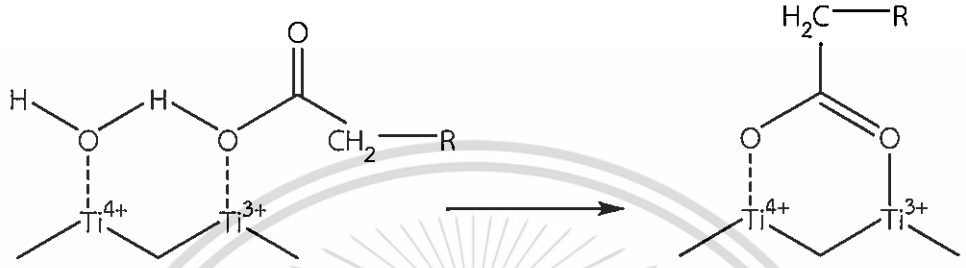

Scheme 4.2

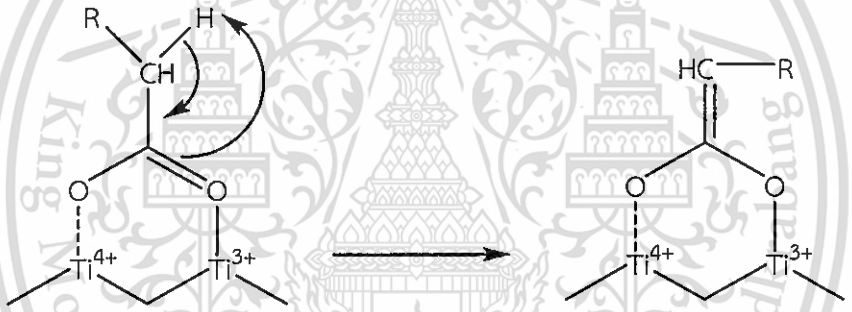

Scheme 4.3

The active semi- enol compound then reacts with another adsorbed heptanoic acid at electrophilic carbon atom, producing a β-keto acid as an important reaction intermediate [25]. The β-keto acid can further rearrange via concerted mechanism to a 6-atom cyclic intermediate, following by decarbonylation which produces an enolic compound, that latter tautomerizes to 7-tridecanone as shown in Scheme 4.4.

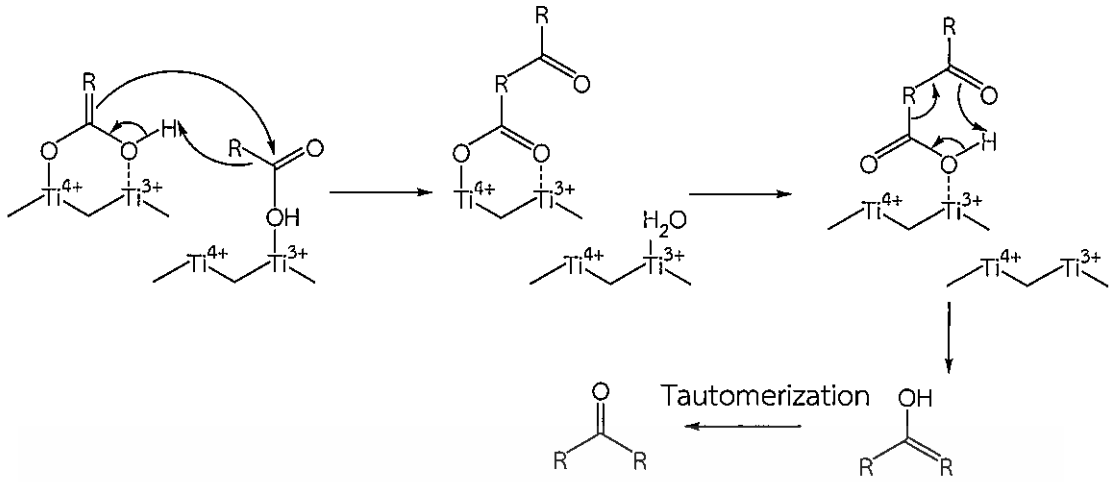

Scheme 4.4

The overall mechanism for the ketonization of heptanoic acid over $K_2Ti_6O_{13}$ collecting product distributions is depicted in Figure 4.19.

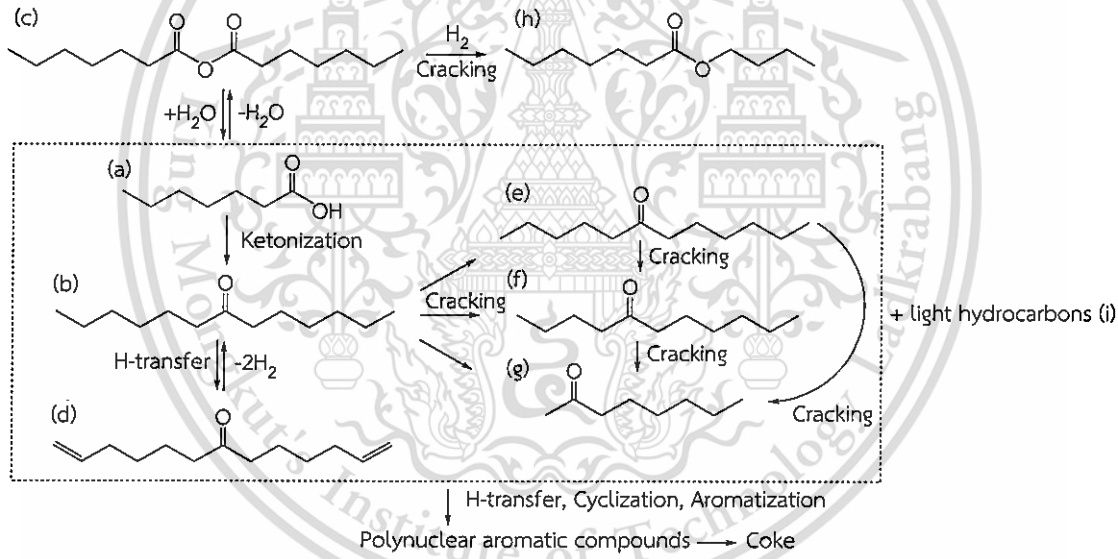

Figure 4.19 Catalytic pathway of the conversion of heptanoic acid in both N_2 and H_2 atmostphere over $K_2Ti_6O_{13}$.

Primarily, heptanoic acid (a) is coupled to 7-tridecanone (b) over oxygen vacancy sites. The presence of heptanoic anhydride (c) may be derived from the dehydration of the acid over some Lewis acid sites. The 7-Tridecanone can be further cracked, producing lower molecular weight ketone (mainly 2-octanone (g)) and some light hydrocarbons (i). 2-Octanone can be further cracked giving smaller products. All products might undergo hydrogen transfer, cyclization, aromatization, or aldol

condensation, resulting in high molecular weight molecules which are the cause of deactivation. The formation of heptanoic butylester (h) is most likely via the hydrogen transfer from coke to heptanoic acid anhydride (c). The presence of H_2 gas enhances the formation of oxygen vacancy sites and regenerate the active sites.

4.2.3 Effect of incorporated metals

From previous section, only major product from deoxygenation is 7-tridecanone. In order to produce long chain olefins, the ketone formed from ketonization can be further hydrogenated (i) to alcohols and subsequently dehydrated (ii) to the olefins [95]. Hydrogenation (i) by metallic Cu, Ni, Co and Pt is well known, while dehydration (ii) can be promoted by surface defect of the support. Accordingly, it is interesting to incorporate active metal such as Co and Pt on $K_2Ti_6O_{13}$ to promote the conversion of fatty acid to long chain olefins via keto-dehydrogenation [96]. As ketonization is carried out at high temperature, sintering of metal can be expected. Hence, Cu and Ni should not be selected in this work [97].

Considering that the metal-free $K_2Ti_6O_{13}$ already shows a complete conversion of heptanoic acid at 200 gh/mol, the contact time in this section should be decreased in order to evaluate the performance of metal-loaded $K_2Ti_6O_{13}$. Contact time of 100 gh/mol (instead of 200 gh/mol) was chosen, while other conditions were kept unchanged (400 °C, and under the stream of H_2).

Figure 4.20 shows the conversion of heptanoic acid and the yields of different products over reduced catalysts with 1wt% Co and 1wt% Pt on the $K_2Ti_6O_{13}$, as compared to the metal-free catalyst.

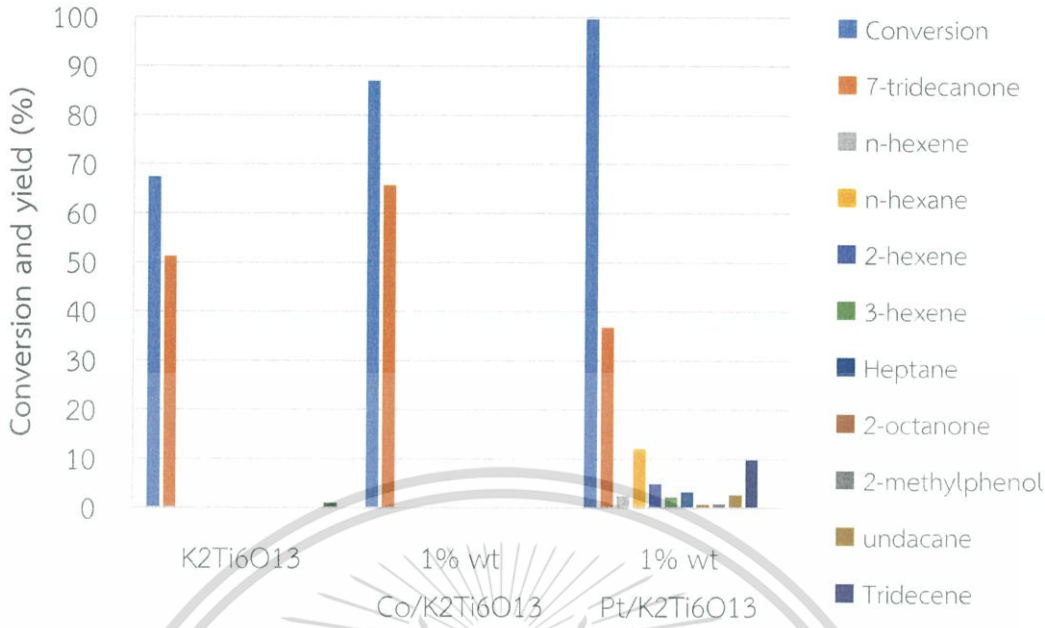

Figure 4.20 The conversion of heptanoic acid and yield of various products over different metal-loaded $K_2Ti_6O_{13}$-based catalysts. *Reaction conditions: $K_2T_6O_{13}$, reduction temperature 400 °C, reaction temperature 400 °C, W/F 100 gh mol^{-1}, atmospheric H_2, at 60 min time on stream.*

It can be seen that the conversion is increased when 1% wt Co and 1% wt Pt are incorporated in $K_2Ti_6O_{13}$. While $K_2Ti_6O_{13}$ gives the conversion of 68%, the cobalt- and platinum-impregnated samples exhibit 89 and 100% conversion, respectively. It is known [98] that these two metals can readily adsorb hydrogen on their surface, thereby assisting the reduction of the $K_2Ti_6O_{13}$ support via a H_2 spillover mechanism (TPR profiles in Figure 4.7). The dissociated hydrogen species on the metal surface can drift through the metal-support interface, enhancing the reduction of the support. As shown in Scheme 4.5, metal assisted hydrogenation boost the surface defects. The highly-active hydrogenation metallic Pt does not only induced H_2-spillover mechanism, but also promoted the Strong Metal-Support Interaction (SMSI). SMSI is a model describing excessive reduction of the surface forming the encapsulated metal sites and novel Ti species [99]. The Ti species, act differentially from the Ti over parent supports, and might be more effective for the ketonization of heptanoic acid.

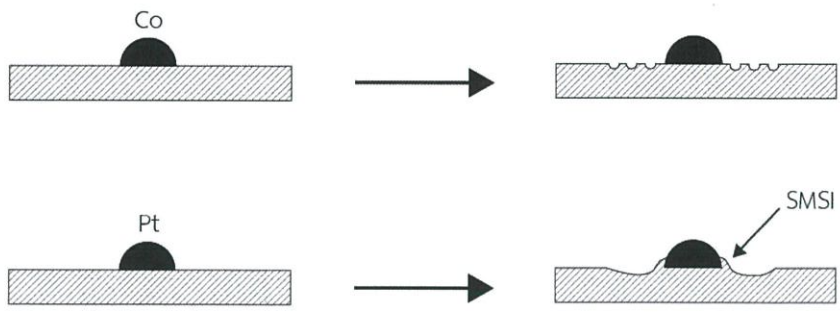

Scheme 4.5

Despite the higher conversion, the selectivity of products over 1%Co/$K_2Ti_6O_{13}$ is rather similar to that over metal-free $K_2Ti_6O_{13}$. This is suggested that Co metal is not active to promote hydrogenation of 7-tridecanone. On the other hand, the different product distribution over 1% Pt/ $K_2Ti_6O_{13}$ could be attributed to the hydrogenation and decarbonylation activity of the SMSI of incorporated Pt. The additional products over 1% wt Pt/$K_2Ti_6O_{13}$ are consisted of all isomers of hexene (8.62 %), hexane (12.03 %), heptane (2.26 %), undecane (2.68 %) and 7-tridecene (9.81 %).

In order to verify the evolution of long chain olefins, 0. 1% wt Pt/ $K_2Ti_6O_{13}$ was tested as a function of the contact time, as depicted in Figure 4.21.

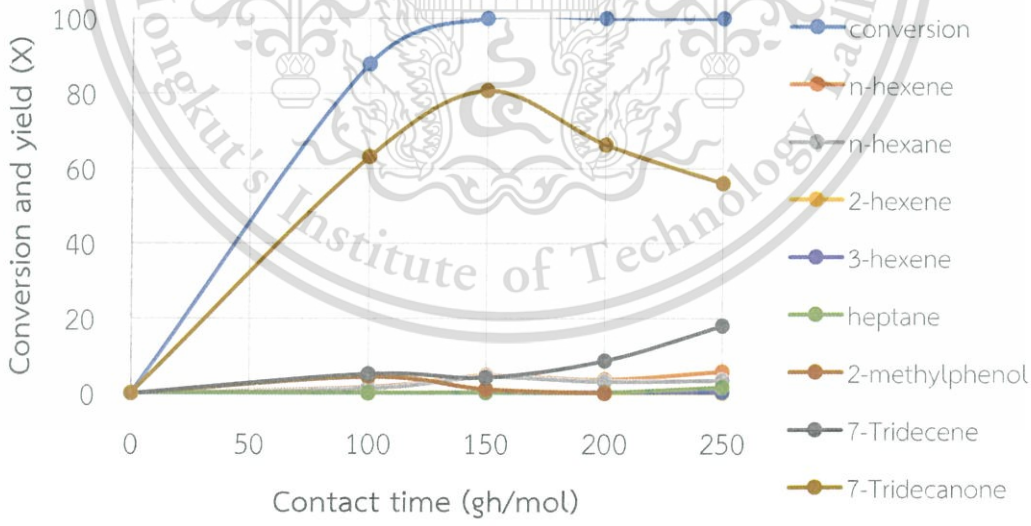

Figure 4.21 The conversion of heptanoic acid and yield of various products at different contact times. *Reaction conditions: 0. 1% wt Pt/ $K_2T_6O_{13}$, reduction temperature 400 °C, reaction temperature 400 °C, atmospheric H_2. The results were averaged from 60-300 min time on stream.*

The yield of 7-tridecanone from heptanoic acid is initially increased with the contact time. However, 7-tridecanone is decreased when the contact time is higher than 150 gh/mol. The decrease in the yield of 7-tridecanone is accompanied by an increase in the yield of 7-tridecene. It is proposed that 7-tridecanone can be hydrated over metallic Pt sites and subsequently dehydrated over Ti^{3+} defects (Equation 4.3).

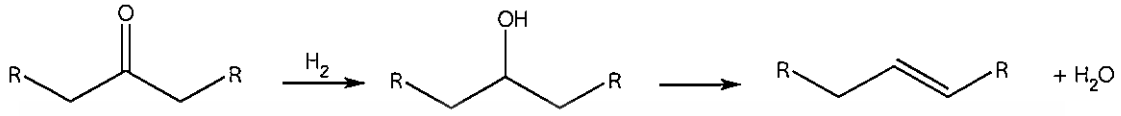

(Equation 4.3)

Furthermore, the presence of heptane at the low contact time suggests that heptanoic acid can be hydrogenolysed over Pt surface (Equation 4.4).

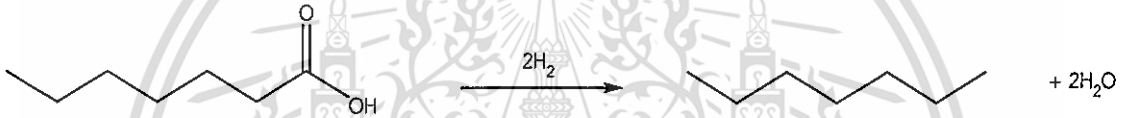

(Equation 4.4)

(Equation 4.5)

The hexenes can be also formed from direct decarbonylation of heptanoic acid (Equation 4.5). Moreover, the Ti^{3+} act as Lewis acid center for the isomerization of hexene to the other isomerism. Considering that various isomers of hexene is increased with the contact time, one can infer that the rate of ketonization (to 7-tridecanone) is faster than that of the decarbonylation (to hexenes).

From the observed results, the extended mechanistic pathway of Pt impregnated sample is proposed in Figure 4.22.

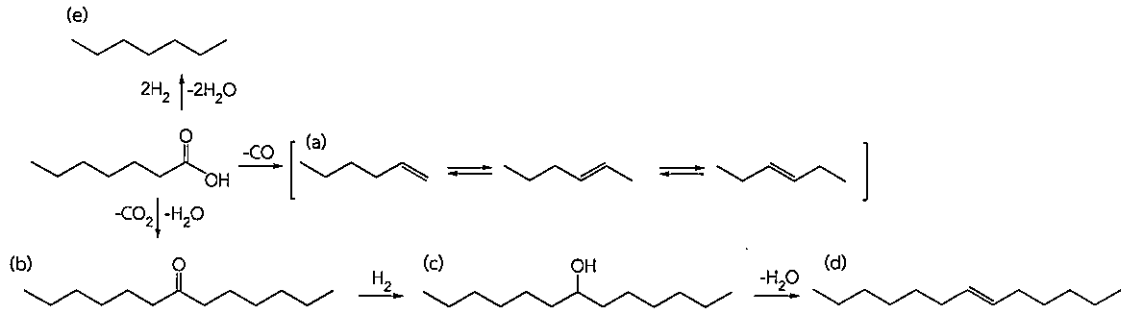

Figure 4.22 the extended mechanistic pathway of $Pt/K_2Ti_6O_{13}$

The decarbonylation and hydrogenolysis of heptanoic acid to form hexene (a) and heptane (e) is directly activated on the Pt surface. The hexene can be isomerized on the Lewis acid Ti^{3+} defects. While the secondary 7-tridecanone obtained can be hydrogenated and dehydrated on the metallic Pt sites to olefins. In other words, the Pt impregnated $K_2Ti_6O_{13}$ yields olefins from (i) directly decarbonylation and (ii) hydrogenation of the ketone produced.

As Pt plays role on the production of long chain olefins, two additional loadings of Pt were applied to $K_2Ti_6O_{13}$ supports are in Figure 4.23.

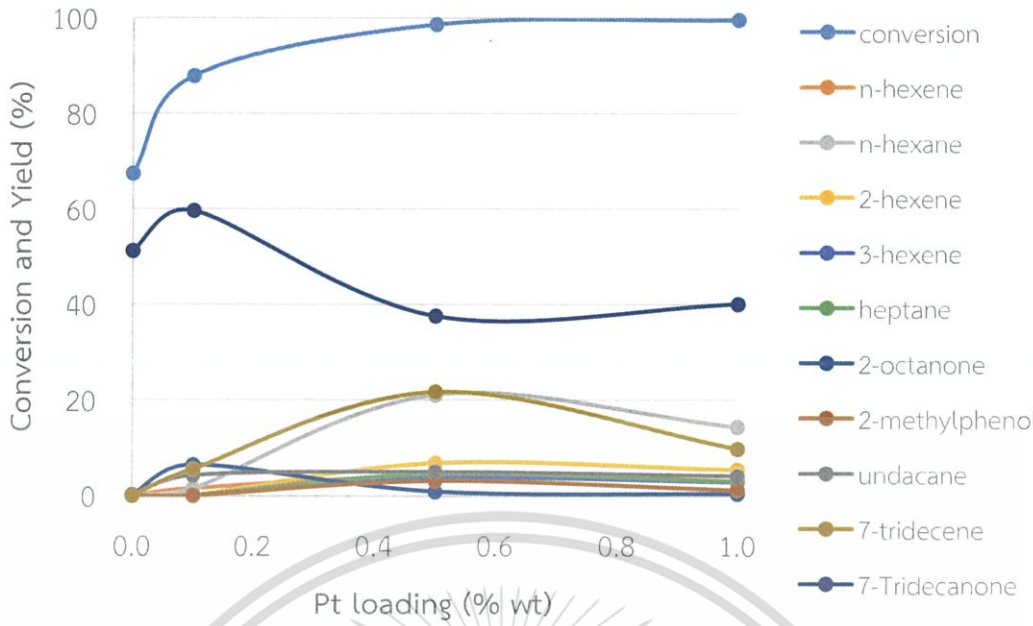

Figure 4.23 The conversion of heptanoic acid and yield of various products over $K_2Ti_6O_{13}$-based catalysts loaded with different amount of Pt. *Reaction conditions: reduction temperature 400 °C, reaction temperature 400 °C, W/F 100 gh/mol, atmospheric H_2, the results were averaged from 60-300 min time on stream.*

The results show that the conversion of heptanoic acid is increased (63.8%, 88.9%, 99.8% and 100.0%) as the Pt loading is increased (free metal $K_2Ti_6O_{13}$, 0.1%, 0.5%, and 1.0%). As mention previously, a metal especially Pt assists the hydrogenation of the support. Yet, the reaction sequence and the product distribution are rather dependent on the Pt loading. The 7-tridecanone is decreased with the increase in Pt loading. While 7-tridecene, hexene, hexane and heptane are increased with higher metallic Pt. These are evidence of decarbonylation and hydrogenation on H_2 of Pt. Metallic Pt can permits the keto- hydrogenation and also extends the direct decarboynylation of heptanoic acid. However, at 1.0 wt of Pt the carbon balance is reduced to 93% while 0.5% wt of Pt is showed up to 97% carbon balance. This is probably because of the extreme hydrogenolysis at excessive metallic Pt sites. The severe hydrogenolysis produces light gas fraction such as methane and ethane.

This valuable information throughout the thesis can be applied for the conversion of fatty acid that composed of higher carbon chain. In this work, lauric acid would be selected as a representative fatty acid derivation.

4.2.4 Production of long chain olefins from lauric acid

0.1% wt $Pt/K_2Ti_6O_{13}$ reduced at 400 °C was studied further as a catalyst on the production of long chain olefins from the higher fatty acid "Lauric acid". The reaction is carried out at 400 °C, W/F 250 gh/mol, under H_2 atmosphere. As shown in Figure 4.24, the conversion of lauric acid is still 100% at contact time 250 gh/mol.

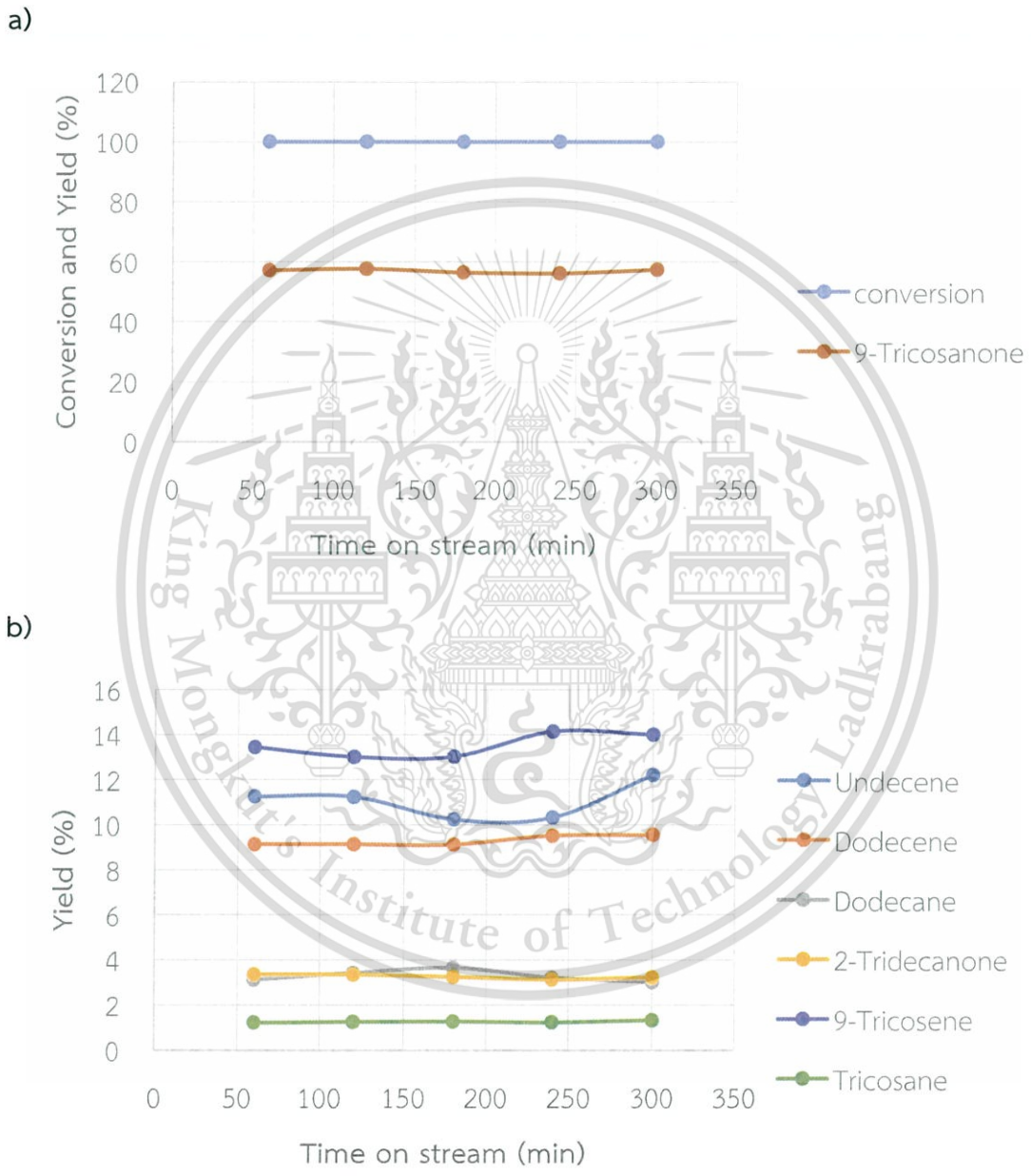

Figure 4.24 The conversion of lauric acid and yield of major product **(a)** and yield of by- products **(b)** *Reaction conditions: 0. 1% Pt/ $K_2T_6O_{13}$, reaction temperature 400 °C, reduction temperature 400 °C, under atmospheric N_2 at 60-300 min time on stream.*

As expected, the ketonization of lauric acid gives 9-tricosanone (56.7%) as a major product and the cracking of this ketone provides 2-tridecanone (3.1%). The hydrocarbon products are undecene (13.8%), dodecene (9.12%) from decarbonylation and hydrogenolysis of lauric acid, respectively. The hydrogenation of dodecene gives dodecane (3.1%). As compared to heptanoic acid (7-tridecanone = 69.2%), the primary ketone is decreased. In contrast, the decarbonylation and hydrogenolysis products are increased with lauric acid (13.8 from 5.8% and 9.1 from 1.6% in heptanoic acid respectively). These results indicate that lauric acid interacts with surface of Pt higher than that of the surface oxygen vacancy. Hence, monomolecular reaction over the Pt would be promoted while the bimolecular reaction over the support is limited.

From the products observed, it is possible to extend the use of fatty acid in industrial and domestic application as demonstrated in Table 4.7

Table 4.7 Application of products derivative from parent fatty acid

Feeds	Applications			
	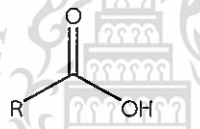	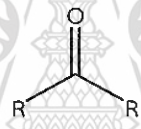		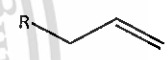
Acetic acid	Vinegar	<u>Acetone</u> • Solvents • Feedstock • Food additives • Remover • Chemical peeling	<u>Ethylene</u> • Feedstock • Fruit ripening	-
Heptanoic acid	• Steroid drugs • Cigarette additives • Artificial flavor	<u>7-tridecanone</u> • Feedstock • Perfumes • Insect resistance	<u>7-tridecene</u> • Feedstock • Solvents • Heat transfer fluid • Liquid fuel	<u>Hexene</u> • Surfactant • Feedstock • Colloidal quantum dot

Table 4.7 Application of products derivative from parent fatty acid (continued)

Feeds	Applications			
	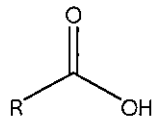	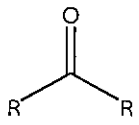	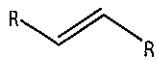	
Lauric acid	• Steroid drugs • Cigarette additives • Artificial flavor	<u>9-tricosanone</u> • Feedstock • Perfumes	<u>9-tricosene</u> • Feedstock • Solvents • Heat transfer fluid • Liquid fuel	<u>Dodecene</u> • Medical treatment • Serum Cholesterol control Surfactant

The ketonization products are mainly used in chemical feedstock or primary products in organic synthesis. Moreover, the higher ketone has been used as fragrance and artificial flavor for food in the last decade. Long chain olefins are used in either of petrochemical and organic synthesis. With the likewise functional molecule, the double bond can be anchored with several of molecules such as sulfonate group and hydroxyl group and even hydrogenated to liquid fuel like gasoline. Especially, α-olefins can be used as cleaning agent, surfactant and soup [33].

CHAPTER 5

Conclusion and Suggestion

5.1 Conclusions

In this thesis, the mechanistic study on the conversion of heptanic acid to long chain olefins over various titanate catalysts were investigated. The effect of structures (tunneled and step-liked layered), compensating cations (Li^+, Na^+ and K^+), impregnated metals (Co and Pt) were investigated.

The structure of tunneled titanates, $A_2Ti_6O_{13}$ (A = Li^+, Na^+ and K^+) is more rigid than that of the layered titanates ($Na_2Ti_3O_7$ and $K_2Ti_6O_{13}$), which relates to high reducibity and activity of the tunneled, as compared to the layered. For the difference compensating cations in the tunneled, the large cation (K) can be easily reduced. Besides, the Li^+ is in distorted LiO_{3+1} square planar geometry can be easily reduced, as compared to Na that are distorted square prismatic polyhedron configuration. The step-liked titanate is thermally stable up to 700 °C. It can be coordinately rearranged into the tunneled structure at high temperature. These samples possessed both of reducibility and basic properties. The high reducible sample shows the high deoxygenation activity. While the basicity is relatively weak, as compared to the typical basic oxide, MgO, and play no role in the conversion of fatty acid to long chain olefins.

Form the mechanistic point of view, the products formed from fatty acid takes place via two mechanisms. The ketonization (i) follows by cracking forming olefins and short chain ketone, and the direct decarbonylation (ii) generating just olefins and CO_2. The reactivity order of the ketonization surely corresponds to the reducibility. However, at relatively high reduction temperature, the activity is suppressed due to the decrease in oxygen vacancy sites by single electron transfer from the surface into the bulk or oxygen replenishment from the bulk to the surface. With the hydrogen assistant, the ketonization of fatty acid is enhanced due to the generation of the reduced site. Moreover, it also prevents the formation of carbon deposits onto the surface of catalysts. The decarbonylation of fatty acid is not observed over all titanates due to the weak basicity. From integral results, it is concluded that just only the first mechanistic pathway, ketonization of fatty acid, is pronounced over the pure titanates.

Metal impregnated samples (Co and Pt) can promote the reduction of parent supports that enhance the ketonization of fatty acid. Especially, Pt impregnated sample, the support is easily reduced due to the Strong Metal Support Interaction (SMSI). The Pt loaded catalyst can also promote the hydrogenation of the ketone formed to the higher secondary alcohol that is further dehydrated to long chain olefins. Moreover, the direct decarbonylation and decarboxylation of fatty acid to relatively shorter olefins, paraffins, CO and CO_2 can be promoted. Nevertheless, the catalyst with relatively high Pt content can also produce light hydrocarbon gas such as methane and ethane by the excessive hydrogenolysis.

Although the titanates show both reducibility and basic property, but only the reducibility predominately affects the long chain olefins production. In addition, the incorporated Pt can promote the formation of long chain olefins via hydrogenation-dehydration of ketone produced instead of cracking of higher ketone to smaller olefins.

5.2 Suggestions

5. 2. 1 An elevated H_2 partial pressure might promotes the hydrogen dissociation compress atmospheric hydrogen on metallic cobalt surface resulting on hydrogenation of 7-tridecanone without hydrogenolysis like Pt.

5. 2. 2 To crash the thermodynamic barrier, H species on the surface that is associated from fatty acid would be discouraged.

5.2.3 Ketonization of bimolecular fatty acid would be increased with the decrease of carrier gas flow rate.

References

[1]. Amin, M.A., Mohsen, Q., Mostafa, N.Y., El-Bagoury, N., Al-Refaie, A., Bairamov, A.K., Al-Maaesab, S., Murill, E.M. and Al-Qahtani, S.A. 2014. "Case study: Corrosion behavior of constructive alloys in linear alpha olefin environment." International Journal of Electrochemical Science. 9 : 2631 – 2648.

[2]. Kurokawa, H., Miura, K., Yamamoto, K., Sakuragi, T., Sugiyama, T., Ohshima, M. and Miura, H. 2013. "Oligomerization of ethylene to produce linear α-olefins using heterogeneous catalyst prepared by immobilization of α-diiminenickel(II) complex into fluorotetrasilicic." Catalysts. 3 : 125-136.

[3]. Zohreh, R.A., Manenti, F., Corbetta, M., Pirola, C. and Ranzi, E. 2015. "Biomass gasification using low-temperature solar-driven steam supply." Renewable Energy. 74 : 671-680.

[4]. Jinhua, J., Gao, Q. and Chen, Z. 2008. "Gold nanocatalysts supported on protonic titanate nanotubes and titania nanocrystals." Journal of Molecular Catalysis A: Chemical. 280(1-2) : 233–239.

[5] Farfan-Arribas, E. and Mardix, R.J. 2003. "Different binding sites for methanol dehydrogenation and deoxygenation on stoichiometric and defective TiO_2 (*110*) surfaces." Surface science. 544(2-3) : 241-260.

[6] Szilvia, P., Laszlo, K., Vera, M., Pegie, C., Etienne, F.V. and Imre, D. 2005. "The influence of temperature on the structural behaviour of sodium tri- and hexa-titanates and their protonated forms." Journal of Solid State Chemistry. 178(5) : 1614–1619.

[7] Gunstone, F.D., 1999. **An Introduction to the chemistry and biochemistry of fatty acids and their glycerides.** London : Chapman and Hall.

[8] Siedlecka, E.M., Kumirska, J., Ossowski, T., Glamowski, P., Gotebiowski, M., Gajdus, J., Kaczynski, Z. and Stepnowski, P. 2008. "Determination of volatile fatty acids in environmental aqueous samples." Journal of Environmental Studies. 17(3) : 351-356.

[9] Jones, J.H. 2000. "The cativa process for the manufacture plant of acetic acid : iridium catalyst improves productivity in an established industrial process." Platinum Metals Review. 44(3) : 94-105.

[10] Gunstone, F.D. 1999. **Fatty Acid and Lipid Chemistry.** Maryland: An Aspen Publication.

[11] Shakhashiri. 2008. Chemical of the week. [Online].

Available : http://scifun.chem.wisc.edu/chemweek/pdf/aceticacid.pdf

[12] Aparadh, V.T. and Karadge, B.A. 2010. "Fatty acid composition of seed oil from some *Cleome* species." Pharmacognosy Journal. 2(10 : 324-327.

[13] Shahidi, F. 2005. **Baily's Industrial Oil and Fat Products.** John Wiley & Sons : German.

[14] Świzdor, A., Panek, A., Milecka-Tronina, N. and Kołek, T. 2012. "Biotransformations ytilizing *β*-oxidation cycle reactions in the synthesis of natural compounds and medicines." International Journal of Molecular Sciences. 13(12) : 16514-16543.

[15] Glinski, M. and Kijenski, J. 2000. "Decarboxylative coupling of heptanoic acid. Manganese, cerium and zirconium oxides as catalysts." Applied Catalysis A: General. 190(1-2) : 87–91.

[16] Lappin, G.R. and Sauer, J.D. 1989. **Alpha Olefins Applications Handbook.** USA : Marcel Dekker.

[17] Alsobaai, A.M., Shaibani, A.M.A., Moustafa, T. and Derhem, A. 2012. "Effect of hydrogenation temperature on the palm mid-fraction fatty acids composition and conversion." Journal of King Saud University-Engineering Sciences. 24(1) : 45-51.

[18] Saeb, M.R., Mohammadi, Y., Ahmadi, M., Khorasani, M.M. and Stadler, F.J. 2015. "A Monte Carlo-based feeding policy for tailoring microstructure of copolymer chains: Reconsidering the conventional metallocene catalyzed polymerization of α-olefins." Chemical Engineering Journal. 274 : 1385-8947.

[19] Chiappero, M., Do, P.T.M., Crossley, S., Lobban, L.L. and Resasco, D.E. 2011. "Direct conversion of triglycerides to olefins and paraffins over noble metal supported catalysts." Fuel. 90(3) : 1155-1165.

[20] Cao, L. and Zhang, S. 2015. "Production and characterization of biodiesel derived from Hodgsonia macrocarpa seed oil." Applied Energy. 146 : 135-140.

[21] Clark, J., 2002, The mechanism for the esterification reaction. [Online]. Available: http://www.chemguide.co.uk/physical/catalysis/esterify.html

[22] L.G. Wade, Jr. 2013. **Organic chemistry.** USA : Pearson education.

[23] Manríquez-Ramírez, M., Gómez, R., Hernández-Cortezc, J.G., Zúniga-Moreno, A., Reza-San Germána, C.M. and Flores-Valle, S.O. 2013. "Advances in the transesterification of triglycerides to biodiesel using MgO–NaOH, MgO–KOH and MgO–CeO_2 as solid basic catalysts." Catalysis Today. 212(1) : 23-30.

[24] Fu , J., Chen, L., Lv, P., Yang, L. and Yuan, Z. 2015. "Free fatty acids esterification for biodiesel production using self- synthesized macroporous cation exchange resin as solid acid catalyst." Fuel. 154(15) : 1-8.

[25] Pham, T.N., Shi, D. and Resasco, D.E. 2014. "Reaction kinetics and mechanism of ketonization of aliphatic carboxylic acids with different carbon chain lengths over Ru/TiO_2 catalyst." Journal of Catalysis. 314 : 149-158.

[26] Santillan-Jimenez, E., Morgan, T., Shoup, J., Harman-Ware, A.E. and Crocker, M. 2014. "Catalytic deoxygenation of triglycerides and fatty acids to hydrocarbons over Ni–Al layered double hydroxide." Catalysis Today. 237 : 136-144.

[27] Yang, C., Nie, R., Fu, J., Hou, Z. and Lu, X. 2013. "Production of aviation fuel via catalytic hydrothermal decarboxylation of fatty acids in microalgae oil." Bioresource Technology. 146 : 569–573.

[28] Hermida, L., Abdullah, A.Z. and Mohamed, A.R. 2015. "Deoxygenation of fatty acid to produce diesel-like hydrocarbons: A review of process conditions, reaction kinetics and mechanism." Renewable and Sustainable Energy Reviews. 42 : 1223–1233.

[29] Guo, D. and Hu, C. 2012. "First-principles study on the electronic structure and optical properties for SnO_2 with oxygen vacancy." Applied Surface Science. 258(18) : 6987–6992.

[30] Curtis, N., Kang, S.C., Choi, S., Oh, S.H. and Park, Y.K. 2015. "A Catalytic Cracking Process for Ethylene and Propylene from Parafin streams: The Advanced Cataltic Olefins (OXO) Process." **Prepared for Presentation at the 2007 Spring National Meeting – Houston.** Texas KBR Internal Reference Paper.

[31] Kurokawa, H., Miura, K., Yamamoto, K., Sakuragi, T., Sugiyama, T., Ohshima, M. and Miura, H. 2013. "Oligomerization of Ethylene to Produce Linear α-Olefins Using Heterogeneous Catalyst Prepared by Immobilization of α-Diiminenickel(II) Complex into Fluorotetrasilicic Mica Interlayer." Catalysts. 3(1) : 125-136.

[32] Arthur, A., Madden, W., Percy, R. and Soliman, E. 2013. "Ethylene to linear alpha olefins (1-hexene & 1-octene)." Chemical Engineering. 459. University of Pennsylvania.

[33] Lappin, G.R. and Sauer, J.D. 1989. **Alpha Olefins Application Handbook.** United State of America : MARCEL DEKKER.

[34] Kolba, N., Winklera, M., Syldatkb, C. and Meier, M. 2014. "Long-chain polyesters and polyamides from biochemically derived fatty acids." European Polymer Journal. 51 : 159–166.

[35] Lennen, R.M. and Pfleger, B.F. 2013. "Microbial production of fatty acid-derived fuels and chemicals." Current Opinion in Biotechnology. 463 : 1044–1053.

[36] Dinga, Y.J., Zhaob, X.E., Zhua, F., Suob, Y.R., Lib, Y.L., Chenb, G.C. and You, J.M. 2007. "Identification of long-chain unsaturated fatty acids in deep-sea fish oil by liquid chromatography/mass spectrometry/atmospheric pressure chemical ionization." Chinese Journal of Analytical Chemistry. 35(3) : 375–381.

[37] Pyla, S.P., Schietekata, C.M., Reyniersa, M.F., Abharib, R., Marina, G.B. and Van Geema, K.M. 2011. "Biomass to olefins: Cracking of renewable naphtha." Chemical Engineering Journal. 176–177 : 178–187

[38] Zakariaa, Z.Y. Amina, N.A.S. and Linnekoskib, J. 2013. "A perspective on catalytic conversion of glycerol to olefins." Biomass and Bioenergy. 55 : 370–385.

[39] Zakariaa, Z.Y., Amina, N.A.S. and. Linnekoskib, J. 2014. "Optimization of catalytic glycerol steam reforming to light olefins using Cu/ZSM-5 catalyst." Energy Conversion and Management. 86 : 735–744.

[40] Kim, K.S. and Barteau, M.A. 1990. "Structure and composition requirements for deoxygenation, dehydration, and ketonization reactions of carboxylic acids on TiO_2(001) single-crystal surfaces." Journal of Catalysis. 125(2) : 353–375.

[41] Xiong, L.B., Li, J.H., Yang, B. and Yu, Y. 2011. "Ti^{3+} in the Surface of Titanium Dioxide: Generation, Properties and Photocatalytic Application." Journal of Nanomaterials. 2012(9) : 13.

[42] Wendt, S., Schaub, R., Matthiesen, J., Vestergaard, E.K., Wahlström, E., Rasmussen, M.D., Thostrup, P., Molina, L.M., Lægsgaard, E., Stensgaard, I., Hammer, B. and Besenbacher, F. 2005. "Oxygen vacancies on TiO_2 (*110*) and their interaction with H_2O and O_2: A combined high-resolution STM and DFT study." Surface Science. 598(1-3) : 226–245.

[43] Zhang, Z., Long, J., Xie, X., Zhuang, H., Zhou, Y., Lin, H., Yuan, R., Dai, W., Ding, Z., Wang, X. and Fu, X. 2012. "Controlling the synergistic effect of oxygen vacancies and N dopants to enhance photocatalytic activity of N-doped TiO_2 by H_2 reduction." Applied Catalysis A: General. 425–426 : 117–124.

[44] Maa, M., Lub, Z., Tangc, Y., Lia, T., Tanga, Z. and Yangb, Z. 2014. "Effect of lattice strain on the oxygen vacancy formation and hydrogen adsorption at CeO_2 (*111*) surface." Physics Letters A. 378(34) : 2570–2575.

[45] Nagashima, O., Sato, S., Takahashi, R. and Sodesawa, T. 2005. "Ketonization of carboxylic acids over CeO_2-based composite oxides." Journal of Molecular Catalysis A: Chemical. 227(1-2) : 231–239.

[46] Laia, C.L., Huangb, H.L., Shena, J.H., Wanga, K.K. and Gana, D. 2015. "The formation of anatase TiO_2 from TiO nanocrystals in sol–gel process." Ceramics International. 41(3) : 5041–5048.

[47] Yang, H.G., Sun, C.H., Qiao, S.Z., Zou, J., Liu, G., Smith, S.C., Cheng, H.M. and Lu, G.Q. 2008. Anatase TiO_2 single crystals with a large percentage of reactive facets. [Online].

Available: http://www.canli.dicp.ac.cn/Gruop%20Seminars%20Pdf/20080607qxus1.pdf

[48] Regalbuto, J. 2007. **Catalyst preparation: science and engineering.** Boca Raton : CEC Press.

[49] Ohno, T., Sarukawa, K., Tokieda, K. and Matsumura, M. 2011. "Morphology of a TiO_2 Photocatalyst (Degussa, P-25) Consisting of Anatase and Rutile Crystalline Phases." Journal of Catalysis. 203(1) : 82–86.

[50] Wanga, C., Liua, H., Liua, Y., Heb, G. and Jiangc, C. 2014. "Comparative activity of TiO_2 microspheres and P25 powder for organic degradation: Implicative importance of structural efects and organic adsorption." Applied Surface Science. 319 : 2–7.

[51] Vijayabalan, A., Selvam, K., Velmurugan, R. and Swaminathan, M. 2009. "Photocatalytic activity of surface fluorinated TiO_2-P25 in the degradation of Reactive Orange 4." Journal of Hazardous Materials. 172(2-3) : 914–921.

[52] Shi, Y., Zhao, L., Wang, S., Li, J., Dong, B., Xu, Z. and Wan, L. 2014. "Double-layer composite film based on hollow TiO_2 boxes and P25 as photoanode for enhanced efficiency in dye-sensitized solar cells." Materials Research Bulletin. 59 : 370–376.

[53] Riedel, R. 2004. **Handbook of ceramic hard materials.** Wiley-VCH : German.

[54] González, F., Munuera, G. and Prieto, J.A. 1978. "Mechanism of ketonization of acetic acid on anatase TiO_2 surfaces." Journal of the Chemical Society, Faraday Transactions 1: Physical Chemistry in Condensed Phases. 74(0) : 1517-1529.

[55] Hyushin, G.D. 2006. "Hydrothermal crystallization of $Na_2Ti_6O_{13}$, $Na_2Ti_3O_7$, and $Na_{16}Ti_{10}O_{28}$ in the NaOH-TiO_2-H_2O system at a temperature of 500°C and a pressure of 0.1 GPa: The structural mechanism of self-assembly of titanates from suprapolyhedral clusters." Crystallography Reports. 51(4) : 715-723.

[56] Zaremba, T. and Hadryś A. 2014. "Synthesis of $K_2Ti_4O_9$ whiskers." Journal of Materials Science. 39(14) : 4561-4568.

[57] Zhaoa, Y., Jinb, J. and Yanga, X. 2007. "Hydrothermal synthesis of titanate nanowire arrays." Materials Letters. 61(2) : 384–388.

[58] Niu, L., Shao, M., Wang, S., Lu, L., Gao, H. and Wang, J. 2008 "Titanate nanotubes: preparation, characterization, and application in the detection of dopamine." Journal of Materials Science. 43(5) : 1510-1514.

[59] Bellat, V., Chassagnon, R., Heintz, O., Saviot, L., Vandroux, D. and Millot, N. 2015. "A multi-step mechanism and integrity of titanate nanoribbons." Dalton Transaction. 44(3) : 1150-1160.

[60] Yin, K. and Zhao, X. 2005. "Titanate nano-whisker electrorheological fluid with high suspended stability and ER activity." Nanotechnology. 17(1) : 192.

[61] Kunadian, I, Lipka, S. M., Le, C., Chen, L. and Christopher, R. 2010 "Electrochemical performance of hydrothermally synthesized lithium titanate nanospheres." **218th ECS Meeting.**

[62] Yua, H., Yua, J., Chenga, B. and Linb, J. 2007. "Synthesis, characterization and photocatalytic activity of mesoporous titania nanorod/titanate nanotube composites." Journal of Hazardous Materials. 147(1-2) : 581–587.

[63] Akimoto, J. and Takei, H. 1990 "$Na_{1.7}Ti_6O_{11}$: A new mixed- valence nonstoichiometric sodium titanate with a tunnel structure." Journal of Solid State Chemistry. 85(1) : 8–14.

[64] Zhang, T., Li, D., Tao, Z. and Chen, J. 2013. "Understanding electrode materials of rechargeable lithium batteries via DFT calculations." Progress in Natural Science: Materials International. 23(3) : 256–272.

[65] Yang, D., Sarina, S., Zhu, H., Liu, H., Zheng, Z., Xie, M., Smith, S.V. and Komarneni, S. 2011. "Capture of radioactive cesium and iodide ions from water by using titanate nanofibers and nanotubes." Angewandte Chemie International Edition. 50(45) : 10594 –10598.

[66] Kiatkittiponga, K., Iwaseb, A., Scottb, J. and Amalb, R. 2013. "Photocatalysis of heat treated sodium- and hydrogen-titanate nanoribbons for water splitting, H_2/O_2 generation and oxalic acid oxidation." Chemical Engineering Science. 93 : 341–349.

[67] Tanaka, T., Kumagai, H., Hattori, H., Kudo, M. and Hasegawa, S. 1991. "Generation of basic sites on TiO_2 by reduction with H_2." Journal of Catalysis. 127(1) : 221–226.

[68] Santillan-Jimenez, E., Morgan, T., Shoup, J., Harman-Ware, A.E. and Crocker, M. 2014. "Catalytic deoxygenation of triglycerides and fatty acids to hydrocarbons over Ni–Al layered double hydroxide." Catalysis Today. 237(15) : 136–144.

[69] HUANG, X., Zhang, Q. Wang, T., Liua, Q., Ma, L. and Zhang, Q. 2012. "Production of jet fuel intermediates from furfural and acetone by aldol condensation over MgO/NaY." Journal of Fuel Chemistry and Technology. 40(8) : 973–978.

[70] Glińskia, M., Zalewskia, G., Burnoa, E. and Jerzakb, A. 2014. "Catalytic ketonization over metal oxide catalysts. XIII. Comparative measurements of activity of oxides of 32 chemical elements in ketonization of propanoic acid." Applied Catalysis A: General. 470, 278–284.

[71] Santillan-Jimenez, E., Morgan, T., Loe, R. and Crocker, M. 2014. "Continuous catalytic deoxygenation of model and algal lipids to fuel-like hydrocarbons over Ni–Al layered double hydroxide." Catalysis Today. 258 : 284-293.

[72] Detonia, C., Bertellab, F., Souzaa, M.M.V.M, Pergherb, S.B.C. and Arandaa, D.A.G. 2014. "Palladium supported on clays to catalytic deoxygenation of soybean fatty acids." Applied Clay Science. 95 : 388–395.

[73] Shima, J., Jeonga, D., Janga, W., Jeona, K., Jeona, B., Choa, S.Y., Roha, H., Nab, J., Koc, C.H., Ohb, Y. and Hanb, S.S. 2014. "Deoxygenation of oleic acid over $Ce_{(1-x)}Zr_{(x)}O_2$ catalysts in hydrogen environment." Renewable Energy. 65 : 36–40.

[74] Dararat, C., Kulrat, T. and Soontontaweesab, S., 2013, "Deoxygenation of palmitic acid over cerium-metal oxide" Faculty of science, **King Mongkut's Institute Technology of Ladkrabang.**

[75] Limsakul, K., Juntarachairot, S. and Sangsan, S., 2013. "Deoxygenation of palmitic acid over Lepidocrocite titanate catalysts", Faculty of science, **King Mongkut's Institute Technology of Ladkrabang.**

[76] Pham, T., Shi, D. and Resasco, D.E. 2014. "Reaction kinetics and mechanism of ketonization of aliphatic carboxylic acids with different carbon chain lengths over Ru/TiO_2 catalyst." Journal of Catalysis. 314 : 149–158.

[77] Cai, J., Zhu, Y., Liu, D., Meng, M., Hu, Z. and Jiang, Z. 2015. "Synergistic effect of Titanate-Anatase heterostructure and hydrogenation-induced surface disorder on photocatalytic water splitting." ACS Catalysis. 5(3) : 1708–1716.

[78] Irawa, H., Klkkawa, S. and Koirunj, M. 1982. "Ion exchange and dehydration of layered titanates, $Na_2Ti_3O_7$ and $K_2Ti_4O_9$." Journal of Physical Chemistry. 86(52) : 5023-5026.

[79] Pappa, S., Korasia, L., Meynenb, V. and Cool, P. 2005. "The influence of temperature on the structural behaviour of sodium tri- and hexa-titanates and their protonated forms." Journal of Solid State Chemistry. 178 : 1614–1619.

[80] Irawa, H., Klkkawa, S. and Koirunj, M. 1982. "Ion exchange and dehydration of layered titanates, $Na_2Ti_3O_7$ and $K_2Ti_4O_9$." Journal of Physical Chemistry. 86 : 5023-5026.

[81] Li, L., Zhang, Y.C. and Zhang, M. 2012. "Low temperature preparation and optical properties of $K_2Ti_6O_{13}$." Materials Letters. 79 : 136–138.

[82] Pérez-Flores, J.C., Kuhn, A. and García-Alvarado, F. 2011. "Synthesis, structure and electrochemical Li insertion behaviour of $Li_2Ti_6O_{13}$ with the $Na_2Ti_6O_{13}$ tunnel-structure." Journal of Power Sources. 196(3) : 1378–1385.

[83] Sauvet, A-L., Baliteau, S., Lopez, C. and Fabry, P. 2004. "Synthesis and characterization of sodium titanates $Na_2Ti_3O_7$ and $Na_2Ti_6O_{13}$." Journal of Solid State Chemistry. 177(12) : 4508–4515.

[84]Pérez-Flores, J.C., García-Alvarado, F., Hoelzel, M., Sobrados, I., Sanzc, J. and Kuhn, A. 2012. "Insight into the channel ion distribution and influence on the lithium insertion properties of hexatitanates $A_2Ti_6O_{13}$ (A = Na, Li, H) as candidates for anode materials in lithium-ion batteries." Dalton Transaction. 41(48) : 14633.

[85] Kikkawa, S., Yasuda, F. and Koizumi, M. 1985. "Ionic conductivities of $Na_2Ti_3O_7$, $K_2Ti_4O_9$ and their related materials." Materials Research Bulletin. 20(10) : 1221–1227.

[86] Zheng, Z.Q. and Zhou, X.P. 2013. "Reduction of Ti^{4+} to Ti^{3+} in boron-doped $BaTiO_3$ at very low temperature." Journal of the American Ceramic Society. 96(11) : 3504-3510.

[87] Bouzoubaa, A., Markovits, A., Calatayud, M. and Minot, C. 2005. "Comparison of the reduction of metal oxide surfaces: TiO_2-anatase, TiO_2-rutile and SnO_2-rutile." Surface Science. 583(1) : 107–117.

[88] Colmenares, J.C., Magdziarz, A., Aramendia, M.A., Marinas, A., Marinas, J.M., Urbano, F.J. and Navio, J.A. 2011. "Influence of the strong metal support interaction effect (SMSI) of Pt/TiO_2 and Pd/TiO_2 systems in the photocatalytic biohydrogen production from glucose solution." Catalysis Communications. 16(1) : 1–6.

[89] de Lange, M.W. 2000. **Selective deoxygenation of carboxylic acid.** Innovation Oriented reseach Programme on Catalysis.

[90] Liu, H., Ma, H.T., Li, X.Z., Li, W.Z., Wu, M. and Bao, X.H. 2003. "The enhancement of TiO_2 photocatalytic activity by hydrogen thermal treatment." Chemosphere. 50(1) : 39-46.

[91] Fa-Qiang, X., Rui-Ling, H., Xu-Xia, L., Jin-Zhen, X., Shu-Ling, L. and Shi-Kong, S., 1997. "Study on the mobility and reactivity of oxygen of ceria-based OCM catalysts by temperature programmed pulse reaction (TPPR)." Journal of Natural Gas Chemistry. 6(4) : 265-274.

[92] Sooknoi, T., Danuthai, T., Lobban, L.L., Mallinson, R.G. and Resasco, D.E. 2008. "Deoxygenation of methylesters over CsNaX." Journal of Catalysis. 258(1) : 199–209.

[93] Marciniak, B. 1988. "Photochemistry of phenyl alkyl ketones: The "Norrish type II" photoreaction: An organic photochemistry experiment." Journal of Chemical Education. 65(9) : 832.

[94] Pham, T.N., Shi, D. and Resasco, D.E. 2014. "Kinetics and Mechanism of Ketonization of Acetic Acid on Ru/TiO_2 Catalyst." Topics in Catalysis. 57(6) : 706-714.

[95] Bryant, D.E. and Kranich, W.L. 1967. "Dehydration of alcohols over zeolite catalysts." Journal of Catalysis. 8(1) : 8–13.

[96] Witsuthammakul, A. and Sooknoi, T. 2015. "Selective hydrodeoxygenation of bio-oil derived products: ketones to olefins." Catalysis Science & Technology. 5(7) : 3639-3648.

[97] Phichitsurathaworn, P., Ketaniruj, S. and Sitthithai, S. 2014. "Conversion of ethanol to gasoline over metal transition loaded H-ZSM-5 zeolite catalysts." Faculty of science. King Mongkut's Institute Technology of Ladkrabang.

[98] Bartholomew, C.H. 1990. "Hydrogen adsorption on supported cobalt, iron, and nickel." Catalysis Letters. 7(1) : 27-51.

[99] Rui, Z., Chen, L., Chen, H. and Ji, H. 2014, "Strong metal-support interaction in Pt/TiO_2 induced by mild HCHO and $NaBH_4$ solution reduction and its effect on catalytic toluene combustion", Industrial & Engineering Chemistry Research. 53 : 15879–15888.

APPENDICES

APPENDIX A

TPR SIGNAL EVALUATION

The electronic signal from the TCD detector during TPR analysis is converted to mmol H_2, employing CuO as a standard. Here, CuO is used because it is a highly-reducible metal with clean and well-known reduction giving Cu metal as a final product following the equation:

$$CuO(s) + H_{2(g)} \rightarrow Cu(s) + H_2O(g)$$

An example of TPR profile of CuO is shown in Figure A1.

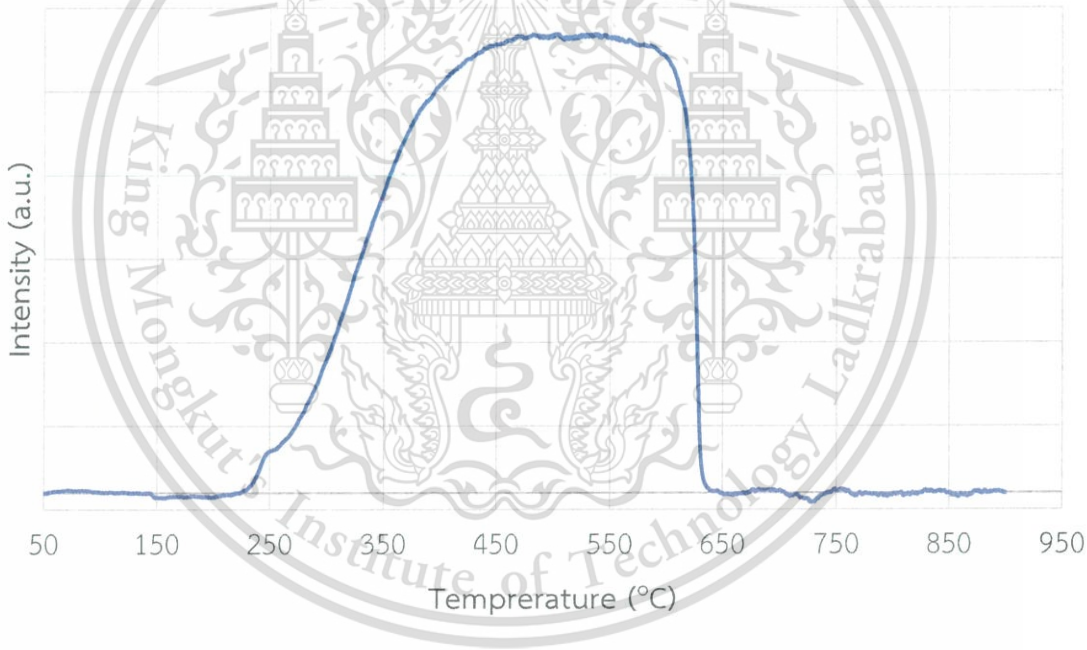

Figure A1 TPR profile of CuO

A few runs were performed by variation of the mass of CuO. Then, the peak area (integrated with **Origin Pro 8.0**) in the range T = 50-900 °C is plotted against the mole of CuO. The resulting plot (**Figure A2**) serves as a calibration curve where the mmol H_2 of any sample could be calculated from the peak area as shown below.

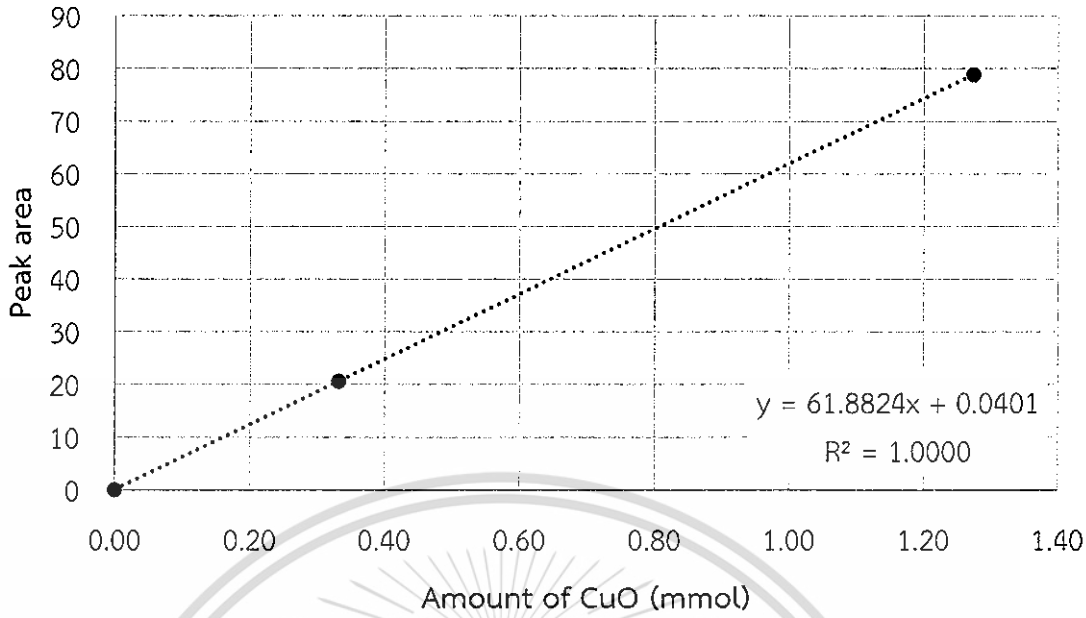

Figure A2 Standard curve of CuO: peak area *vs* the number of mole of CuO

From TPR results, $Na_2Ti_6O_{13}$ (0.1016 g) gives the peak area of 7.5521. Substituting this number into the equation in Figure A2 gives:

y = 61,882.3584x + 0.0401

7.5521 = 61,882.3584x + 0.0401

x = mmol CuO = 0.01214 mmol

As the mole ratio of CuO to H2 is 1:1, the number of mmol of H_2 consumed by $Na_2Ti_6O_{13}$ equals 0.01214 mol as well. So, the reducibility of $Na_2Ti_6O_{13}$ is 0.01214 mmol / 0.1016 g = 1.14 mmol H_2/g of catalyst.

CO_2 TPD SIGNAL EVALUATION

The electronic signal from the TCD detector during TPR analysis is converted to mmol CO_2, employing $CaCO_3$ as a standard. $CaCO_3$ is basic catalyst that can be decomposed giving CaO and CO_2. These CO2 molecules is used as signal reference material. The decomposition of CO_2 released during the heating are expressed by this equation;

$$CaCO_3(s) \rightarrow CaO(s) + CO_2(g)$$

An example of the decomposition of $CaCO_3$ is shown in Figure A2.

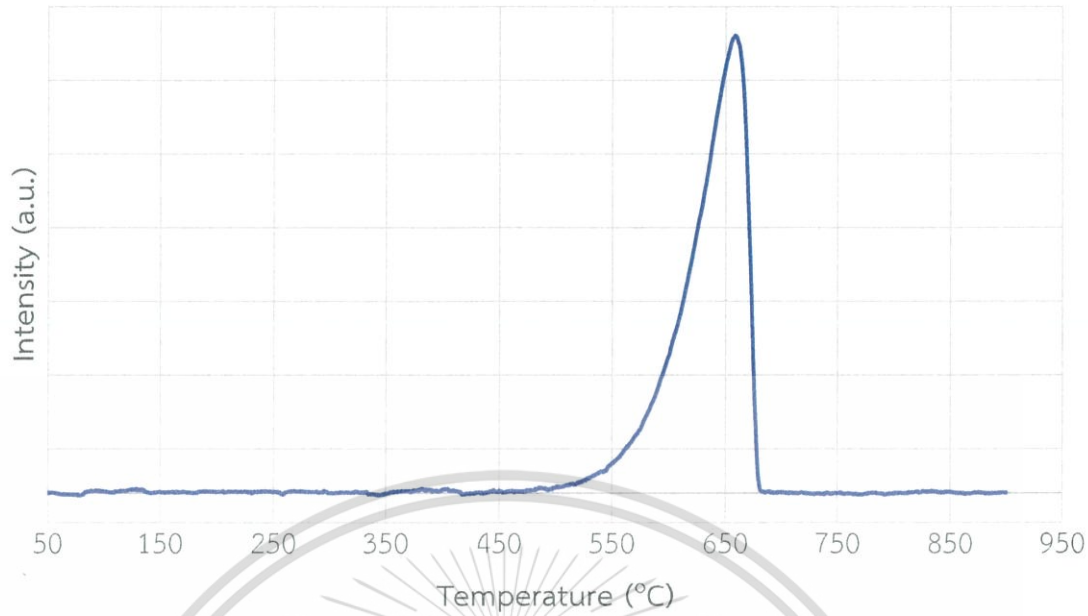

Figure A3 Decomposition profile of $CaCO_3$

The resulting plot (Figure A4) as a calibration curve and the mmol CO_2 of any sample could be calculated from the peak area similar to TPR

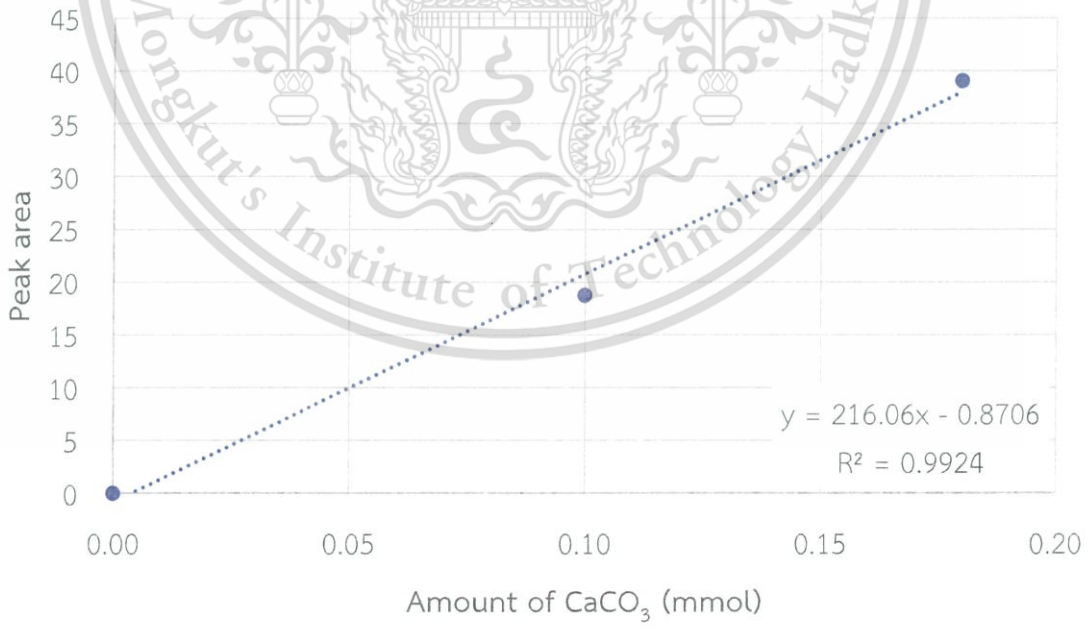

Figure A4 Standard curve of $CaCO_3$: peak area *vs* the number of mole of $CaCO_3$

APPENDIX B

CALCULATION

Contact time, W/F

Contact time (W/F) is expressed as:

$$W/F = \frac{\text{Weight of catalyst (g)}}{\text{Molar feed rate (mol/h)}}$$

This parameter can be tuned by varying the mass of catalyst, keeping the feed rate unchanged. The molar feed rate is fixed at 1.45 mmol/h (or 2.0 mL/h for acetic acid, and XXX mL/h for heptanoic acid). Slower feed rate render producible catalytic results difficult. For example, at the required W/F = 100 gh/mol, the weight of catalyst needed is:

$$100 \text{ gh/mol} = \frac{\text{Weight of catalyst (g)}}{0.00145 \text{ mol/h}}$$

$$\text{Weight of catalyst} = 0.1450 \text{ g}$$

Evaluation of obtained products

1. **Conversion** - the feed changed after the reaction.

$$\% \text{ Conversion} = \frac{\text{Corrected area of initial feed - Corrected of feed at any time}}{\text{Corrected area of initial feed}} \times 100$$

2. **Yield** - the products that are obtained after reaction

$$\% \text{ Yield} = \frac{\text{Corrected area of each product}}{\text{Corrected area of initial feed} \times \text{Response factor}} \times 100$$

Corrected area is a mathematic term where the area of interested is divided by the area of the standard.

$$\text{Corrected area of A} = \text{Area of} \frac{A}{\text{internal standard}}$$

Table B1 Product distribution* from the measurement by GC-FID

Product	Peak area	Response factor
2-octanone	28.3	1.21
5-undecane	15.2	1.42
6-Dodecanone	48.2	1.21
1,12-Tridecadien-7-one	0	1.21
Heptanoic anhydride	0	-
7-Tridecanone	12585.4	1.21
Heptanoic buthyl ester	33.1	1.35
Heptanophenone	94.1	1.21
Heptanoic acid (feed)	19985.2	1.00
p-xylene (internal standard)	1014507	-

* $K_2Ti_6O_{13}$, reduced at 400 °C for 2 h, W/F 250 gh/mol, reaction at 400 °C in N_2 at 60 min on stream.

For example;

Corrected area of initial feed is 0.0319

1. Conversion

$$\text{Conversion} = \frac{[0.0319-(19985.2/1014507)]}{0.0319} \times 100$$

$$= 38.24\ \%$$

2. Yield of 7-tridecanone

$$\text{Yield} = \frac{(11285.4/\ 1014507]}{0.0319 \times 1.21} \times 100$$

$$= 28.11\ \%$$

APPENDIX C

GC-CHROMATOGRAM

Prior to analysis, the products were identified by GC-MS (Gas chromatography equipped with Mass Spectrometer detector). Then, quantitative analysis was carried out with GC-FID (Gas chromatography equipped with Flame Ionization Detector). The analytical conditions of products from the ketonization of acetic acid and heptanoic acid are shown in Table C1 and Table C2 respectively.

Table C1 GC conditions for product analysis from ketonization of acetic acid

Column	DB-WAX, 30 m x 0.53 mm i.d., 1 Micrometer
Temperature program	Isothermal, 140°C for 15 min
Carrier gas	Nitrogen gas 1.5 mL/mol (34 cm/sec)
Injector	250 °C (splitting 1:100 at 0.01 s)
Injection volume	0.1 microliter
Detector	FID (300 °C)
Internal standard	*n*-propanol

Table B2 GC conditions for product analysis from ketonization of heptanoic acid

Column	DB-1, 30 m x 0.32 mm i.d., 5 Micrometer
Temperature program	40 °C for 5 min to 280 °C at rate 15 °C/min for 24 min
Carrier gas	Nitrogen gas 1.2 mL/mol (39 cm/sec)
Injector	265 °C (splitless)
Injection volume	0.1 microliter
Detector	FID (275 °C)
Internal standard	p-xylene or n-dodecane(for only $Pt/K_2Ti_6O_{13}$)

The products from the ketonization of acetic acid (heptanoic acid) were identified by comparing the retention time to that of the known substances as listed in Table C3 (Table C4).

Table C3 Products distribution from the ketonization of acetic acid

Feed or products	Retention time (min)
Acetone	1.396
n-propanol	1.633
Acetic acid	2.281

Table C4 Products distribution from the reaction of heptanoic acid

Feed or products	Retention time (min)
n-hexene	8.250
n-hexane	8.530
2-hexene	8.633
3-hexene	8.867
heptane	10.694
2-octanone	13.685
2-methylphenol	15.621
Heptanoic acid	15.881
undacane	16.395
n-dodecane	17.560
7-Tridecene	18.502
7-Tridecanone	20.036

APPENDIX D

REACTION DATA

1. The ketonization activity of all catalysts studied acetic acid?

Table D1 The ketonization of all catalysts studied acetic acid?

catalysts	No reduction		Reduction at 400 °C for 2 h	
	Conversion	Acetone	Conversion	Acetone
Anatase TiO_2	0.0	0.0	0.3	0.2
$Li_2Ti_6O_{13}$	4.8	3.9	14.3	13.2
$Na_2Ti_6O_{13}$	4.5	2.7	25.0	17.5
$K_2Ti_6O_{13}$	6.1	3.4	33.0	27.0
$Na_2Ti_3O_7$	0.9	0.7	4.3	3.7
$K_2Ti_4O_9$	4.9	3.7	14.0	10.0

* W/F 15 gh/mol, 400 °C in 90 mL/min N_2 at 1 atm. results average from time on stream 60-360 min.

2. The effect of reduction temperature of the ketonization of acetic acid

Table D2 The effect of reduction temperature over $K_2Ti_6O_{13}$

Time	Reduction temperature (°C)					
	400		450		500	
	Conversion	Acetone	Conversion	Acetone	Conversion	Acetone
60	32.3	26.9	35.2	27.9	23.7	18.9
120	35.00	26.1	35.1	28.1	24.7	18.9
180	32.8	26.5	34.3	27.8	24.7	18.5
240	33.1	27.5	34.3	28.2	25.8	18.7
300	33.0	27.5	34.2	29.5	25.4	19.4
360	32.9	27.5	33.6	30.7	24.8	19.4

* $K_2Ti_6O_{13}$, W/F 15 gh/mol, reaction at 400 °C in 90 mL/min N_2 at 1 atm.

3. The temperature scanning of the production of long chain olefins from heptanoic acid

Table D3 The heptanoic conversion over $K_2Ti_6O_{13}$ and the product distribution at 400 °C

Time on stream (min)	Conversion (%)	Yield (%)							
		octanone	D-nonalactone	5-undecane	6-Dodecanone	7-Tridecanone	Heptanoic buthyl ester	Heptanophenone	1-(4-methylphenyl) -1-pentanone
60	24.2	0.1	0.3	0.1	0.2	18.2	0.2	0.0	0.1
120	18.9	0.1	0.1	0.1	0.2	14.3	0.1	0.0	0.0
180	15.6	0.1	0.3	0.0	0.0	11.7	0.1	0.1	0.0
240	16.5	0.2	0.1	0.0	0.1	12.5	0.0	0.0	0.0
300	15.1	0.0	0.1	0.0	0.1	11.5	0.0	0.0	0.1

* non-reduced $K_2Ti_6O_{13}$, W/F 250 gh/mol, 400 °C in 90 mL/min N_2 at 1 atm.

Table D4 The heptanoic conversion over $K_2Ti_6O_{13}$ and the product distribution at 450 °C

Time on stream (min)	Conversion (%)	Yield (%)							
		octanone	D-nonalactone	5-undecane	6-Dodecanone	7-Tridecanone	Heptanoic buthyl ester	Heptanophenone	1-(4-methylphenyl) -1-pentanone
60	99.9	1.3	0.1	0.4	0.4	73.1	0.3	0.5	0.0
120	100.0	1.5	0.0	1.4	1.4	71.4	0.4	0.1	0.0
180	100.0	1.5	0.0	1.5	1.5	71.6	0.0	0.0	0.0
240	100.0	1.5	0.0	0.9	0.9	72.4	0.4	0.1	0.0
300	99.9	1.2	0.0	1.1	1.1	72.0	0.5	0.1	0.0

* non-reduced $K_2Ti_6O_{13}$, W/F 250 gh/mol, 450 °C in 90 mL/min N_2 at 1 atm.

Table D5 Heptanoic conversion over $K_2Ti_6O_{13}$ and the product distribution at 500 °C

Time on stream (min)	Conversion (%)	Yield (%)							
		octanone	D-nonalactone	5-undecane	6-Dodecanone	7-Tridecanone	Heptanoic buthyl ester	Heptanophenone	1-(4-methylphenyl) -1-pentanone
60	99.6	3.9	0.1	0.0	1.9	67.7	0.3	0.5	0.0
120	99.8	2.4	0.1	0.0	2.1	69.7	0.2	0.2	0.0
180	99.8	2.4	0.1	0.3	1.9	71.2	0.0	0.0	0.0
240	100.0	2.4	0.1	0.2	1.8	70.8	0.5	0.2	0.0
300	99.9	3.0	0.0	0.7	1.7	70.1	0.5	0.1	0.0

* non-reduced $K_2Ti_6O_{13}$, W/F 250 gh/mol, 500 °C in 90 mL/min N_2 at 1 atm.

4. The contact time scanning for the production of long chain olefins from heptanoic acid over $K_2Ti_6O_{13}$

4.1 Contact time scanning in N_2 atmosphere

Table D6 Heptanoic conversion over $K_2Ti_6O_{13}$ and the product distribution at various contact times in N_2

Contact time (gh/mol)	Conversion (%)	Yield (%)							
		octanone	D-nonalactone	5-undecane	6-Dodecanone	7-Tridecanone	Heptanoic buthyl ester	Heptanophenone	1-(4-methylphenyl) -1-pentanone
0.0	0.0	0.0	0.0	0.0	0.0	0.0	0.0	0.0	0.0
100	27.2	0.1	0.1	0.1	0.1	20.1	0.5	0.3	0.0
150	35.7	0.0	0.1	0.0	0.1	26.5	0.2	0.0	0.0
200	40.8	0.0	0.0	0.0	0.1	30.5	0.2	0.0	0.0
250	38.2	0.1	0.1	0.1	0.2	29.2	0.1	0.3	0.1

* $K_2Ti_6O_{13}$, reduced at 400 °C for 2 h, reaction at 400 °C in 90 mL/min N_2 at 1 atm.

4.2 Contact time scanning in H_2 atmosphere

Table D7 Heptanoic conversion over $K_2Ti_6O_{13}$ and the product distribution at various contact time in H_2

Contact time (gh/mol)	Conversion (%)	Yield (%)							
		octanone	D-nonalactone	5-undecane	6-Dodecanone	7-Tridecanone	Heptanoic buthyl ester	Heptanophenone	1-(4-methylphenyl) -1-pentanone
0	0.0	0.0	0.0	0.0	0.0	0.0	0.0	0.1	0.1
100	67.4	0.1	0.1	0.0	0.1	50.9	0.3	0.5	0.1
150	77.0	0.0	0.1	0.0	0.2	58.1	0.1	0.1	0.1
200	99.8	0.0	0.1	0.1	0.4	75.4	0.1	0.1	0.1
250	99.4	0.1	0.0	0.1	0.4	75.6	0.1	0.1	0.1

* $K_2Ti_6O_{13}$, reduced at 400 °C for 2 h, reaction at 400 °C in 90 mL/min H_2 at 1 atm.

5. The effect of metal loading

Table D8 Heptanoic conversion over 1% wt $Co/K_2Ti_6O_{13}$ and the product distribution

Time on stream (min)	Conversion (%)	Yield (%)							
		octanone	D-nonalactone	5-undecane	6-Dodecanone	7-Tridecanone	Heptanoic buthyl ester	Heptanophenone	1-(4-methylphenyl) -1-pentanone
60	87.0	0.1	0.1	0.2	0.3	77.1	0.3	0.0	0.0
120	90.3	0.0	0.1	0.1	0.5	62.9	0.2	0.2	0.0
180	91.4	0.0	0.1	0.0	0.4	72.0	0.0	0.0	0.0
240	91.8	0.0	0.0	0.0	0.3	73.0	0.1	0.0	0.0
300	92.0	0.0	0.0	0.0	0.3	69.5	0.2	0.0	0.0

1% wt $Co/K_2Ti_6O_{13}$, reduced at 400 °C for 2 h, W/F 100 gh/mol, reaction at 400 °C in 90 mL/min H_2 at 1 atm.

Table D9 Heptanoic conversion over 1% wt $Pt/K_2Ti_6O_{13}$ and the product distribution

Time on stream (min)	Conversion (%)	Yield									
		n-hexene	n-hexane	2-hexene	3-hexene	heptane	2-octanone	2-methylphenol	undacane	7-Tridecene	7-Tridecanone
60	99.6	2.8	14.3	5.3	2.8	3.0	0.5	1.3	4.1	9.7	47.0
120	99.4	6.54	17.4	7.4	4.4	5.9	0.5	2.3	5.5	13.1	49.4
180	99.6	2.15	12.5	4.5	1.9	3.0	0.3	1.2	2.8	8.6	40.4
240	99.4	6.1	18.2	8.5074	3.8	6.2	1.0	2.2	6.8	13.5	46.1
300	100.0	4.9	22.8	10.6	3.7	8.0	0.8	2.5	5.9	16.1	55.9

* 1% wt $Pt/K_2Ti_6O_{13}$, reduced at 400 °C for 2 h, W/F 100 gh/mol, reaction at 400 °C in 90 mL/min H_2 at 1 atm.

Table D10 Heptanoic conversion over 0.5% wt $Pt/K_2Ti_6O_{13}$ and the product distribution

Time on stream (min)	Conversion (%)	Yield									
		n-hexene	n-hexane	2-hexene	3-hexene	heptane	2-octanone	2-methylphenol	undacane	7-Tridecene	7-Tridecanone
60	98.4	4.0	21.1	6.8	3.6	4.6	1.0	3.6	4.9	21.7	44.0
120	98.9	3.8	19.2	6.4	3.7	3.7	0.8	3.1	4.6	20.3	41.6
180	98.8	3.3	21.4	6.0	3.0	4.4	0.6	3.0	4.0	21.9	46.1
240	98.7	4.0	13.4	6.6	3.3	3.5	0.9	2.8	4.0	20.5	40.6
300	98.5	2.6	19.4	7.9	2.8	4.6	1.3	3.6	2.2	15.9	47.1

* 0.5% wt $Pt/K_2Ti_6O_{13}$, reduced at 400 °C for 2 h, W/F 100 gh/mol, reaction at 400 °C in 90 mL/min H_2 at 1 atm.

Table D11 Heptanoic conversion over 0.1% wt $Pt/K_2Ti_6O_{13}$ and the product distribution

Time on stream (min)	Conversion (%)	Yield											
		n-hexene	n-hexane	2-hexene	3-hexene	heptane	2-octanone	2-methylphenol	undacane	7-Tridecene	7-Tridecanone	Heptanoic buthyl ester	Heptanophenone
60	90.3	1.5	1.4	.00	0.0	0.0	7.5	0.0	4.2	5.5	69.9	1.5	1.4
120	87.0	0.4	1.4	0.0	0.0	0.0	5.2	0.0	4.5	5.6	66.4	0.4	1.4
180	86.6	0.4	1.7	0.0	0.0	0.0	4.7	0.0	5.1	5.0	72.1	0.4	1.7
240	88.3	0.6	1.0	0.0	0.0	0.0	6.0	0.0	7.8	3.8	72.9	0.6	1.0
300	87.1	0.4	1.5	0.0	0.0	0.0	6.3	0.0	6.7	3.1	72.5	0.4	1.5

* 0.1% wt $Pt/K_2Ti_6O_{13}$, reduced at 400 °C for 2 h, W/F 100 gh/mol, reaction at 400 °C in 90 mL/min H_2 at 1 atm.

5. The contact time scanning for the production of long chain olefins from heptanoic acid over 0.1% wt $Pt/K_2Ti_6O_{13}$

Table D12 Heptanoic conversion over 0.1% wt $Pt/K_2Ti_6O_{13}$ and the product distribution at 150 gh/mol

Time on stream (min)	Conversion (%)	Yield									
		n-hexene	n-hexane	2-hexene	3-hexene	heptane	2-octanone	2-methylphenol	undacane	7-Tridecene	7-Tridecanone
60	100	4.7	4.3	0.3	0.3	0.2	13.9	0.0	1.0	4.3	80.7
120	100	4.7	4.1	0.0	0.3	0.2	16.4	0.0	0.0	3.8	80.0
180	100	4.2	3.6	0.0	0.2	0.1	15.1	0.0	0.0	3.2	79.7
240	100	4.7	3.9	0.0	0.3	0.2	18.0	0.0	0.0	4.0	82.6
300	100	4.7	3.9	0.0	0.2	0.2	8.1	0.0	0.0	3.4	79.6

* 0.1% wt $Pt/K_2Ti_6O_{13}$, reduced at 400 °C for 2 h, reaction at 400 °C in 90 mL/min H_2 at 1 atm.

Table D13 Heptanoic conversion over 0.1% wt $Pt/K_2Ti_6O_{13}$ and the product distribution at 200 gh/mol

Time on stream (min)	Conversion (%)	Yield									
		n-hexene	n-hexane	2-hexene	3-hexene	heptane	2-octanone	2-methylphenol	undacane	7-Tridecene	7-Tridecanone
60	100	3.5	3.1	0.0	0.2	0.1	17.1	0.0	0.0	3.7	77.0
120	100	4.3	3.6	0.0	0.3	0.9	16.0	0.0	0.0	3.9	75.7
180	100	4.6	0.4	0.0	0.3	1.0	18.1	0.0	0.0	4.1	76.5
240	100	4.4	3.4	0.0	0.3	1.0	17.5	0.0	0.0	3.5	77.4
300	100	5.0	3.8	0.0	0.3	1.1	19.9	0.0	0.0	3.8	76.0

* 0.1% wt $Pt/K_2Ti_6O_{13}$, reduced at 400 °C for 2 h, reaction at 400 °C in 90 mL/min H_2 at 1 atm.

APPENDIX E

ADSORPTION-DESORPTION ISOTHERM

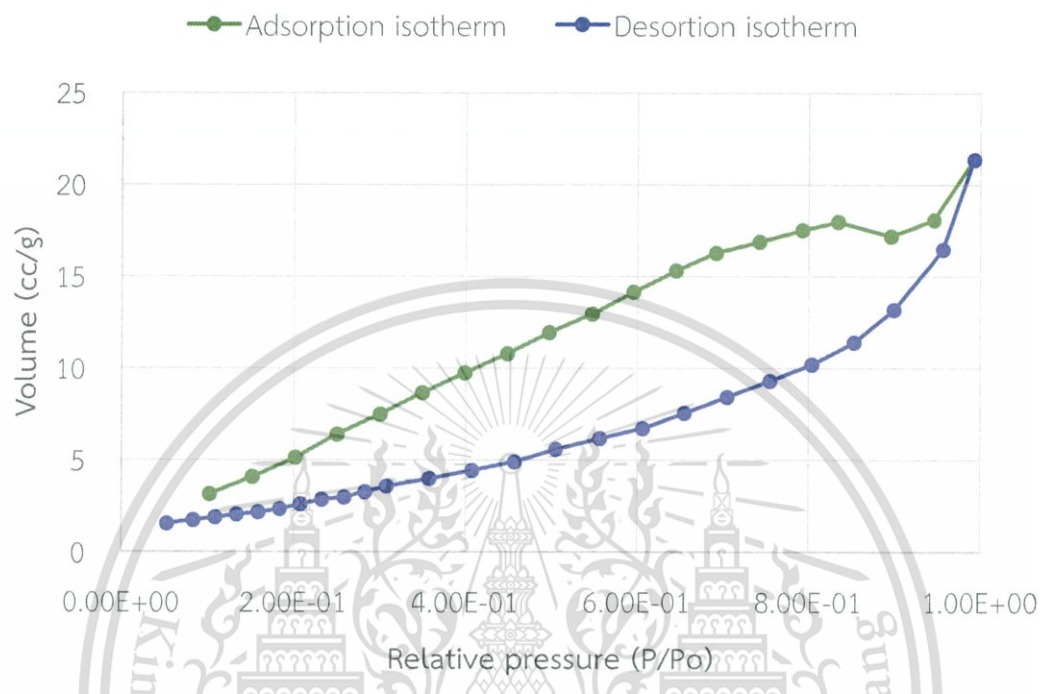

Figure E1 Adsorption-desorption isotherm of $Na_2Ti_6O_{13}$

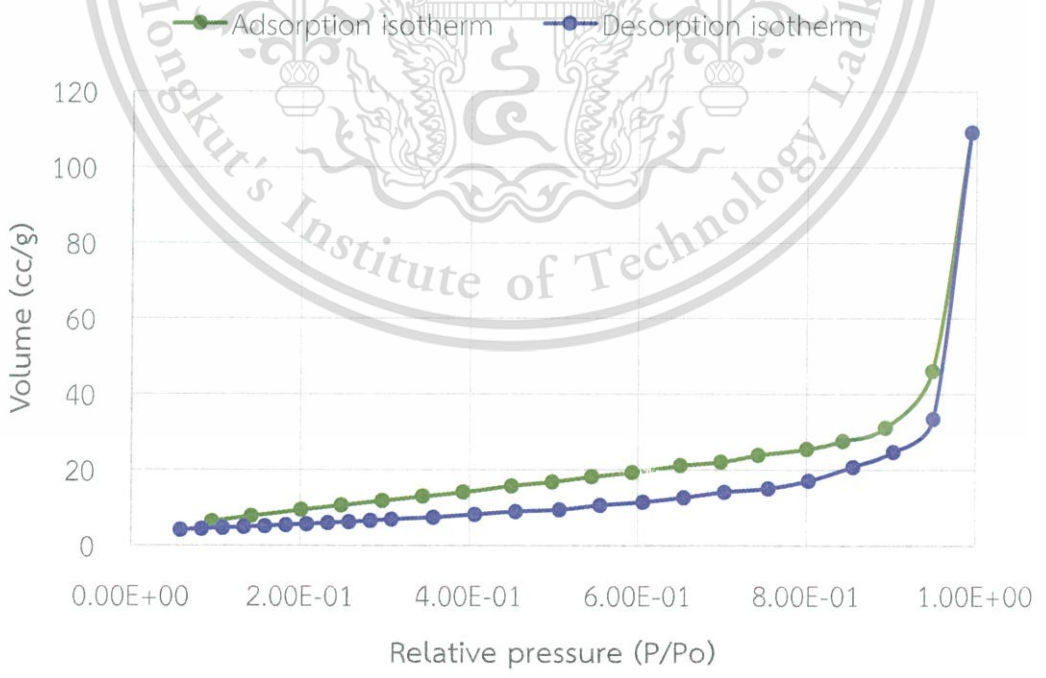

Figure E2 Adsorption-desorption isotherm of $K_2Ti_6O_{13}$

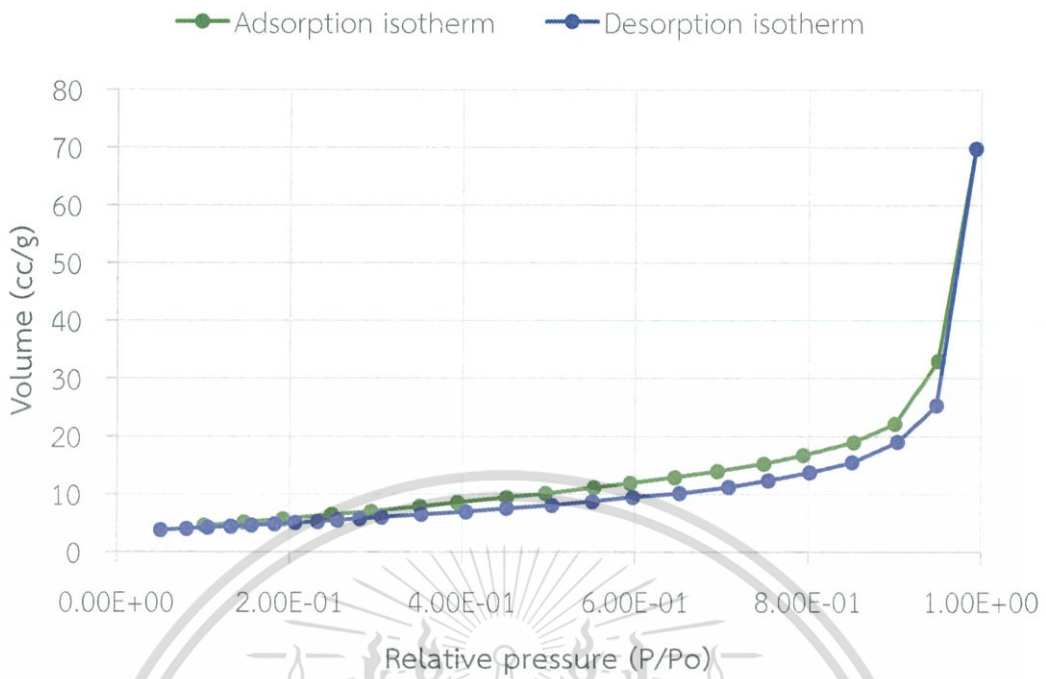

Figure E3 Adsorption-desorption isotherm of $Li_2Ti_6O_{13}$

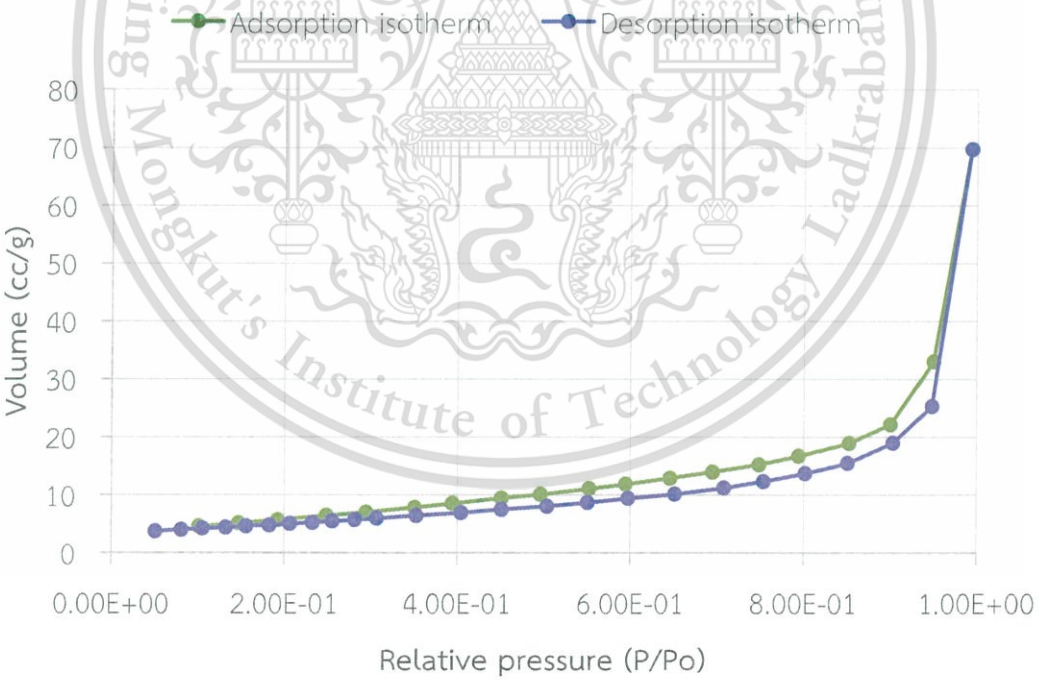

Figure E4 Adsorption-desorption isotherm of commercial $Na_2Ti_3O_7$

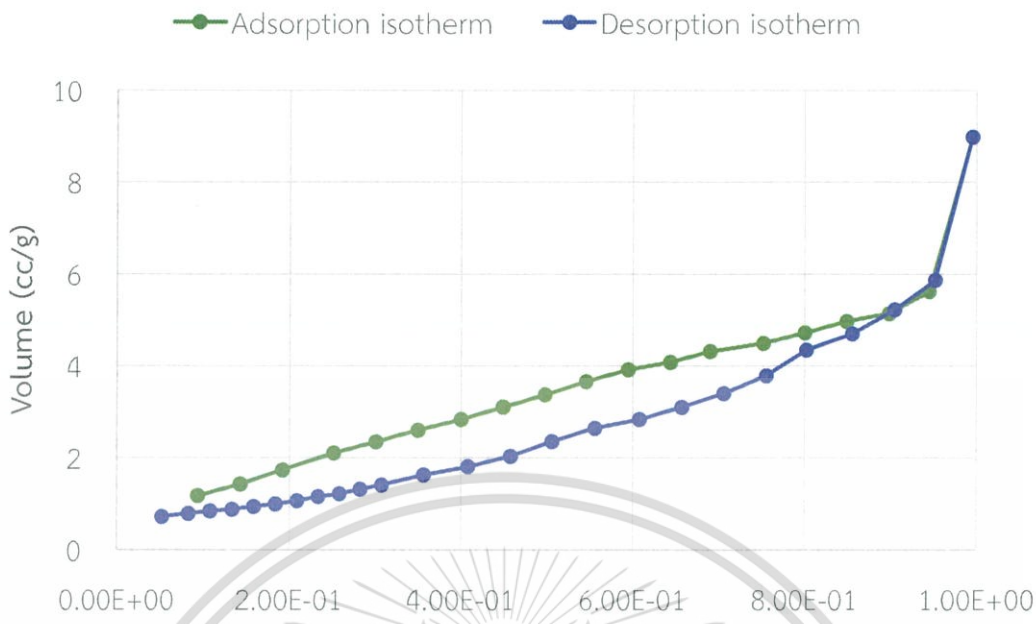

Figure E5 Adsorption-desorption isotherm of $Na_2Ti_3O_7$

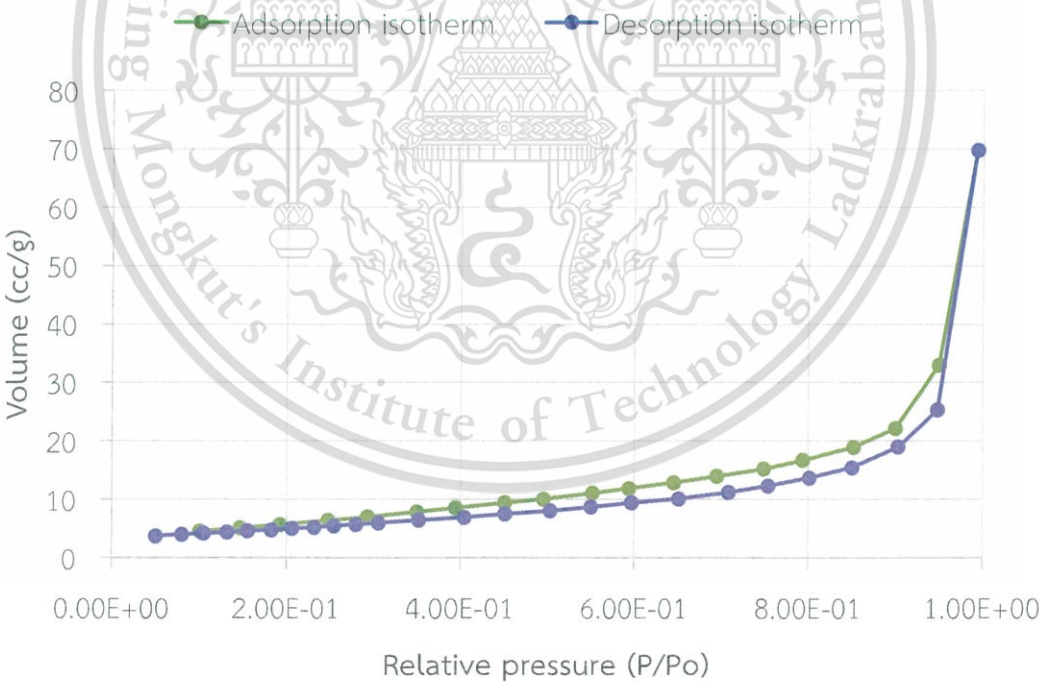

Figure E6 Adsorption-desorption isotherm of Nanotube $Na_2Ti_3O_7$

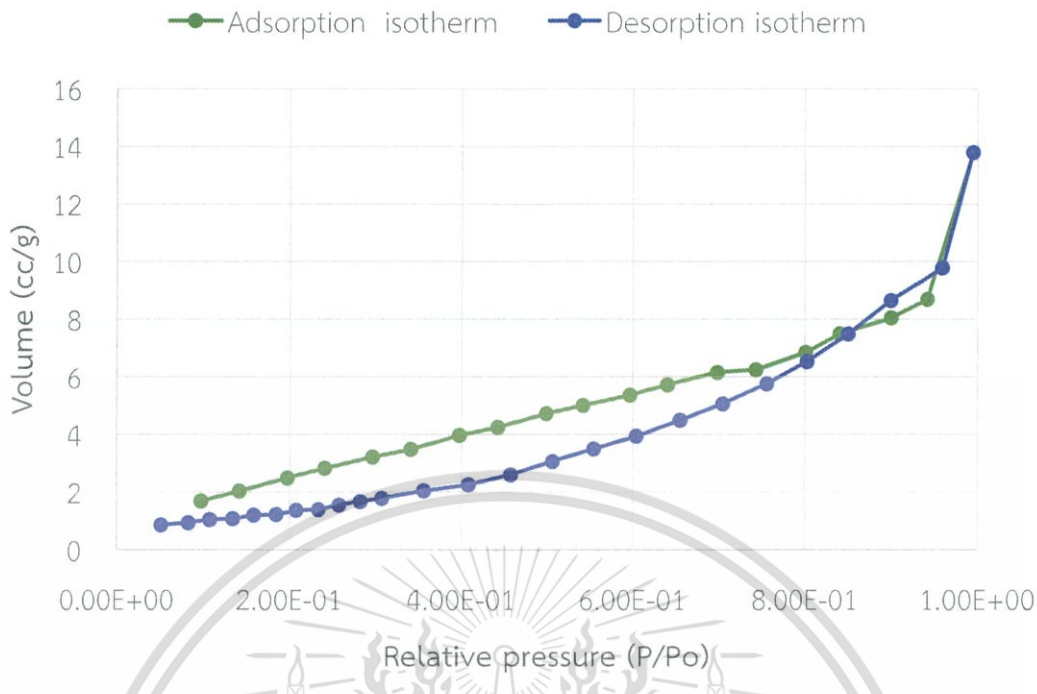

Figure E7 Adsorption-desorption isotherm of $K_2Ti_4O_9$

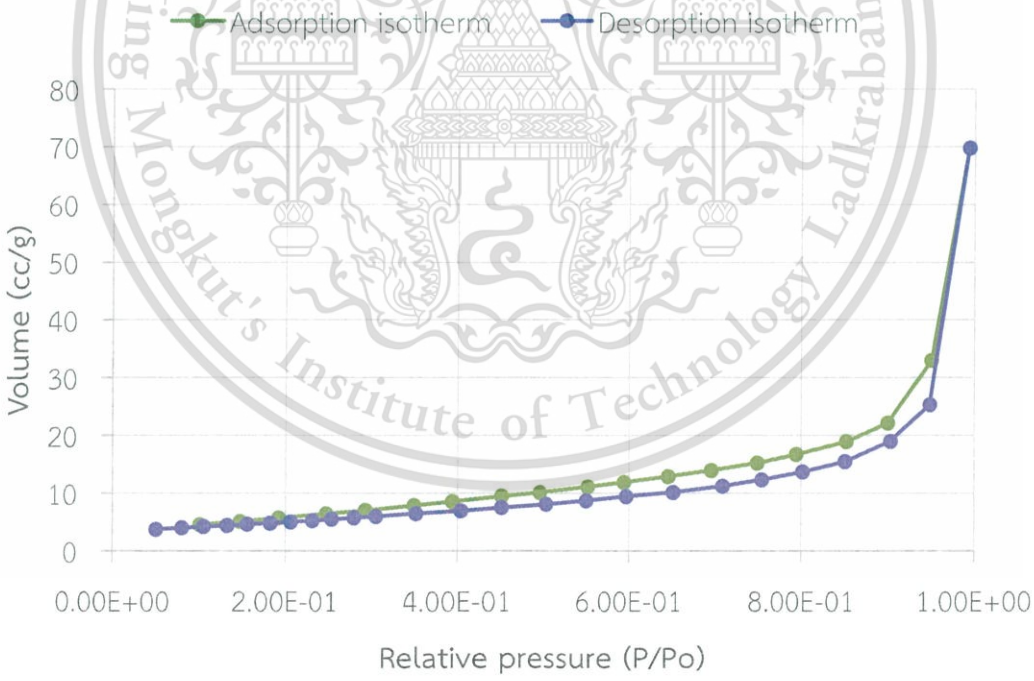

Figure E8 Adsorption-desorption isotherm of 1% wt $Co/K_2Ti_6O_{13}$

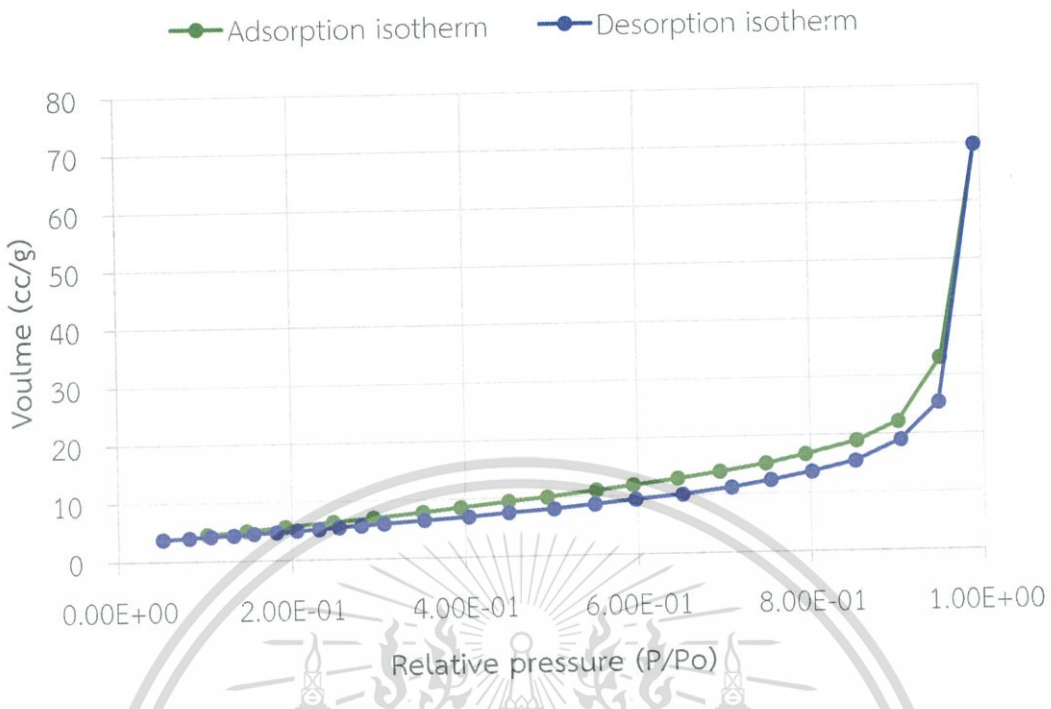

Figure E9 Adsorption-desorption isotherm of 0.1% wt $Pt/K_2Ti_6O_{13}$

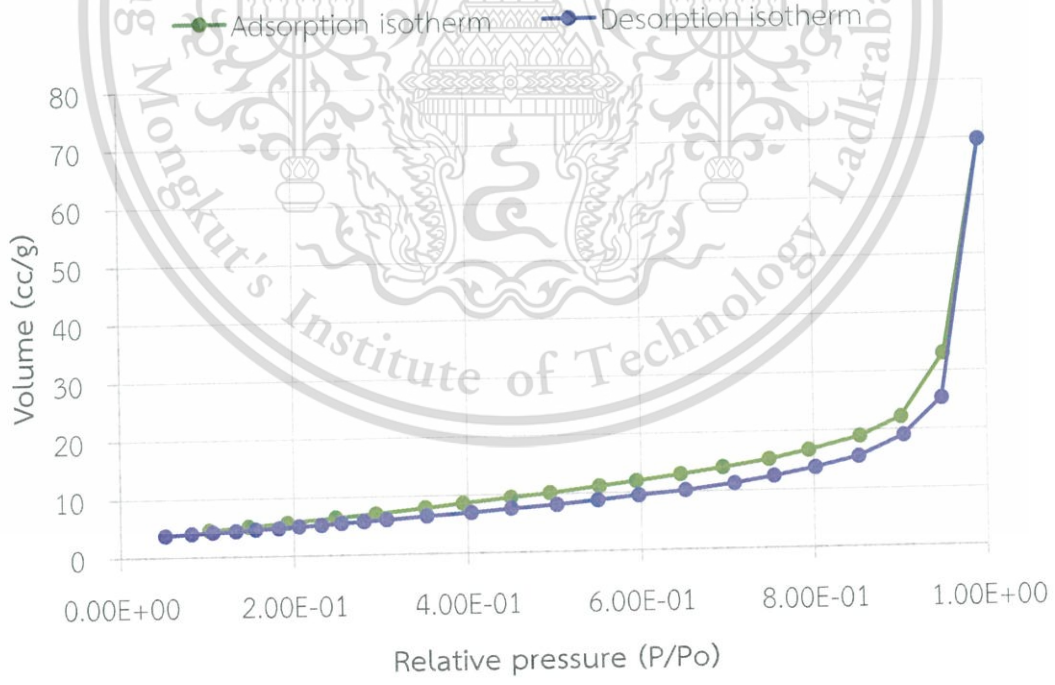

Figure E10 Adsorption-desorption isotherm of 0.5% wt $Pt/K_2Ti_6O_{13}$

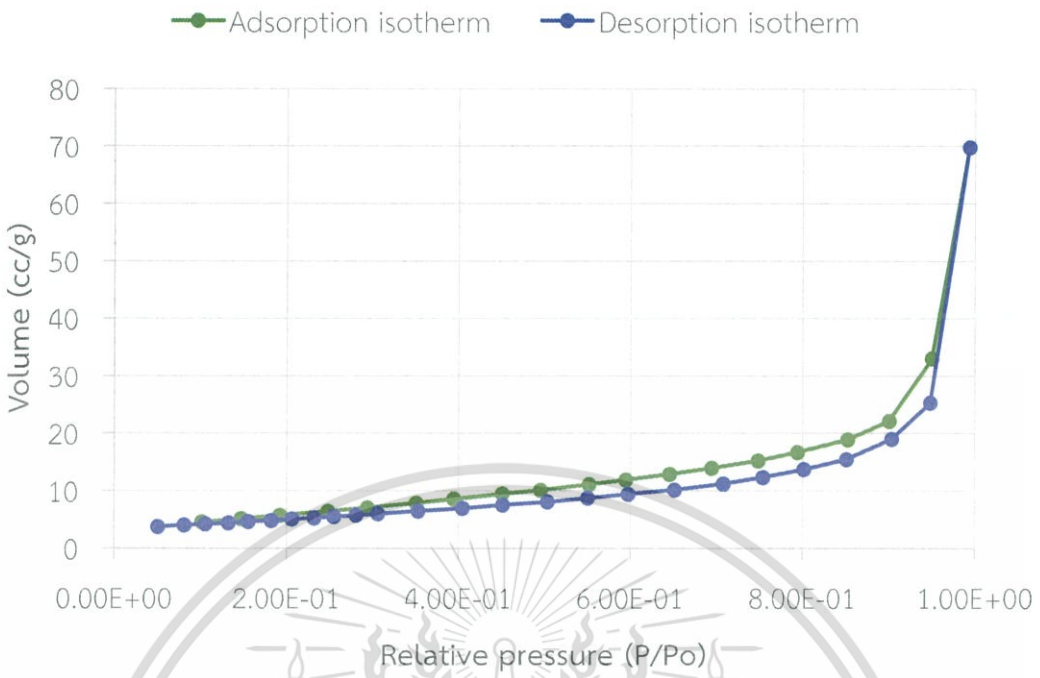

Figure E11 Adsorption-desorption isotherm of 1% wt $Pt/K_2Ti_6O_{13}$

AURTHER BIOGRAPHY

Name Mr. Pratya Promchana

Date of Birth 22 April 1991

Address 88/3 Village no.2 Huisai Sub-district Maerim District Chiang mai 50180

Education (2014) Bachelor of Science in Science and Technology GPA 3.79
Chiang mai Rajabhat University

International Conferences

1. Pratya Promchana, Tawan Sooknoi and Tosapol Maluangnont, "***The ketonization of acetic acid over alkali metal titanates with tunneled and layered structure***", PACCON 2015, Poster presentation, Amari Watergate hotel, Bangkok, Thailand.

2. Sarawut Somnam* , Pratya Promchana, Kamolcharal Hyumtha and Miki Kanna. ***"The Recovery of Silver from Some Electronic Waste to Prepare $AgNO_3$"***, PACCON 2013, Poster presentation, The Tide resort, Chon buri, Thailand.

Award

1. (2014) Best Schorlar in Faculty of Science and Technology, CMRU